
	<p>Research and Development Programme on Seismic Ground Motion</p> <p>CONFIDENTIAL  <i>Restricted to SIGMA scientific partners and members of the consortium, please do not pass around</i></p>	<p>Ref : SIGMA-2013-D3-97  Version : 01</p> <p>Date :  Page :</p>
--	---	---



# CHARACTERIZATION OF CLASSES OF SITES WITH A LARGE POTENTIAL TO CAUSE SITE EFFECTS TAKING INTO ACCOUNT THE GEOLOGICAL HETEROGENEITIES (METHODOLOGICAL APPROACH)

(Deliverable D3-97)

AUTHORS			REVIEW			APPROVAL		
NOM	DATE	VISA	NOM	DATE	VISA	NOM	DATE	VISA
P. Moczo University of Bratislava			A. Pecker Geodynamique Consulting	In written review attached		F. Hollender		
			P.Y. Bard IsTerre	In written review attached		G. Senfaute		

	<p style="text-align: center;">Research and Development Programme on Seismic Ground Motion</p> <p style="text-align: center;">CONFIDENTIAL <i>Restricted to SIGMA scientific partners and members of the consortium, please do not pass around</i></p>	<p>Ref : SIGMA-2013-D3-97 Version : 01</p> <hr/> <p>Date : 21/10/2013 Page : 2</p>
--	--	--

## Executive Summary


We present methodology of extensive numerical modelling of seismic motion and its interpretation for a set of selected models of surface sedimentary structures. 8 models representing important local surface sedimentary structures include canonical model, simplified models and realistic models. Here realistic means sufficiently geometrically and rheologically complex, and, at the same time, potentially well approximating reality in terms of the most important features of seismic motion.

The numerical simulations of seismic motion are performed using the Fortran95 computer code 3DFD\_VS. The computational algorithm is based on the (2,4) velocity-stress staggered-grid finite-difference explicit heterogeneous scheme on Cartesian discontinuous spatial grid. Here, (2,4) means the 2<sup>nd</sup>-order accuracy in time and 4<sup>th</sup>-order accuracy in space.


The direct results of the numerical simulations, the synthetic velocity seismograms in case of the plane wave incidence and accelerograms in case of kinematic point or finite source, will be used for determination of the site transfer properties, the Fourier transfer functions. The Fourier transfer functions and selected real and synthetic accelerograms will be used for determination of the amplification factors.

These characteristics of seismic motion will be used for comparing 3D, 2D and 1D modelling approaches.

Specific variations of the selected models will be subject of predominantly 3D modelling in order to investigate sensitivity of characteristics of seismic motion to model features. The main goal will be to identify the key features of representative 3D structures for forming seismic motion and determining characteristics of seismic motion.

	<p style="text-align: center;">Research and Development Programme on Seismic Ground Motion</p> <p style="text-align: center;">CONFIDENTIAL <i>Restricted to SIGMA scientific partners and members of the consortium, please do not pass around</i></p>	<p>Ref : SIGMA-2013-D3-97 Version : 01</p> <hr/> <p>Date : 21/10/2013 Page : 3</p>
--	--	--

<b>1.</b>	<b>INTRODUCTION.....</b>	<b>4</b>
<b>2.</b>	<b>LOCAL SURFACE GEOLOGICAL STRUCTURES.....</b>	<b>4</b>
2.1.	CANONICAL MODEL.....	5
2.2.	REAL AND VIRTUAL SITES.....	5
<b>3.</b>	<b>NUMERICAL SIMULATIONS OF SEISMIC MOTION .....</b>	<b>7</b>
3.1.	SIMULATIONS .....	7
	3D SIMULATIONS.....	7
	2D SIMULATIONS.....	7
	1D SIMULATIONS.....	7
3.2.	METHOD OF NUMERICAL SIMULATIONS.....	7
	3.2.1. Numerical method.....	7
	3.2.2. Computational domain and grid.....	8
	3.2.3. Model of medium and governing equations.....	9
	3.2.4. Discrete representation of the medium.....	12
	3.2.5. FD scheme for interior grid points.....	19
	3.2.6. Simulation of the planar free surface.....	21
	3.2.7. Simulation of the non-reflecting boundary.....	23
	3.2.8. Wavefield excitation.....	24
<b>4.</b>	<b>ANALYSIS OF NUMERICAL SIMULATIONS .....</b>	<b>24</b>
4.1.	TRANSFER PROPERTIES AT A SITE – 3D.....	25
4.2.	AMPLIFICATION FACTOR – 3D.....	26
4.3.	TRANSFER PROPERTIES AND AMPLIFICATION FACTOR AT A SITE – 2D .....	27
4.4.	TRANSFER PROPERTIES AND AMPLIFICATION FACTOR AT A SITE – 1D .....	28
<b>5.</b>	<b>GRENOBLE VALLEY, FRANCE.....</b>	<b>36</b>
5.1.	INTRODUCTION.....	36
5.2.	COMPUTATIONAL MODEL.....	36
5.3.	COMPUTATIONAL PARAMETERS .....	41
5.4.	ILLUSTRATIVE NUMERICAL EXAMPLE.....	41
	5.4.1. Pseudoimpulse responses.....	41
	5.4.2. Selected accelerograms.....	42
	5.4.3. Amplification factors.....	42
	5.4.4. Average amplification factors obtained from the 1D, 2D and 3D numerical simulations .....	43
<b>6.</b>	<b>CONCLUSIONS .....</b>	<b>46</b>
<b>7.</b>	<b>REFERENCES.....</b>	<b>46</b>
<b>8.</b>	<b>APPENDIX.....</b>	<b>49</b>

	<p style="text-align: center;">Research and Development Programme on Seismic Ground Motion</p> <p style="text-align: center;">CONFIDENTIAL <i>Restricted to SIGMA scientific partners and members of the consortium, please do not pass around</i></p>	<p>Ref : SIGMA-2013-D3-97 Version : 01</p> <hr/> <p>Date : 21/10/2013 Page : 4</p>
--	--	--

## 1. Introduction

The main goal of the SIGMA project is to develop robust and stable estimates of seismic hazard. Specific site condition (e.g., surface sedimentary structures or distinct free-surface topography) can significantly contribute to the earthquake ground motion at a site. The Work Package #3 (WP3) therefore aims to develop methods

- of predicting whether a site of interest needs a special investigation with respect to its site conditions,
- for including site effects in the seismic hazard assessment.

The collaboration between CUB and EdF should contribute to the following tasks


- X3-5 – Identification of important site parameters using sensitivity study,
- X3-6 – Evaluation of numerical simulation tools in terms of an impact of uncertainty in geotechnical model on results of numerical simulations,
- X3-9 – Application of the numerical-modelling methods to a set of representative real and/or virtual sites.

The present study is focused on investigations of potential of selected specific sites to cause site effects and their estimation using 1D, 2D and 3D numerical simulations. The investigations should contribute to identifying key parameters responsible for site effects.

We first briefly introduce set of selected site model (models of surface local sedimentary structures), and intended 3D, 2D and 1D numerical simulations of seismic motion. Then we continue by exposition of the numerical methodology. The exposition covers all aspects of the methodology but pays more attention to those aspects that dominantly determine accuracy with respect to material heterogeneity and realistic attenuation. Further we detail characteristics of seismic motion that will be used for the comparative and sensitivity investigations. Finally, we present an example of numerical simulations and their evaluation for the realistic model of the Grenoble valley.

## 2. Local surface geological structures

A set of representative/important types of local surface sedimentary structures has been selected for performing the intended comparative and sensitivity investigations. The all models may be divided

	<p>Research and Development Programme on Seismic Ground Motion</p> <p>CONFIDENTIAL <i>Restricted to SIGMA scientific partners and members of the consortium, please do not pass around</i></p>	<p>Ref : SIGMA-2013-D3-97 Version : 01</p> <hr/> <p>Date : 21/10/2013 Page : 5</p>
--	--	--

into three groups – canonical (or reference) model, virtual sites and real sites. All they have flat (horizontal planar) free surface. The models are schematically illustrated in Tab. 2.1.

In the process of investigations, modifications of the selected models may be defined in order

- to estimate sensitivity of characteristics of seismic motion with respect to geometry and material properties,
- to identify key features of the models determining characteristics of seismic motion.

## 2.1. Canonical model

The homogeneous halfspace is a reasonable reference canonical model because the only effect on the incident wave is the effect of the planar free surface. In case of the horizontal flat free surface and vertically incident plane wave the interference of the incident and reflected wave at any frequency leads to amplification by factor of 2. Whereas in the hazard analysis it is reasonable to recognize a soft soil, standard rock and hard rock, in the linear numerical modelling we incorporate all these three cases in one model of the homogeneous halfspace.


## 2.2. Real and virtual sites

Real sites 1 – 3 and virtual sites 4 – 6 represent realistic models important for the SIGMA project. Here ‘realistic’ means considerably more complicated (in terms of geometry and rheology) from what we would classify as canonical or simplified. The relativity of the concept is, of course, obvious. The seismic motion at a free surface can be hardly intuitively estimated because even for a canonical vertically incident plane wave it is a result of complex interference, diffraction and resonant wave phenomena.

The virtual site 7 may represent a simplified model of a 2D shallow valley – a uniform long sedimentary valley in a limited frequency range related to the valley dimensions and speeds of seismic waves in sediments. A 2D modelling can give reasonable approximation for a vertical or nearly vertical incidence if wavefront has relatively large radius of curvature. If these conditions are not met, a 3D modelling for the 2D structural model can considerably better approximate reality. For modelling at relatively low frequencies the 2D model of the real prolonged valley likely may be insufficient.

**Tab. 2.1 Model codes, names and schematic depictions**

model code and name	schematic picture
<b>canonical model</b>	
9 homogeneous halfspace representing soil, standard rock and hard rock	
<b>real sites</b>	
1 EuroSeistest	
2 Grenoble	
3 Argostoli	
<b>virtual sites</b>	
4 RS4	
5 RS5	
6 3D meander	
7 2D shallow valley	

	<p style="text-align: center;">Research and Development Programme on Seismic Ground Motion</p> <p style="text-align: center;">CONFIDENTIAL <i>Restricted to SIGMA scientific partners and members of the consortium, please do not pass around</i></p>	<p>Ref : SIGMA-2013-D3-97 Version : 01</p> <hr/> <p>Date : 21/10/2013 Page : 7</p>
--	--	--

### 3. Numerical simulations of seismic motion

#### 3.1. Simulations

Forward numerical simulations of seismic motion in the selected models of local surface structures will be performed using the finite-difference method. Because the accuracy and computational efficiency of the numerical simulations is crucial for the intended investigations, we will describe the simulations and the method itself with an appropriate level of detail in order to make reader aware of the essential aspects of the modelling of seismic motion in relatively complex 3D models.

##### 3D simulations

3D simulations will be performed selectively for

- a vertical incidence of three plane waves; each wave will be polarized in a coordinate direction,
- point double-couple source,
- finite kinematic source.

##### 2D simulations

2D simulations will be performed for selected 2D profiles of the 3D models assuming a vertical incidence of P, SV and SH waves. The discrete grid models of the selected 2D model profiles will be prepared from the 3D model.

##### 1D simulations


1D simulations will be performed for local vertical model profiles at selected receiver positions in 3D model.

#### 3.2. Method of numerical simulations

##### 3.2.1. Numerical method

The numerical simulations of seismic motion are performed using the Fortran95 computer code 3DFD\_VS. The computational algorithm is based on the (2,4) velocity-stress staggered-grid finite-difference explicit heterogeneous scheme on Cartesian discontinuous spatial grid. Here, (2,4) means the 2<sup>nd</sup>-order accuracy in time and 4<sup>th</sup>-order accuracy in space. In the finite-difference method both medium and wavefield are represented by values in the discrete space-time grid. An explicit scheme



	Research and Development Programme on Seismic Ground Motion  CONFIDENTIAL <i>Restricted to SIGMA scientific partners and members of the consortium,          please do not pass around</i>	Ref : SIGMA-2013-D3-97 Version : 01  Date : 21/10/2013 Page : 8
--	--	---

for updating a particle velocity at a spatial position is obtained by a discrete approximation of the equation of motion and linear stress-strain relation formulated in the particle velocity vector and stress tensor.

References for the applied method are Moczo et al. (2000, 2002, 2004, 2007a,b, 2011, 2014), Kristek et al. (2002, 2009, 2010), Kristek and Moczo (2003), Moczo and Kristek (2005).

In the next subsections we describe the numerical method in 3D. For the purpose of the numerical simulations for the SIGMA project we developed new codes for 2D and 1D simulations – they are directly derived from the code for the 3D simulations. This effort should pay off by the overall efficiency of the methodologically and algorithmically consistent 3D, 2D and 1D numerical simulations.


### 3.2.2. Computational domain and grid

The computational domain is a rectangular parallelepiped. Its horizontal top side represents a planar free surface. The four vertical sides and the bottom side optionally represent transparent boundaries or boundaries with prescribed boundary conditions for the particle velocity (e.g., symmetry or antisymmetry plane, rigid surface).

The computational domain is covered either by a uniform Cartesian grid or by a discontinuous grid. The discontinuous grid may be advantageously applied if the minimum wave speed in an upper part of the computational model is smaller than that in a lower part of the model. The discontinuous grid consists of a finer grid (with the grid spacing  $h$ ), covering the upper part of the model, and a coarser grid (with the grid spacing  $H > h$ ) covering the lower part of the model. A total number of grid points in such a discontinuous spatial grid can be significantly smaller than that in a uniform grid. Consequently, the computer memory and time requirements can be significantly reduced compared to those in case of the uniform grid.

Due to the structure of the staggered grid, the ratio of the spatial grid spacings in the coarser and finer grids has to be an odd number. In other words, depending on the model of medium, it is possible to choose a 1:1 (uniform) grid, or 1:3, 1:5, ... discontinuous grid. The key feature of the algorithm is the application of the Lanczos downsampling filter. The algorithm allows for large numbers of time levels without inaccuracy and instability due to numerical noise that is generated at the contact of the two grids with different spatial-grid spacings. For more details see Kristek et al. (2010) and Moczo et al. (2014).



	Research and Development Programme on Seismic Ground Motion  CONFIDENTIAL <i>Restricted to SIGMA scientific partners and members of the consortium,          please do not pass around</i>	Ref : SIGMA-2013-D3-97 Version : 01  Date : 21/10/2013 Page : 9
--	--	---

### 3.2.3. Model of medium and governing equations

The realistic model of attenuation is one of the key aspects of numerical modelling of seismic wave propagation and seismic motion especially in the surface sedimentary structures.

Real medium is approximated by a linear viscoelastic medium. Viscoelasticity is described by rheology of the generalized Maxwell body (GMB-EK) in definition by Emmerich and Korn (1987). GMB-EK is equivalent to the generalized Zener body (GZB). Specifically, it is assumed that one GMB-EK/GZB describes a viscoelastic bulk modulus and the other GMB-EK/GZB describes a viscoelastic shear modulus. The reason for using GMB-EK/GZB is the possibility to approximate an arbitrary  $Q(\omega)$ -law with an optional accuracy.

The equation of motion is

$$\rho \dot{v}_i = \sigma_{ij,j} + f_i, \quad (1.1)$$


the stress-strain relation is

$$\begin{aligned} \frac{\partial}{\partial t} \sigma_{ij} = & \kappa \frac{\partial}{\partial t} \varepsilon_{kk} \delta_{ij} + 2\mu \left( \frac{\partial}{\partial t} \varepsilon_{ij} - \frac{1}{3} \frac{\partial}{\partial t} \varepsilon_{kk} \delta_{ij} \right) \\ & - \sum_{l=1}^n \left[ Y_l^\kappa \kappa \xi_l^{kk} \delta_{ij} + 2Y_l^\mu \mu \left( \xi_l^{ij} - \frac{1}{3} \xi_l^{kk} \delta_{ij} \right) \right] \end{aligned} \quad (1.2)$$

$$\frac{\partial}{\partial t} \xi_l^{ij}(t) + \omega_l \xi_l^{ij}(t) = \omega_l \frac{\partial}{\partial t} \varepsilon_{ij}(t) \quad , \quad l=1, \dots, n. \quad (1.3)$$

Here, in a Cartesian coordinate system  $(x_1, x_2, x_3)$ ,  $\rho(x_i)$ ;  $i \in \{1, 2, 3\}$ , is density,  $\kappa(x_i)$  and  $\mu(x_i)$  unrelaxed (elastic) bulk and shear modules,  $Y_l^\kappa$  and  $Y_l^\mu$  anelastic coefficients,  $\vec{v}(x_i, t)$  particle-velocity vector,  $t$  time,  $\vec{f}(x_i, t)$  body force per unit volume,  $\sigma_{ij}(x_k, t)$  and  $\varepsilon_{ij}(x_k, t)$ ;  $i, j, k \in \{1, 2, 3\}$  stress and strain tensors,  $\xi_l^{ij}$  material-independent anelastic functions (memory variables), and  $\omega_l$  relaxation angular frequencies. Summation convention does not apply to index  $l$ .

Consider for simplicity a viscoelastic modulus  $M(\omega)$ . The attenuation corresponding to  $M(\omega)$  is quantified by

	<p>Research and Development Programme on Seismic Ground Motion</p> <p>CONFIDENTIAL <i>Restricted to SIGMA scientific partners and members of the consortium, please do not pass around</i></p>	<p>Ref : SIGMA-2013-D3-97 Version : 01</p> <p>Date : 21/10/2013 Page : 10</p>
--	--	---

$$\frac{1}{Q(\omega)} = \frac{M_{\text{imag}}(\omega)}{M_{\text{real}}(\omega)} = \frac{\sum_{l=1}^n Y_l \frac{\omega_l \omega}{\omega_l^2 + \omega^2}}{1 - \sum_{l=1}^n Y_l \frac{\omega_l^2}{\omega_l^2 + \omega^2}} \quad (1.4)$$


The equation can be rewritten as

$$Q^{-1}(\omega) = \sum_{l=1}^n \frac{\omega_l \omega + \omega_l^2 Q^{-1}(\omega)}{\omega_l^2 + \omega^2} Y_l \quad (1.5)$$

Assume that values of  $Q(\omega)$  in a frequency range of interest are known – they are measured or estimated. We can choose the number and values of frequencies  $\omega_l$  in order to reasonably cover the frequency range of interest. (Frequencies  $\omega_l$  are the same for the whole computational domain.) Considering, e.g.,  $Q$  values at frequencies  $\tilde{\omega}_k$ , a system of equations (1.5), one equation for each  $Q(\tilde{\omega}_k)$ , is obtained. The system can be solved for the anelastic coefficients  $Y_l$  using the least square method. The application of the least square method leads to system of  $n$  equations for  $n$  unknown anelastic coefficients.

Emmerich and Korn (1987) demonstrated that a sufficiently accurate approximation to nearly constant  $Q(\omega)$  is obtained if frequencies  $\omega_l$  cover the frequency range of interest logarithmically equidistantly. One possibility is to consider  $Q$  values at  $2n-1$  frequencies  $\tilde{\omega}_k$ , and  $\omega_1 = \tilde{\omega}_1$ ,  $\omega_2 = \tilde{\omega}_3$ , ...,  $\omega_n = \tilde{\omega}_{2n-1}$ . Emmerich and Korn (1987) showed that  $n=3$  is sufficient for the frequency range  $[\omega_{\min}, 100\omega_{\min}]$ . A simple possible choice is  $\tilde{\omega}_1 = \omega_{\min}$ . A more detailed discussion of the frequency range and its sampling by frequencies  $\tilde{\omega}_k$  can be found in the article by Graves and Day (2003; Eqs. 13 and 14). For an efficient and accurate determination of the parameters of the GMB-EK see Liu and Archuleta (2006).

If a phase velocity at certain reference frequency  $\omega_{ref}$ , that is  $c(\omega_{ref})$ , is known from measurements, the unrelaxed modulus  $M_U$  can be determined from the value of  $c(\omega_{ref})$  and viscoelastic modulus. The phase velocity is

	<p>Research and Development Programme on Seismic Ground Motion</p> <p>CONFIDENTIAL Restricted to SIGMA scientific partners and members of the consortium, please do not pass around</p>	<p>Ref : SIGMA-2013-D3-97 Version : 01</p> <p>Date : 21/10/2013 Page : 11</p>
--	---	---

$$\frac{1}{c(\omega)} = \text{Re} \left\{ \left( \frac{M(\omega)}{\rho} \right)^{-1/2} \right\} \quad (1.6)$$

The unrelaxed modulus is then (Moczo et al. 1997)

$$M_U = \rho c^2(\omega_{ref}) \frac{R + \Theta_1}{2R^2} \quad (1.7)$$

where

$$R = (\Theta_1^2 + \Theta_2^2)^{1/2}, \quad (1.8)$$

$$\Theta_1 = 1 - \sum_{l=1}^n Y_l \frac{\omega_l^2}{\omega_l^2 + \omega_{ref}^2}, \quad \Theta_2 = \sum_{l=1}^n Y_l \frac{\omega_l \omega_{ref}}{\omega_l^2 + \omega_{ref}^2}$$

Thus, if we know  $Q(\omega)$  and  $c(\omega_{ref})$  from measurements, and if we assume viscoelastic rheology of GMB-EK, we can determine parameters of the viscoelastic stress-strain relation using Eqs. (1.5) and (1.7) for a chosen set of frequencies  $\omega_l$  reasonably covering the frequency range of interest.

Return now to the 3D problem with two viscoelastic modules and two wave speeds. Assume that the quality factors for P and S waves, that is  $Q_\alpha(\omega)$  and  $Q_\beta(\omega)$ , are known (measured or estimated). Here  $\alpha$  and  $\beta$  are the P-wave and S-wave speeds, respectively:

$$\alpha = \left[ \left( \kappa + \frac{4}{3} \mu \right) / \rho \right]^{1/2}, \quad \beta = [\mu / \rho]^{1/2} \quad (1.9)$$


The anelastic functions corresponding to  $Q_\alpha(\omega)$  and  $Q_\beta(\omega)$  are  $Y_l^\alpha$  and  $Y_l^\beta$ . They are obtained by solving system of equations

$$Q_\gamma^{-1}(\tilde{\omega}_k) = \sum_{l=1}^n \frac{\omega_l \tilde{\omega}_k + \omega_l^2 Q_\gamma^{-1}(\tilde{\omega}_k)}{\omega_l^2 + \tilde{\omega}_k^2} Y_l^\gamma; \quad k=1, \dots, 2n-1; \quad \gamma \in \{\alpha, \beta\} \quad (1.10)$$

using the least square method. The anelastic coefficients  $Y_l^\kappa$  and  $Y_l^\mu$  are obtained from

$$Y_l^\kappa = \left( \alpha^2 Y_l^\alpha - \frac{4}{3} \beta^2 Y_l^\beta \right) / \left( \alpha^2 - \frac{4}{3} \beta^2 \right), \quad Y_l^\mu = Y_l^\beta, \quad l=1, \dots, n. \quad (1.11)$$

In case of using modules  $\lambda$  and  $\mu$  instead of  $\kappa$  and  $\mu$  we have

	<p>Research and Development Programme on Seismic Ground Motion</p> <p>CONFIDENTIAL <i>Restricted to SIGMA scientific partners and members of the consortium, please do not pass around</i></p>	<p>Ref : SIGMA-2013-D3-97 Version : 01</p> <hr/> <p>Date : 21/10/2013 Page : 12</p>
--	--	---

$$\frac{\partial}{\partial t} \sigma_{ij} = \lambda \frac{\partial}{\partial t} \varepsilon_{kk} \delta_{ij} + 2\mu \frac{\partial}{\partial t} \varepsilon_{ij} - \sum_{l=1}^n \left[ Y_l^\lambda \lambda \xi_l^{kk} \delta_{ij} + 2Y_l^\mu \mu \xi_l^{ij} \right] \quad (1.12)$$

instead of Eq. (1.2). The anelastic coefficients  $Y_l^\lambda$  are obtained from

$$Y_l^\lambda = \left( \alpha^2 Y_l^\alpha - 2\beta^2 Y_l^\beta \right) / \left( \alpha^2 - 2\beta^2 \right) , \quad l=1, \dots, n. \quad (1.13)$$

### 3.2.4. Discrete representation of the medium

Sufficiently accurate and computationally efficient incorporation of the smooth and discontinuous heterogeneities of the medium is a key aspect of the numerical modelling of seismic motion especially in surface sedimentary structures. Therefore we describe the representation of the medium in the grid with adequate attention.

Models of the Earth's interior and surface geological structures have to include layers/blocks of different materials. Their contact, material interface, is a material discontinuity at which material parameters change discontinuously. At a welded material interface, the boundary conditions are continuity of the displacement (or particle-velocity) and traction vector.

One possible approach is to apply a) a FD scheme for the smoothly heterogeneous medium at grid points outside the discontinuity, b) FD schemes obtained by a proper incorporation of the boundary conditions at grid points at or near the interface. Such approach had been called homogeneous. A homogeneous FD scheme is specific for a particular problem. Whereas feasible for simple interface geometry, its application to curved material discontinuities is difficult and therefore is considered impractical. In any case, the approach requires stable and sufficiently accurate FD approximation of the boundary conditions which is not a trivial problem.

In the alternative heterogeneous approach only one FD scheme is used for all interior grid points (points not lying on boundaries of a grid) no matter what their positions are with respect to the material interface. The presence of the interface is accounted for only by values of effective material parameters assigned to grid positions. Therefore, the heterogeneous approach is the most dominant approach to incorporate continuous and discontinuous heterogeneity of medium.

Clearly, a heterogeneous FD scheme should approximate solution of the equation of motion and stress-strain relation valid both for the smoothly heterogeneous medium and interface. For more details see Moczo et al. (2002, 2007a,b, 2014).

Hooke's law for a smooth isotropic medium. Defining the stress vector, strain vector and elasticity matrix

$$\vec{\sigma} \equiv [\sigma_{xx}, \sigma_{yy}, \sigma_{zz}, \sigma_{xy}, \sigma_{yz}, \sigma_{zx}]^T, \quad \vec{\varepsilon} \equiv [\varepsilon_{xx}, \varepsilon_{yy}, \varepsilon_{zz}, \varepsilon_{xy}, \varepsilon_{yz}, \varepsilon_{zx}]^T \quad (1.14)$$

$$\mathbf{E} \equiv \begin{bmatrix} \lambda + 2\mu & \lambda & \lambda & 0 & 0 & 0 \\ \lambda & \lambda + 2\mu & \lambda & 0 & 0 & 0 \\ \lambda & \lambda & \lambda + 2\mu & 0 & 0 & 0 \\ 0 & 0 & 0 & 2\mu & 0 & 0 \\ 0 & 0 & 0 & 0 & 2\mu & 0 \\ 0 & 0 & 0 & 0 & 0 & 2\mu \end{bmatrix} \quad (1.15)$$

the stress-strain relation may be written in the matrix form

$$\vec{\sigma} = \mathbf{E} \vec{\varepsilon} \quad (1.16)$$

**Boundary conditions at the welded material interface.** Consider surface  $S$  with normal vector  $\vec{v}$  defining the geometry of the material interface at which elastic modules  $\lambda$  and  $\mu$  have a discontinuity of the zero order. The welded-interface boundary conditions are continuity of displacement and traction vectors across the surface at each point  $\vec{\eta}$  of surface  $S$ :


$$\vec{u}^+(\vec{\eta}) = \vec{u}^-(\vec{\eta}), \quad \vec{T}^+(\vec{\eta}; \vec{v}) = \vec{T}^-(\vec{\eta}; \vec{v}) \quad (1.17)$$

**Planar Interface Parallel to a Coordinate Plane.** Assume a planar interface parallel to the  $xy$ -coordinate plane. The normal vector in this case is  $\vec{v} = (0, 0, 1)$ . Then the stress-strain relation for a point at the interface may be written as

$$\vec{\sigma}^A = \tilde{\mathbf{E}} \vec{\varepsilon}^A \quad (1.18)$$

where

$$\tilde{\mathbf{E}} = \begin{bmatrix} \bar{\mathbf{R}} & \bar{\mathbf{P}} \\ \bar{\mathbf{P}}^T & \bar{\mathbf{S}} \end{bmatrix} = \begin{bmatrix} 2\mu^H & 0 & 0 & 0 & 0 & 0 \\ 0 & 2\mu^H & 0 & 0 & 0 & 0 \\ 0 & 0 & (\lambda + 2\mu)^H & \Psi & \Psi & 0 \\ 0 & 0 & \Psi & \Lambda + 2\mu^A & \Lambda & 0 \\ 0 & 0 & \Psi & \Lambda & \Lambda + 2\mu^A & 0 \\ 0 & 0 & 0 & 0 & 0 & 2\mu^A \end{bmatrix} \quad (1.19)$$

	<p style="text-align: center;">Research and Development Programme on Seismic Ground Motion</p> <p style="text-align: center;">CONFIDENTIAL <i>Restricted to SIGMA scientific partners and members of the consortium, please do not pass around</i></p>	<p>Ref : SIGMA-2013-D3-97 Version : 01</p> <hr/> <p>Date : 21/10/2013 Page : 14</p>
--	--	---

$$\Psi = \left( \frac{\lambda}{\lambda + 2\mu} \right)^A (\lambda + 2\mu)^H$$

$$\Lambda = \left[ \left( \frac{\lambda}{\lambda + 2\mu} \right)^A \right]^2 (\lambda + 2\mu)^H + 2 \left( \frac{\lambda}{\lambda + 2\mu} \mu \right)^A \quad (1.20)$$

Here superscripts  $A$  and  $H$  indicate the arithmetic and harmonic averages, respectively. Equation (1.18) is the stress-strain relation for a point at the interface. It has the same form as Hooke's law (1.16) and, importantly, is consistent with the boundary conditions at the welded material interface.

An important difference between matrices  $\tilde{\mathbf{E}}$  and  $\bar{\mathbf{E}}$  (that is, the difference between any of the two original smooth media and the averaged medium at the interface) is that matrix  $\tilde{\mathbf{E}}$  for any of the two isotropic media in contact has only 2 independent nonzero elements whereas matrix  $\bar{\mathbf{E}}$  has 5 independent nonzero elements. The averaged medium is transversely isotropic with the axis of symmetry perpendicular to the interface. This means that the exact heterogeneous formulation for a planar welded material interface parallel with a coordinate plane increases the number of the elastic coefficients necessary to describe the medium from 2 to 5.


***A planar interface in a general orientation.*** The normal vector to the interface,  $\vec{\nu} = (\nu_x, \nu_y, \nu_z)$ , has all components nonzero. In this case we obtain a symmetric elasticity matrix which may have all elements nonzero although only 5 of them independent. All nonzero elements of the averaged elasticity matrix mean real complication: a) all strain-tensor components are necessary to calculate each stress-tensor component at a point of the interface, b) 21 nonzero elastic coefficients are necessary at the point.

If the geometry of the interface is defined by a nonplanar smooth surface  $S$ , the surface may be locally approximated by a planar surface tangential to surface  $S$  at a given point.

Algorithmically we have two possibilities: 1) Calculate 21 nonzero elastic coefficients for each grid point and store them in memory during the entire FD time-integration. 2) to store only 2+2 elastic coefficients (2 per medium in contact) and 2 angles (specifying orientation of an approximating tangential planar interface) for each grid point and calculate the elasticity matrix at each time step at each grid point.

The situation is even more complicated for the staggered grid in which not all strain-tensor components are defined at each grid position of the stress-tensor components.



	<p>Research and Development Programme on Seismic Ground Motion</p> <p>CONFIDENTIAL Restricted to SIGMA scientific partners and members of the consortium, please do not pass around</p>	<p>Ref : SIGMA-2013-D3-97 Version : 01</p> <p>Date : 21/10/2013 Page : 15</p>
--	---	---

**Consideration on averaging.** Matrix  $\bar{\mathbf{E}}$  rearranged into the structure corresponding to the stress and strain vectors in Eqs. (1.14) is

$$\bar{\mathbf{E}} = \begin{bmatrix} \Lambda + 2\mu^A & \Lambda & \Psi & 0 & 0 & 0 \\ \Lambda & \Lambda + 2\mu^A & \Psi & 0 & 0 & 0 \\ \Psi & \Psi & (\lambda + 2\mu)^H & 0 & 0 & 0 \\ 0 & 0 & 0 & 2\mu^A & 0 & 0 \\ 0 & 0 & 0 & 0 & 2\mu^H & 0 \\ 0 & 0 & 0 & 0 & 0 & 2\mu^H \end{bmatrix} \quad (1.21)$$

The matrix is symmetric with 9 elements. For the planar interface perpendicular to the  $z$ -axis only 5 of the 9 elements are independent. In case of a planar interface perpendicular to other coordinate axis the positions of the 9 elements will not change because these positions are given by the structure of the stress and strain vectors. The positions of the 5 independent elements will be, however, different – due to the orientation of the interface. This means that for any of 3 canonical orientations of an interface we need at each point 5 independent coefficients plus 1 index of orientation in order to construct matrix  $\bar{\mathbf{E}}$ .

The above consideration and the fact that the general orientation requires 21 nonzero coefficients (too many and inconsistent with the staggered distribution of the field variables) may lead to a compromise with 9 independent coefficients. 9 independent coefficients are consistent with the above consideration on the interface orientation and with the structure of the staggered grid. Moreover, and very importantly for the computational efficiency, a stress-tensor component is determined by the same strain-tensor components as in the isotropic medium.

Medium described by 9 independent elastic coefficients is medium with the orthorhombic anisotropy. It has 3 axes of symmetry that are identical with the coordinate axes.

**Effective elastic coefficients for the orthorhombic medium.** Being decided for the orthorhombic medium, the problem may be formulated in this way: find such averaging of the elastic coefficients which reduces to the transversal anisotropy for any of the three canonical orientations of the material interface. The sought elasticity matrix has the form



$$\mathbf{E}^{\text{ort}} \equiv \begin{pmatrix} \Pi_x & \lambda_{xy} & \lambda_{zx} & 0 & 0 & 0 \\ \lambda_{xy} & \Pi_y & \lambda_{yz} & 0 & 0 & 0 \\ \lambda_{zx} & \lambda_{yz} & \Pi_z & 0 & 0 & 0 \\ 0 & 0 & 0 & \mu_{xy} & 0 & 0 \\ 0 & 0 & 0 & 0 & \mu_{yz} & 0 \\ 0 & 0 & 0 & 0 & 0 & \mu_{zx} \end{pmatrix} \quad (1.22)$$

and, consequently, the stress-strain relation may be written in the form

$$\begin{aligned} \sigma_{xx} &= \Pi_x \varepsilon_{xx} + \lambda_{xy} \varepsilon_{yy} + \lambda_{zx} \varepsilon_{zz} \\ \sigma_{yy} &= \lambda_{xy} \varepsilon_{xx} + \Pi_y \varepsilon_{yy} + \lambda_{yz} \varepsilon_{zz} \\ \sigma_{zz} &= \lambda_{zx} \varepsilon_{xx} + \lambda_{yz} \varepsilon_{yy} + \Pi_z \varepsilon_{zz} \\ \sigma_{xy} &= \mu_{xy} \varepsilon_{xy}, \quad \sigma_{yz} = \mu_{yz} \varepsilon_{yz}, \quad \sigma_{zx} = \mu_{zx} \varepsilon_{zx} \end{aligned} \quad (1.23)$$

with

$$\Pi_x = \left( \int_x [\mathbf{P}_{yz}(\lambda, \mu)]^{-1} dl \right)^{-1}, \quad \Pi_y = \left( \int_y [\mathbf{P}_{xz}(\lambda, \mu)]^{-1} dl \right)^{-1} \quad (1.24)$$

$$\Pi_z = \left( \int_z [\mathbf{P}_{xy}(\lambda, \mu)]^{-1} dl \right)^{-1}$$

$$\mu_{zx} = \left( \iint_{zx} \left[ \int_y \mu dl \right]^{-1} dS \right)^{-1}, \quad \mu_{yz} = \left( \iint_{yz} \left[ \int_x \mu dl \right]^{-1} dS \right)^{-1} \quad (1.25)$$


$$\mu_{xy} = \left( \iint_{xy} \left[ \int_z \mu dl \right]^{-1} dS \right)^{-1}$$

$$\begin{aligned} \lambda_{xz} &= \Psi_{xz}(\Lambda_y(\lambda, \mu), \mathbf{P}_y(\lambda, \mu)) \\ \lambda_{yz} &= \Psi_{yz}(\Lambda_x(\lambda, \mu), \mathbf{P}_x(\lambda, \mu)) \\ \lambda_{xy} &= \Psi_{xy}(\Lambda_z(\lambda, \mu), \mathbf{P}_z(\lambda, \mu)) \end{aligned} \quad (1.26)$$

where

$$\begin{aligned} \mathbf{P}_{\xi\xi}(\lambda, \mu) &= \left[ \iint_{\xi\xi} \frac{\lambda}{\lambda+2\mu} dS \right]^2 \left( \iint_{\xi\xi} \frac{1}{\lambda+2\mu} dS \right)^{-1} + \iint_{\xi\xi} \left( \lambda+2\mu - \frac{\lambda^2}{\lambda+2\mu} \right) dS \\ \Lambda_{\xi\xi}(\lambda, \mu) &= \mathbf{P}_{\xi\xi}(\lambda, \mu) - 2 \iint_{\xi\xi} \mu dS \end{aligned} \quad (1.27)$$

$$\Psi_{\xi\xi}(a, b) = \iint_{\xi\xi} \frac{a}{b} dS \left( \iint_{\xi\xi} \frac{1}{b} dS \right)^{-1}$$

	<p>Research and Development Programme on Seismic Ground Motion</p> <p>CONFIDENTIAL Restricted to SIGMA scientific partners and members of the consortium, please do not pass around</p>	<p>Ref : SIGMA-2013-D3-97 Version : 01</p> <p>Date : 21/10/2013 Page : 17</p>
--	---	---

The auxiliary parameters  $a$  and  $b$  stand for an appropriate  $P_{\xi}(\lambda, \mu)$  and  $\Lambda_{\xi}(\lambda, \mu)$ , respectively.

The two latter parameters are evaluated as

$$\begin{aligned}
 P_{\xi}(\lambda, \mu) &= \left[ \int_{\xi} \frac{\lambda}{\lambda + 2\mu} dl \right]^2 \left( \int_{\xi} \frac{1}{\lambda + 2\mu} dl \right)^{-1} + \int_{\xi} \left( \lambda + 2\mu - \frac{\lambda^2}{\lambda + 2\mu} \right) dl \\
 \Lambda_{\xi}(\lambda, \mu) &= P_{\xi}(\lambda, \mu) - 2 \int_{\xi} \mu dl
 \end{aligned} \tag{1.28}$$


The double subscript  $\xi, \zeta$  indicates averaging over the  $\xi, \zeta$ -plane. The single subscript  $\xi$  indicates averaging along the  $\xi$ -axis. An integral is evaluated for a grid cell. Prior to the integration the volume of a grid cell is split into homogeneous isotropic subcells of a uniform size. The effective elastic coefficients are determined at the grid positions of the stress-tensor components – according to the structures of vectors  $\bar{\sigma}$  and  $\bar{\varepsilon}$  given by Eqs. (1.14) and matrix  $\mathbf{E}^{\text{ort}}$  given by Eq. (1.22). All  $\Pi_x, \Pi_y, \Pi_z$  and  $\lambda_{xy}, \lambda_{yz}, \lambda_{zx}$  are determined at the grid position shared by the normal stress-tensor components. Coefficients  $\mu_{xy}, \mu_{yz}$  and  $\mu_{zx}$  are determined at the grid positions of  $\sigma_{xy}, \sigma_{yz}$  and  $\sigma_{zx}$ , respectively.

In 3D, at each grid position of the particle-velocity component an effective grid density is determined as a volume arithmetic average of density within a volume of the grid cell centred at the grid position. The averaging applies to both smoothly and discontinuously heterogeneous media. The averages are evaluated by numerical integration. Consider, e.g., the grid position of the  $v_x$  at the grid point  $I, K + 1/2, L + 1/2$ . Then the effective density is evaluated as

$$\rho_{I, K+1/2, L+1/2}^A = \frac{1}{h^3} \int_{x_{I-1/2}}^{x_{I+1/2}} \int_{y_K}^{y_{K+1}} \int_{z_L}^{z_{L+1}} \rho \, dx \, dy \, dz \tag{1.29}$$

with superscript  $A$  indicating the arithmetic averaging and  $h$  standing for the grid spacing.

**Material Interface in the Viscoelastic Medium.** Assume one set of relaxation frequencies  $\omega_l$ ;  $l=1, 2, \dots, n$  for both media in contact. Each medium is described by a real density  $\rho$ , elastic (unrelaxed) modules (e.g.,  $\kappa$  and  $\mu$ ), and corresponding viscoelastic (complex frequency-dependent) modules. We need to determine average (effective) density, elastic modules, and

	<p>Research and Development Programme on Seismic Ground Motion</p> <p>CONFIDENTIAL <i>Restricted to SIGMA scientific partners and members of the consortium, please do not pass around</i></p>	<p>Ref : SIGMA-2013-D3-97 Version : 01</p> <hr/> <p>Date : 21/10/2013 Page : 18</p>
--	--	---

anelastic coefficients  $Y_l^{\bar{M}}$ ;  $l=1, \dots, n$  ( $\bar{M}$  indicating any of the determined averaged modules) for an averaged medium that would represent the contact of two viscoelastic media.

The average density is evaluated in the same way as in case of the elastic media. Averaged viscoelastic modules can be determined by numerical integration according to relations (1.24) – (1.28) in which complex viscoelastic modules in the frequency domain are used instead of the real elastic modules. From the averaged viscoelastic modules, the quality factors corresponding to these modules can be determined at frequencies  $\tilde{\omega}_k$ ;  $k=1, \dots, 2n-1$ , using

$$Q_{\bar{M}}(\tilde{\omega}_k) = \frac{\bar{M}_{\text{real}}}{\bar{M}_{\text{imag}}}; \quad k=1, 2, \dots, 2n-1. \quad (1.30)$$

Having values  $Q_{\bar{M}}(\tilde{\omega}_k)$ ;  $k=1, 2, \dots, 2n-1$ , for each averaged modulus  $\bar{M}$  we can apply the least-square method to system of equations (compare with (1.10))


$$Q_{\bar{M}}^{-1}(\tilde{\omega}_k) = \sum_{l=1}^n \frac{\omega_l \tilde{\omega}_k + \omega_l^2 Q_{\bar{M}}^{-1}(\tilde{\omega}_k)}{\omega_l^2 + \tilde{\omega}_k^2} Y_l^{\bar{M}}; \quad k=1, 2, \dots, 2n-1. \quad (1.31)$$

What remains to be determined are the unrelaxed (elastic) averaged modules. The unrelaxed modulus of any viscoelastic modulus is

$$\bar{M}_U = \lim_{\omega \rightarrow \infty} \bar{M}(\omega) \quad (1.32)$$

Consequently, the averaging of the viscoelastic modulus gives in the limit the averaging of the unrelaxed modulus. This means that the unrelaxed (elastic) modulus  $\bar{M}_U$  for the averaged viscoelastic medium can be obtained in the same way as in the perfectly elastic medium, e.g., using relations (1.24)–(1.28).

If we do not know directly viscoelastic modules  $\kappa(\omega)$  and  $\mu(\omega)$  (or  $\lambda(\omega)$  and  $\mu(\omega)$ ) for each of the two media in contact but, instead, we know measured or estimated  $Q_\alpha(\omega)$  for P wave and  $Q_\beta(\omega)$  for S wave, we have to proceed as follows. We will assume the GMB-EK/GZB rheology of each medium as well as of the averaged medium. For each of the two media we first determine  $Y_l^\alpha$

	<p>Research and Development Programme on Seismic Ground Motion</p> <p>CONFIDENTIAL <i>Restricted to SIGMA scientific partners and members of the consortium, please do not pass around</i></p>	<p>Ref : SIGMA-2013-D3-97 Version : 01</p> <p>Date : 21/10/2013 Page : 19</p>
--	--	---

and  $Y_l^\beta$  using Eqs. (1.10) and then  $Y_l^k$  and  $Y_l^\mu$  or  $Y_l^\lambda$  and  $Y_l^\mu$  using Eqs. (1.11) or (1.13). Then, assuming known unrelaxed modules for each medium, we can determine viscoelastic modules using

$$M(\omega) = M_U \left[ 1 - \sum_{l=1}^n Y_l \frac{\omega_l}{\omega_l + i\omega} \right] \quad (1.33)$$

for each modulus. Then we can proceed with the numerical averaging of the modules in the frequency domain, determination of the corresponding quality factors, and determination of the anelastic coefficients as described before.

### 3.2.5. FD scheme for interior grid points

Here we show the scheme for updating the  $x$ -component of the particle velocity,  $xx$ -component of the stress tensor, and the  $xx$  anelastic function, that is, for  $v_x$ ,  $\sigma_{xx}$ , and  $\xi_l^{xx}$ . Schemes for the other components are easily obtained. Denote the discrete grid values of the particle velocity components  $v_x, v_y, v_z$  by  $VX, VY, VZ$ , respectively. Similarly denote the stress-tensor components  $\sigma_{xx}, \sigma_{xy}, \sigma_{zx}$  by  $TXX, TXY, TZX$ .  $\Delta$ ,  $h$ ,  $f$  and  $\bar{\rho}$  denote time step, grid spacing, body-force term (body force per unit volume) and volume arithmetic average of density.  $m$  denotes a time level,  $I$ ,  $K$  and  $L$  denote spatial grid indices in the  $x$ ,  $y$  and  $z$  coordinate directions. Note that, for simplicity, the overbar  $\bar{\cdot}$  is not used for indicating that the modules are the averaged modules. The schemes for  $v_x$  and  $\sigma_{xx}$  are then

$$\begin{aligned}
VX_{I, K+1/2, L+1/2}^{m+1/2} &= VX_{I, K+1/2, L+1/2}^{m-1/2} + \frac{\Delta}{\bar{\rho}_{I, K+1/2, L+1/2}} f_{I, K+1/2, L+1/2}^m \\
&+ \frac{1}{\bar{\rho}_{I, K+1/2, L+1/2}} \frac{\Delta}{h} \left[ \frac{9}{8} \left( TXX_{I+1/2, K+1/2, L+1/2}^m - TXX_{I-1/2, K+1/2, L+1/2}^m \right) \right. \\
&\quad - \frac{1}{24} \left( TXX_{I+3/2, K+1/2, L+1/2}^m - TXX_{I-3/2, K+1/2, L+1/2}^m \right) \\
&\quad + \frac{9}{8} \left( TXY_{I, K+1, L+1/2}^m - TXY_{I, K, L+1/2}^m \right) \\
&\quad - \frac{1}{24} \left( TXY_{I, K+2, L+1/2}^m - TXY_{I, K-1, L+1/2}^m \right) \\
&\quad + \frac{9}{8} \left( TZX_{I, K+1/2, L+1}^m - TZX_{I, K+1/2, L}^m \right) \\
&\quad \left. - \frac{1}{24} \left( TZX_{I, K+1/2, L+2}^m - TZX_{I, K+1/2, L-1}^m \right) \right] \quad (1.34)
\end{aligned}$$


$$\begin{aligned}
& TXX_{I+1/2, K+1/2, L+1/2}^m = TXX_{I+1/2, K+1/2, L+1/2}^{m-1} \\
& + \frac{\Delta}{h} \left\{ \tilde{M}XX_{I+1/2, K+1/2, L+1/2} \left[ \frac{9}{8} \left( VX_{I+1, K+1/2, L+1/2}^{m-1/2} - VX_{I, K+1/2, L+1/2}^{m-1/2} \right) \right. \right. \\
& \quad \left. \left. - \frac{1}{24} \left( VX_{I+2, K+1/2, L+1/2}^{m-1/2} - VX_{I-1, K+1/2, L+1/2}^{m-1/2} \right) \right] \right. \\
& \quad + \tilde{M}XY_{I+1/2, K+1/2, L+1/2} \left[ \frac{9}{8} \left( VY_{I+1/2, K+1, L+1/2}^{m-1/2} - VY_{I+1/2, K, L+1/2}^{m-1/2} \right) \right. \\
& \quad \left. \left. - \frac{1}{24} \left( VY_{I+1/2, K+2, L+1/2}^{m-1/2} - VY_{I+1/2, K-1, L+1/2}^{m-1/2} \right) \right] \right. \\
& \quad \left. + \tilde{M}ZX_{I+1/2, K+1/2, L+1/2} \left[ \frac{9}{8} \left( VZ_{I+1/2, K+1/2, L+1}^{m-1/2} - VZ_{I+1/2, K+1/2, L}^{m-1/2} \right) \right. \right. \\
& \quad \left. \left. - \frac{1}{24} \left( VZ_{I+1/2, K+1/2, L+2}^{m-1/2} - VZ_{I+1/2, K+1/2, L-1}^{m-1/2} \right) \right] \right\} \\
& - \Delta \sum_{l=1}^n \left( \tilde{Y}_{l; I+1/2, K+1/2, L+1/2}^{MXX} \xi_{l; I+1/2, K+1/2, L+1/2}^{xx; m} \right. \\
& \quad + \tilde{Y}_{l; I+1/2, K+1/2, L+1/2}^{MXY} \xi_{l; I+1/2, K+1/2, L+1/2}^{yy; m} \\
& \quad \left. + \tilde{Y}_{l; I+1/2, K+1/2, L+1/2}^{MZX} \xi_{l; I+1/2, K+1/2, L+1/2}^{zz; m} \right) \quad (1.35)
\end{aligned}$$

$$\begin{aligned}
\xi_{l; I+1/2, K+1/2, L+1/2}^{xx; m} &= \frac{2 - \omega_l \Delta}{2 + \omega_l \Delta} \xi_{l; I+1/2, K+1/2, L+1/2}^{xx; m-1} \\
& + \frac{2\omega_l \Delta}{2 + \omega_l \Delta} \frac{1}{h} \left[ \frac{9}{8} \left( VX_{I+1, K+1/2, L+1/2}^{m-1/2} - VX_{I, K+1/2, L+1/2}^{m-1/2} \right) \right. \\
& \quad \left. - \frac{1}{24} \left( VX_{I+2, K+1/2, L+1/2}^{m-1/2} - VX_{I-1, K+1/2, L+1/2}^{m-1/2} \right) \right] \quad (1.36)
\end{aligned}$$

$$\begin{aligned}
\tilde{M}XX_{I+1/2, K+1/2, L+1/2} &= \tilde{\Pi}_{x; I+1/2, K+1/2, L+1/2} \\
\tilde{M}XY_{I+1/2, K+1/2, L+1/2} &= \tilde{\lambda}_{xy; I+1/2, K+1/2, L+1/2} \\
\tilde{M}ZX_{I+1/2, K+1/2, L+1/2} &= \tilde{\lambda}_{zx; I+1/2, K+1/2, L+1/2}
\end{aligned} \quad (1.37)$$

$$\begin{aligned}
\tilde{Y}_{l; I+1/2, K+1/2, L+1/2}^{MXX} &= \tilde{Y}_{l; I+1/2, K+1/2, L+1/2}^{\Pi_x} \\
\tilde{Y}_{l; I+1/2, K+1/2, L+1/2}^{MXY} &= \tilde{Y}_{l; I+1/2, K+1/2, L+1/2}^{\lambda_{xy}} \\
\tilde{Y}_{l; I+1/2, K+1/2, L+1/2}^{MZX} &= \tilde{Y}_{l; I+1/2, K+1/2, L+1/2}^{\lambda_{zx}}
\end{aligned} \quad (1.38)$$

where

	<p style="text-align: center;">Research and Development Programme on Seismic Ground Motion</p> <p style="text-align: center;">CONFIDENTIAL <i>Restricted to SIGMA scientific partners and members of the consortium, please do not pass around</i></p>	<p>Ref : SIGMA-2013-D3-97 Version : 01</p> <hr/> <p>Date : 21/10/2013 Page : 21</p>
--	--	---

$$\begin{aligned}
\tilde{\Pi}_x &= \Pi_x \left( 1 + \sum_{l=1}^n G_{1l} Y_l^{\Pi_x} \right) \\
\tilde{Y}_l^{\Pi_x} &= G_{2l} \Pi_x Y_l^{\Pi_x} \\
G_{1l} &= \frac{\omega_l \Delta}{2 - \omega_l \Delta} \quad , \quad G_{2l} = \frac{2}{2 - \omega_l \Delta}
\end{aligned} \tag{1.39}$$

and similar relations apply to the two other modules necessary for updating  $\sigma_{xx}$ .

### 3.2.6. Simulation of the planar free surface

Assuming vacuum above the Earth's surface, the Earth's surface can be considered a traction-free surface. If  $\vec{T}(\vec{n})$  is the traction vector at surface  $S$  with normal vector  $\vec{n}$ , the traction-free condition at surface  $S$  is

$$\vec{T}(\vec{n}) = 0 \tag{1.40}$$

or, equivalently,


$$\sigma_{ij} n_j = 0 . \tag{1.41}$$

For surface  $S$  planar and perpendicular to the  $z$ -axis,  $\vec{n} = (0, 0, -1)$ , the condition is

$$\sigma_{iz} = 0 \quad ; \quad i \in \{x, y, z\} . \tag{1.42}$$

Since Levander's (1988) article, the most popular method of simulating the planar free surface in the velocity-stress staggered-grid finite-difference schemes has been the stress-imaging method. Rodrigues (1993) and Kristek et al. (2002) demonstrated that the spatial sampling applicable inside the medium is insufficient in the stress-imaging method especially if Rayleigh surface waves should be propagated without considerable grid dispersion. Rodrigues (1993) therefore combined the stress-imaging technique with a vertically refined grid near the free surface and achieved good accuracy. A disadvantage of the approach is three times smaller time step applied to the whole grid. Therefore, Kristek et al. (2002) and Moczo et al. (2004) developed the 4<sup>th</sup>-order scheme with adjusted FD approximations (AFDA) and demonstrated its better accuracy compared to the stress imaging.

The calculation of the stress-tensor and particle-velocity components in the W-AFDA approach can be summarized as follows:

	<p style="text-align: center;">Research and Development Programme on Seismic Ground Motion</p> <p style="text-align: center;">CONFIDENTIAL Restricted to SIGMA scientific partners and members of the consortium, please do not pass around</p>	<p>Ref : SIGMA-2013-D3-97 Version : 01</p> <hr/> <p>Date : 21/10/2013 Page : 22</p>
--	---	---

**Direct application of the boundary condition:**

$$TZX(0) = 0, TYZ(0) = 0.$$

**4<sup>th</sup>-order approximations of the  $z$  derivative:**

The following 4<sup>th</sup>-order approximations of the 1<sup>st</sup> derivative with respect to the  $z$ -coordinate are used in calculations of the stress-tensor and particle-velocity vector components:

$$\begin{aligned} \frac{\partial \Phi}{\partial z}(z_0) = \frac{1}{h} \left[ -\frac{352}{105} \Phi(z_0) + \frac{35}{8} \Phi\left(z_0 + \frac{1}{2}h\right) - \frac{35}{24} \Phi\left(z_0 + \frac{3}{2}h\right) \right. \\ \left. + \frac{21}{40} \Phi\left(z_0 + \frac{5}{2}h\right) - \frac{5}{56} \Phi\left(z_0 + \frac{7}{2}h\right) \right] + O(h^4) \end{aligned} \quad (1.43)$$

$$\begin{aligned} \frac{\partial \Phi}{\partial z}(z_0) = \frac{1}{h} \left[ -\frac{11}{12} \Phi\left(z_0 - \frac{1}{2}h\right) + \frac{17}{24} \Phi\left(z_0 + \frac{1}{2}h\right) + \frac{3}{8} \Phi\left(z_0 + \frac{3}{2}h\right) \right. \\ \left. - \frac{5}{24} \Phi\left(z_0 + \frac{5}{2}h\right) + \frac{1}{24} \Phi\left(z_0 + \frac{7}{2}h\right) \right] + O(h^4) \end{aligned} \quad (1.44)$$

$$\begin{aligned} \frac{\partial \Phi}{\partial z}(z_0) = \frac{1}{h} \left[ -\frac{1}{12} h \Phi(z_0 - h) - \frac{577}{528} \Phi\left(z_0 - \frac{1}{2}h\right) + \frac{201}{176} \Phi\left(z_0 + \frac{1}{2}h\right) \right. \\ \left. - \frac{9}{176} \Phi\left(z_0 + \frac{3}{2}h\right) + \frac{1}{528} \Phi\left(z_0 + \frac{5}{2}h\right) \right] + O(h^4) \end{aligned} \quad (1.45)$$

$$\begin{aligned} \frac{\partial \Phi}{\partial z}(z_0) = \frac{1}{h} \left[ \frac{16}{105} \Phi(z_0 - h) - \frac{31}{24} \Phi\left(z_0 - \frac{1}{2}h\right) + \frac{29}{24} \Phi\left(z_0 + \frac{1}{2}h\right) \right. \\ \left. - \frac{3}{40} \Phi\left(z_0 + \frac{3}{2}h\right) + \frac{1}{168} \Phi\left(z_0 + \frac{5}{2}h\right) \right] + O(h^4) \end{aligned} \quad (1.46)$$

Depending on the particular configuration,  $\Phi$  may stand for a particle-velocity or stress-tensor components and  $z_0$  for 0,  $h/2$  or  $h$ .

a) Calculation of the stress-tensor components


$TXX(h/2)$  is obtained from the 4<sup>th</sup>-order approximation of the temporal derivative of the stress-strain relation for  $\sigma_{xx}$ ;  $\frac{\partial v_z}{\partial z}$  is approximated using Eq. (1.44).

$TYY(h/2)$  and  $TZZ(h/2)$  – analogous to  $TXX(h/2)$ .

$TZX(h)$  is obtained from the 4<sup>th</sup>-order approximation of the temporal derivative of the stress-strain relation for  $\sigma_{zx}$ ;  $\frac{\partial v_x}{\partial z}$  is approximated using Eq. (1.45) in which  $\frac{\partial v_x}{\partial z}(0)$  is replaced by

$\frac{\partial v_z}{\partial x}(0)$  due to condition  $\sigma_{zx}(0) = 0$ .



	<p>Research and Development Programme on Seismic Ground Motion</p> <p>CONFIDENTIAL <i>Restricted to SIGMA scientific partners and members of the consortium, please do not pass around</i></p>	<p>Ref : SIGMA-2013-D3-97 Version : 01</p> <hr/> <p>Date : 21/10/2013 Page : 23</p>
--	--	---

$TYZ(h)$  is obtained from the 4<sup>th</sup>-order approximation of the temporal derivative of the stress-strain relation for  $\sigma_{yz}$ ;  $\frac{\partial v_y}{\partial z}$  is approximated using Eq. (1.45) in which  $\frac{\partial v_y}{\partial z}(0)$  is replaced by  $\frac{\partial v_z}{\partial y}(0)$  due to condition  $\sigma_{yz}(0) = 0$ .

b) Calculation of the particle-velocity components

$VZ(0)$  is obtained from the 4<sup>th</sup>-order approximation of the equation for  $v_z$ ;  $\frac{\partial \sigma_{zz}}{\partial z}$  is approximated using Eq. (1.43) in which condition  $\sigma_{zz}(0) = 0$  is used.

$VX(h/2)$  is obtained from the 4<sup>th</sup>-order approximation of the equation for  $v_x$ ;  $\frac{\partial \sigma_{zx}}{\partial z}$  is approximated using Eq. (1.44).

$VY(h/2)$  is obtained from the 4<sup>th</sup>-order approximation of the equation for  $v_y$ ;  $\frac{\partial \sigma_{yz}}{\partial z}$  is approximated using Eq. (1.44).


$VZ(h)$  is obtained from the 4<sup>th</sup>-order approximation of the equation for  $v_z$ ;  $\frac{\partial \sigma_{zz}}{\partial z}$  is approximated using Eq. (1.46) in which condition  $\sigma_{zz}(0) = 0$  is used.

The corresponding effective grid material parameters are evaluated as integral averages in the half grid-cell volumes, that is, the upper half of the volume located above the free surface is not taken into account. For example,

$$\rho_{I+1/2, K+1/2, 0}^A = \frac{2}{h^3} \int_{x_I}^{x_{I+1}} \int_{y_K}^{y_{K+1}} \int_{z_0}^{z_{1/2}} \rho \, dx \, dy \, dz \quad (1.47)$$

### 3.2.7. Simulation of the non-reflecting boundary

We efficiently simulate non-reflecting boundaries of the grid using the unsplit formulation of the perfectly matched layer (PML) with our time-integration algorithm that is computationally slightly more efficient than the other published algorithm. The corresponding theory is described by Kristek

	<p style="text-align: center;">Research and Development Programme on Seismic Ground Motion</p> <p style="text-align: center;">CONFIDENTIAL <i>Restricted to SIGMA scientific partners and members of the consortium, please do not pass around</i></p>	<p>Ref : SIGMA-2013-D3-97 Version : 01</p> <hr/> <p>Date : 21/10/2013 Page : 24</p>
--	--	---

et al. (2009) and Moczo et al. (2014). Here we just note that the convolutional unsplit PML is really necessary for avoiding spurious artificial reflections from the grid boundaries.

### 3.2.8. Wavefield excitation

In our computer code we implemented four possible excitations of the wavefield:

- Point double-couple source
- Finite kinematic source
- Vertical incidence of plane S wave (this option was implemented for the E2VP project)
- Vertical incidence of plane P wave (this option was implemented for the SIGMA project)


The point double-couple source can be simulated either using the body-force term, as introduced for the staggered-grid schemes by Graves (1996), or using the incremental stress, as introduced for the staggered-grid schemes by Virieux (1986) and Coutant et al. (1995). In both cases the point source is described by the time-dependent moment tensor.

The finite kinematic source is simulated using spatial distribution of point double-couple sources. Each point source is described by individual time-dependent moment tensor.

The vertical incidence of plane wave is based on the wavefield decomposition. The total wavefield is decomposed into the wavefield produced by a source and the residual (or scattered) wavefield. The principle of the wavefield decomposition is, in general, an efficient tool for "injecting" an analytical source wavefield in the grid. By a) distinguishing separate grid field variables for the source, residual and total wavefields, b) prescribing just the source wavefield, and c) calculating the residual and total wavefields we do not violate physical causality. The variables for the total and residual wavefields share grid positions only in the algorithmically necessary strip of grid planes – ensuring thus the computational efficiency. For the theory we refer to Moczo et al. (2007a,b, 2014).

## 4. Analysis of numerical simulations

The direct results of the numerical simulations are time histories of the particle velocity at specified (receiver) positions possibly anywhere at or beneath the free surface. For the purpose of the intended investigations the time histories will be used for calculation of the selected important characteristics of the seismic motion. These characteristics will be subject of basically two types of comparisons:

	<p style="text-align: center;">Research and Development Programme on Seismic Ground Motion</p> <p style="text-align: center;">CONFIDENTIAL <i>Restricted to SIGMA scientific partners and members of the consortium, please do not pass around</i></p>	<p>Ref : SIGMA-2013-D3-97 Version : 01</p> <hr/> <p>Date : 21/10/2013 Page : 25</p>
--	--	---

- comparisons of characteristics obtained from 3D modelling of seismic motion in the basic model with those for modified models,
- comparisons of characteristics obtained from 3D modelling of seismic motion with characteristics obtained from 2D and 1D modelling.

Before we define the characteristics, we specify the coordinate systems. In all cases we consider Cartesian right-handed coordinate systems. One coordinate system may be defined for both the 3D and 1D modelling:

### 3D, 1D

- $x$ -direction = West → East direction (EW component)
- $y$ -direction = South → North direction (NS component)
- $z$ -direction = vertical upward direction (UD component)

## 4.1. Transfer properties at a site – 3D

We define the pseudoimpulse input signal in the particle velocity using the Gabor signal


$$p(t) = \exp\left\{-\left[\omega_p(t-t_s)/\gamma_s\right]^2\right\} \cos\left[\omega_p(t-t_s) + \theta\right]. \quad (2.1)$$

Here  $\omega_p = 2\pi f_p$ ,  $\gamma_s$  controls the width of the signal,  $\theta$  is a phase shift. For this study we chose  $f_p = 0.45$ ,  $\gamma_s = 0.35$ ,  $\theta = \pi/2$  and  $t_s = 0.5$ . (In many simulations, it is sufficient to use a smaller value determined by formula  $t_s = 0.45\gamma_s/f_p$ . Here we chose large  $t_s$  in order to have a smaller onset of the signal.) The signal, and its amplitude and phase Fourier spectra are shown in Fig. 4.1. For obtaining the transfer properties at a site for a vertical incidence of a plane wave it is reasonable to assume

$$p_x(t) = p_y(t) = p_z(t) = p(t) \quad (2.2)$$

The Fourier spectrum of the input signal may be denoted by  $\mathcal{F}p(f)$ .

A plane wave polarized in the  $x$ -direction results in the time-domain pseudoimpulse responses  $r_{xx}(t)$ ,  $r_{xy}(t)$  and  $r_{xz}(t)$ . The second index indicates the component of the response. Analogously, a plane wave polarized in the  $y$ -direction results in responses  $r_{yx}(t)$ ,  $r_{yy}(t)$ ,  $r_{yz}(t)$ , and a plane wave polarized in the  $z$ -direction results in responses  $r_{zx}(t)$ ,  $r_{zy}(t)$ ,  $r_{zz}(t)$ . The Fourier spectrum

	<p style="text-align: center;">Research and Development Programme on Seismic Ground Motion</p> <p style="text-align: center;">CONFIDENTIAL <i>Restricted to SIGMA scientific partners and members of the consortium, please do not pass around</i></p>	<p>Ref : SIGMA-2013-D3-97 Version : 01</p> <hr/> <p>Date : 21/10/2013 Page : 26</p>
--	--	---

of the time-domain response  $r_{\xi\eta}(t)$  may be denoted by  $\mathcal{F}r_{\xi\eta}(f)$ . Having Fourier spectra of all time-domain responses, we can obtain a matrix of the Fourier transfer functions as

$$\begin{bmatrix} \mathcal{F}TF_{xx}(f) & \mathcal{F}TF_{yx}(f) & \mathcal{F}TF_{zx}(f) \\ \mathcal{F}TF_{xy}(f) & \mathcal{F}TF_{yy}(f) & \mathcal{F}TF_{zy}(f) \\ \mathcal{F}TF_{xz}(f) & \mathcal{F}TF_{yz}(f) & \mathcal{F}TF_{zz}(f) \end{bmatrix} = \frac{1}{\mathcal{F}p(f)} \begin{bmatrix} \mathcal{F}r_{xx}(f) & \mathcal{F}r_{yx}(f) & \mathcal{F}r_{zx}(f) \\ \mathcal{F}r_{xy}(f) & \mathcal{F}r_{yy}(f) & \mathcal{F}r_{zy}(f) \\ \mathcal{F}r_{xz}(f) & \mathcal{F}r_{yz}(f) & \mathcal{F}r_{zz}(f) \end{bmatrix} \quad (2.3)$$

Having the transfer functions it is possible to proceed with calculations of the amplification factor for a set of selected real and synthetic accelerograms.

## 4.2. Amplification factor – 3D

Components of the  $i$ -th of  $n$  selected accelerograms may be denoted as  $a_{x,i}(t)$ ,  $a_{y,i}(t)$  and  $a_{z,i}(t)$ . The Fourier spectrum of  $a_{\xi,i}(t)$  may be denoted by  $\mathcal{F}a_{\xi,i}(f)$ . The response spectrum of  $a_{\xi,i}(t)$  may be denoted by  $\mathcal{R}a_{\xi,i}(f)$ .

Assuming the vertical incidence of a plane wave with the  $a_{x,i}(t)$ ,  $a_{y,i}(t)$  and  $a_{z,i}(t)$  components, the components of the site acceleration (site time-domain response to the input accelerograms) may be denoted as  $s_{x,i}(t)$ ,  $s_{y,i}(t)$  and  $s_{z,i}(t)$ . They are obtained as

$$\begin{pmatrix} s_{x,i}(t) \\ s_{y,i}(t) \\ s_{z,i}(t) \end{pmatrix} = \mathcal{F}^{-1} \left\{ \begin{bmatrix} \mathcal{F}TF_{xx}(f) & \mathcal{F}TF_{yx}(f) & \mathcal{F}TF_{zx}(f) \\ \mathcal{F}TF_{xy}(f) & \mathcal{F}TF_{yy}(f) & \mathcal{F}TF_{zy}(f) \\ \mathcal{F}TF_{xz}(f) & \mathcal{F}TF_{yz}(f) & \mathcal{F}TF_{zz}(f) \end{bmatrix} \begin{pmatrix} \mathcal{F}a_{x,i}(f) \\ \mathcal{F}a_{y,i}(f) \\ \mathcal{F}a_{z,i}(f) \end{pmatrix} \right\}, \quad (2.4)$$


where  $\mathcal{F}^{-1}$  denotes the inverse Fourier transform.

The response spectrum of  $s_{\xi,i}(t)$  may be denoted by  $\mathcal{R}s_{\xi,i}(f)$ . Then the amplification factor for the  $\xi$ -component is obtained as

$$AF_{\xi,i}(f) = \frac{\mathcal{R}s_{\xi,i}(f)}{\mathcal{R}a_{\xi,i}(f)} \quad (2.5)$$

We may also obtain the amplification factor for the horizontal component as

$$AF_{h,i}(f) = \sqrt{\frac{\mathcal{R}s_{x,i}(f) \mathcal{R}s_{y,i}(f)}{\mathcal{R}a_{x,i}(f) \mathcal{R}a_{y,i}(f)}} \quad (2.6)$$

	<p>Research and Development Programme on Seismic Ground Motion</p> <p>CONFIDENTIAL <i>Restricted to SIGMA scientific partners and members of the consortium, please do not pass around</i></p>	<p>Ref : SIGMA-2013-D3-97 Version : 01</p> <hr/> <p>Date : 21/10/2013 Page : 27</p>
--	--	---

The average amplification factor for a set of  $n$  input accelerograms for the  $\xi$ -component is obtained as

$$\overline{AF}_{\xi}(f) = \sqrt[n]{\prod_{i=1}^n AF_{\xi,i}(f)} \quad (2.7)$$

Here,  $\xi \in \{x, y, z, h\}$ .

The characteristics of the seismic motion at a site are summarized in Tables 4.1 and 4.2.

### 4.3. Transfer properties and amplification factor at a site – 2D

Because the selected 2D profiles are not necessarily aligned with one of the EW or NS directions we consider a local coordinate system. The coordinates in the local system are indicated by a prime except the  $z$ -coordinate which is identical with the  $z$ -coordinate of the 3D system. We thus have

$x'$ -direction = direction of the profile (along the horizontal surface profile line)

$y'$ -direction = direction perpendicular to the profile

$z$ -direction = vertical upward direction

We may denote the angle between the  $x$ -axis and  $x'$  axis as  $\phi$ .


In the local coordinate system, assuming a vertical incidence of a plane wave,  $x'$ ,  $y'$  and  $z$  indicate the SV, SH and P waves, respectively. Relations (2.2) can be modified as

$$p(t) = p_{x'}(t) = p_{y'}(t) = p_z(t) . \quad (2.8)$$

In the 2D modelling the SH wavefield does not interact with the P-SV wavefield (the two wavefields are independent). Consequently, a plane wave polarized in the  $y'$ -direction results only in the time-domain pseudoimpulse response  $r_{y'y'}(t)$ . A plane wave polarized in the  $x'$ -direction results in responses  $r_{x'x'}(t)$  and  $r_{x'z}(t)$ , and a plane wave polarized in the  $z$ -direction results in responses  $r_{zx'}(t)$  and  $r_{zy'}(t)$ . The Fourier spectrum of the time-domain response  $r_{\xi'\eta'}(t)$  may be denoted by  $\mathcal{F}r_{\xi'\eta'}(f)$ . Having Fourier spectra of all time-domain responses, we can obtain an SH Fourier transfer function and a P-SV matrix of the Fourier transfer functions as

$$\mathcal{F}T\mathcal{F}_{y'y'}(f) = \frac{\mathcal{F}r_{y'y'}(f)}{\mathcal{F}p(f)} \quad (2.9)$$

and

	<p style="text-align: center;">Research and Development Programme on Seismic Ground Motion</p> <p style="text-align: center;">CONFIDENTIAL <i>Restricted to SIGMA scientific partners and members of the consortium, please do not pass around</i></p>	<p>Ref : SIGMA-2013-D3-97 Version : 01</p> <hr/> <p>Date : 21/10/2013 Page : 28</p>
--	--	---

$$\begin{bmatrix} FT\mathcal{F}_{x'x'}(f) & FT\mathcal{F}_{zx'}(f) \\ FT\mathcal{F}_{x'z}(f) & FT\mathcal{F}_{zz}(f) \end{bmatrix} = \frac{1}{\mathcal{F}p(f)} \begin{bmatrix} \mathcal{F}r_{x'x'}(f) & \mathcal{F}r_{zx'}(f) \\ \mathcal{F}r_{x'z}(f) & \mathcal{F}r_{zz}(f) \end{bmatrix} \quad (2.10)$$

Components of the  $i$ -th of  $n$  selected accelerograms (rotated to the local 2D-problem coordinate system) may be denoted as  $a_{y',i}(t)$  and  $a_{x',i}(t), a_{z,i}(t)$ . The Fourier spectrum of  $a_{\xi',i}(t)$  may be denoted by  $\mathcal{F}a_{\xi',i}(f)$ .

The components of the site acceleration are obtained as

$$s_{y',i}(t) = \mathcal{F}^{-1} \left\{ \mathcal{F}a_{y',i}(f) FT\mathcal{F}_{y'y'}(f) \right\} \quad (2.11)$$

and

$$\begin{pmatrix} s_{x',i}(t) \\ s_{z,i}(t) \end{pmatrix} = \mathcal{F}^{-1} \left\{ \begin{bmatrix} FT\mathcal{F}_{x'x'}(f) & FT\mathcal{F}_{zx'}(f) \\ FT\mathcal{F}_{x'z}(f) & FT\mathcal{F}_{zz}(f) \end{bmatrix} \begin{pmatrix} \mathcal{F}a_{x',i}(f) \\ \mathcal{F}a_{z,i}(f) \end{pmatrix} \right\} \quad (2.12)$$

The rotated site acceleration components are obtained as

$$\begin{pmatrix} s_{x,i}(t) \\ s_{y,i}(t) \end{pmatrix} = \begin{bmatrix} \cos \phi & -\sin \phi \\ \sin \phi & \cos \phi \end{bmatrix} \begin{pmatrix} s_{x',i}(t) \\ s_{y',i}(t) \end{pmatrix} \quad (2.13)$$

where  $\phi = \angle x x'$ . From the obtained site accelerations  $s_{x,i}(t), s_{y,i}(t)$  and  $s_{z,i}(t)$  we can obtain the amplification factors and average amplification factors in the same way as in 3D.


All characteristics of seismic motion specific for the 2D modelling are summarized in Tab. 4.3 and 4.4.

#### 4.4. Transfer properties and amplification factor at a site – 1D

The coordinate system is the same as in the 3D modelling. Relations (2.2) can be modified as

$$p(t) = p_h(t) = p_z(t) \quad (2.14)$$

where  $h$  indicates a horizontal component of S wave, i.e., any of the  $x$ - and  $y$ - components, and  $z$  indicates P wave. A plane wave polarized in the  $h$ -direction results in the time-domain pseudoimpulse response  $r_h(t)$ , and a plane wave polarized in the  $z$ -direction results in the time-

	<p>Research and Development Programme on Seismic Ground Motion</p> <p>CONFIDENTIAL <i>Restricted to SIGMA scientific partners and members of the consortium, please do not pass around</i></p>	<p>Ref : SIGMA-2013-D3-97 Version : 01</p> <hr/> <p>Date : 21/10/2013 Page : 29</p>
--	--	---

domain pseudoimpulse response  $r_z(t)$ . The Fourier spectrum of the time-domain response  $r_z(t)$  may be denoted by  $\mathcal{F}r_z(f)$ . The Fourier transfer functions are obtained as

$$\mathcal{F}T\mathcal{F}_h(f) = \frac{\mathcal{F}r_h(f)}{\mathcal{F}p(f)} \quad \mathcal{F}T\mathcal{F}_z(f) = \frac{\mathcal{F}r_z(f)}{\mathcal{F}p(f)} \quad (2.15)$$

The site accelerations are then obtained as

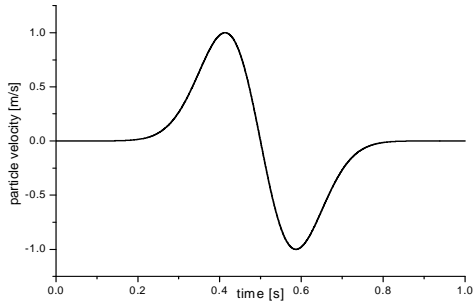
$$\begin{aligned} s_{x,i}(t) &= \mathcal{F}^{-1}\{\mathcal{F}a_{x,i}(f) \mathcal{F}T\mathcal{F}_h(f)\} \\ s_{y,i}(t) &= \mathcal{F}^{-1}\{\mathcal{F}a_{y,i}(f) \mathcal{F}T\mathcal{F}_h(f)\} \\ s_{z,i}(t) &= \mathcal{F}^{-1}\{\mathcal{F}a_{z,i}(f) \mathcal{F}T\mathcal{F}_z(f)\} \end{aligned} \quad (2.16)$$

From the site accelerations  $s_{x,i}(t)$ ,  $s_{y,i}(t)$  and  $s_{z,i}(t)$  we can obtain the amplification factors and average amplification factors in the same way as in 3D.

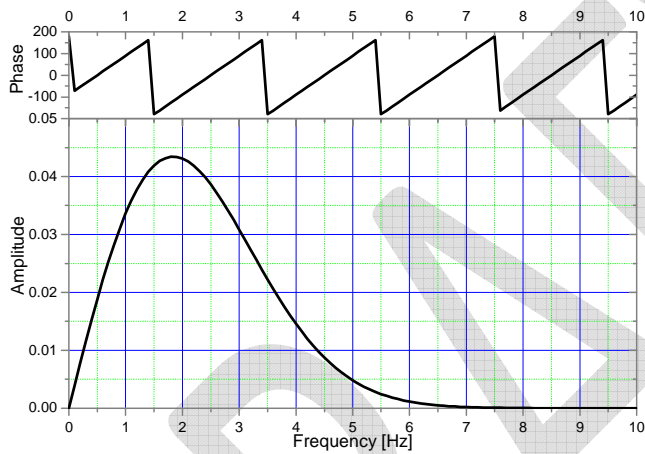
All characteristics of seismic motion specific for the 1D modelling are summarized in Tab. 4.5 and 4.6.

DRAFT

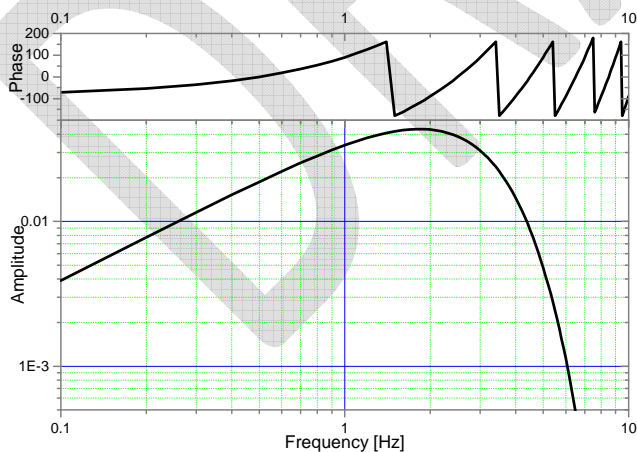




Pseudoimpulse input signal in the particle velocity



Amplitude and phase Fourier spectra of the input signal



Loglog amplitude and log phase Fourier spectra of the input signal

**Fig. 4.1 The input signal and its spectra**

**Tab. 4.1 Transfer properties at a site**

<b>3D</b>		
<b>characteristic of seismic motion</b>	<b>abbreviation and/or mathematical symbol</b>	<b>note/legend</b>
pseudoimpulse input signal in the particle velocity	$p_x(t) = p_y(t) = p_z(t) = p(t)$	assuming a vertical incidence of a plane wave, $x$ and $y$ indicate S wave, $z$ indicates P wave
Fourier spectrum of the pseudoimpulse input signal	$\mathcal{F}p(f)$	
time-domain pseudoimpulse response	$r_{xx}(t) \quad r_{yx}(t) \quad r_{zx}(t)$ $r_{xy}(t) \quad r_{yy}(t) \quad r_{zy}(t)$ $r_{xz}(t) \quad r_{yz}(t) \quad r_{zz}(t)$	$r_{xy}(t) =$ y-component of response to $p_x(t)$
Fourier spectrum of the pseudoimpulse response	$\begin{bmatrix} \mathcal{F}r_{xx}(f) & \mathcal{F}r_{yx}(f) & \mathcal{F}r_{zx}(f) \\ \mathcal{F}r_{xy}(f) & \mathcal{F}r_{yy}(f) & \mathcal{F}r_{zy}(f) \\ \mathcal{F}r_{xz}(f) & \mathcal{F}r_{yz}(f) & \mathcal{F}r_{zz}(f) \end{bmatrix}$	
matrix of the Fourier transfer functions	$\begin{bmatrix} \mathcal{F}TF_{xx}(f) & \mathcal{F}TF_{yx}(f) & \mathcal{F}TF_{zx}(f) \\ \mathcal{F}TF_{xy}(f) & \mathcal{F}TF_{yy}(f) & \mathcal{F}TF_{zy}(f) \\ \mathcal{F}TF_{xz}(f) & \mathcal{F}TF_{yz}(f) & \mathcal{F}TF_{zz}(f) \end{bmatrix}$	$\mathcal{F}TF_{xx}(f) = \frac{\mathcal{F}r_{xx}(f)}{\mathcal{F}p(f)}$

**Tab 4. 2 Seismic motion at a site**


<b>3D</b>		
characteristic of seismic motion	abbreviation and/or mathematical symbol	note/legend
input real/synthetic accelerogram	$a_{x,i}(t) \quad a_{y,i}(t) \quad a_{z,i}(t)$	$i$ – sequential number of the $i$ -th of $n$ accelerograms
Fourier spectrum of the accelerogram	$\mathcal{F}a_{x,i}(f) \quad \mathcal{F}a_{y,i}(f) \quad \mathcal{F}a_{z,i}(f)$	
response spectrum of the input accelerogram	$\mathcal{R}a_{x,i}(f) \quad \mathcal{R}a_{y,i}(f) \quad \mathcal{R}a_{z,i}(f)$	
site acceleration (site time-domain response to the input accelerogram)	$s_{x,i}(t) \quad s_{y,i}(t) \quad s_{z,i}(t)$	$s_{x,i}(t) = \mathcal{F}^{-1} \{ \mathcal{F}a_{x,i}(f) \mathcal{F}TF_{xx}(f) + \mathcal{F}a_{y,i}(f) \mathcal{F}TF_{yx}(f) + \mathcal{F}a_{z,i}(f) \mathcal{F}TF_{zx}(f) \}$ analogously for $s_{y,i}(t), s_{z,i}(t)$
response spectrum of the site acceleration	$\mathcal{R}s_{x,i}(f) \quad \mathcal{R}s_{y,i}(f) \quad \mathcal{R}s_{z,i}(f)$	
amplification factors	$AF_{x,i}(f) \quad AF_{y,i}(f) \quad AF_{z,i}(f)$ $AF_{h,i}(f)$	$AF_{x,i}(f) = \frac{\mathcal{R}s_{x,i}(f)}{\mathcal{R}a_{x,i}(f)}$ analogously for $AF_{y,i}(f), AF_{z,i}(f)$  $AF_{h,i}(f) = \sqrt{\frac{\mathcal{R}s_{x,i}(f) \mathcal{R}s_{y,i}(f)}{\mathcal{R}a_{x,i}(f) \mathcal{R}a_{y,i}(f)}}$ $h$ indicates the horizontal component
average amplification factors	$\overline{AF}_x(f) \quad \overline{AF}_y(f) \quad \overline{AF}_z(f)$ $\overline{AF}_h(f)$	$\overline{AF}_x(f) = \sqrt[n]{\prod_{i=1}^n AF_{x,i}(f)}$ analogously for $\overline{AF}_y(f), \overline{AF}_z(f), \overline{AF}_h(f)$

**Tab. 4.3 Transfer properties at a site**

<b>2D</b>		
<b>characteristic of seismic motion</b>	<b>abbreviation and/or mathematical symbol</b>	<b>note/legend</b>
pseudoimpulse input signal in the particle velocity	$p(t) = p_{x'}(t) = p_{y'}(t) = p_z(t)$	assuming a vertical incidence of a plane wave, $x'$ , $y'$ and $z$ indicate SV, SH and P waves, respectively
time-domain pseudoimpulse response  SH  P-SV	$r_{y'y'}(t)$  $\begin{matrix} r_{x'x'}(t) & r_{zx'}(t) \\ r_{x'z}(t) & r_{zz}(t) \end{matrix}$	$r_{y'y'}(t) = r_{SH}(t)$  $r_{x'z}(t) = z\text{-component}$ of response to $p_{x'}(t)$
Fourier spectrum of the pseudoimpulse response	$\mathcal{F}r_{y'y'}(f)$  $\begin{bmatrix} \mathcal{F}r_{x'x'}(f) & \mathcal{F}r_{zx'}(f) \\ \mathcal{F}r_{x'z}(f) & \mathcal{F}r_{zz}(f) \end{bmatrix}$	
SH transfer function  P-SV matrix of the Fourier transfer functions	$\mathcal{FTF}_{y'y'}(f)$  $\begin{bmatrix} \mathcal{FTF}_{x'x'}(f) & \mathcal{FTF}_{zx'}(f) \\ \mathcal{FTF}_{x'z}(f) & \mathcal{FTF}_{zz}(f) \end{bmatrix}$	$\mathcal{FTF}_{y'y'}(f) =$ $\mathcal{F}r_{y'y'}(f) / \mathcal{F}p(f)$ analogously for the other four transfer functions


**Tab. 4.4 Seismic motion at a site**

<b>2D</b>		
<b>characteristic of seismic motion</b>	<b>abbreviation and/or mathematical symbol</b>	<b>note/legend</b>
input real/synthetic accelerogram	$a_{y',i}(t)$ $a_{x',i}(t) \quad a_{z,i}(t)$	$i$ – sequential number of the accelerogram
Fourier spectrum of the accelerogram	$\mathcal{F}a_{y',i}(f)$ $\mathcal{F}a_{x',i}(f) \quad \mathcal{F}a_{z,i}(f)$	
site acceleration (site time- domain response to the input accelerogram)	$s_{y',i}(t)$ $s_{x',i}(t) \quad s_{z,i}(t)$	$s_{y',i}(t) =$ $\mathcal{F}^{-1}\{\mathcal{F}a_{y',i}(f) \mathcal{F}TF_{y'y'}(f)\}$ $s_{x',i}(t) =$ $\mathcal{F}^{-1}\{\mathcal{F}a_{x',i}(f) \mathcal{F}TF_{x'x'}(f)$ $+ \mathcal{F}a_{z,i}(f) \mathcal{F}TF_{zx'}(f)\}$ analogously for $s_{z,i}(t)$
rotated site acceleration	$s_{x,i}(t) \quad s_{y,i}(t) \quad s_{z,i}(t)$	$\begin{pmatrix} s_{x,i}(t) \\ s_{y,i}(t) \end{pmatrix} = \begin{bmatrix} \cos \phi & -\sin \phi \\ \sin \phi & \cos \phi \end{bmatrix} \begin{pmatrix} s_{x',i}(t) \\ s_{y',i}(t) \end{pmatrix}$ $\phi = \angle x x'$

	Research and Development Programme on Seismic Ground Motion	Ref : SIGMA-2013-D3-97 Version : 01
	CONFIDENTIAL Restricted to SIGMA scientific partners and members of the consortium, please do not pass around	Date : 21/10/2013 Page : 35

Tab. 4.5 Transfer properties at a site		
1D		
characteristic of seismic motion	abbreviation and/or mathematical symbol	note/legend
pseudoimpulse input signal in the particle velocity	$p(t) = p_h(t) = p_z(t)$	$h$ indicates a horizontal component of S wave, i.e., any of the $x$ and $y$ components, $z$ indicates P wave
time-domain pseudoimpulse response	$r_h(t) \quad r_z(t)$	
Fourier spectrum of the pseudoimpulse response	$\mathcal{F}r_h(f) \quad \mathcal{F}r_z(f)$	
Fourier transfer functions	$\mathcal{F}TF_h(f) \quad \mathcal{F}TF_z(f)$	$\mathcal{F}TF_h(f) = \mathcal{F}r_h(f) / \mathcal{F}p(f)$ analogously for $\mathcal{F}TF_z(f)$

Tab. 4.6 Seismic motion at a site		
1D		
characteristic of seismic motion	abbreviation and/or mathematical symbol	note/legend
site acceleration (site time-domain response to the input accelerogram)	$s_{x,i}(t) \quad s_{y,i}(t) \quad s_{z,i}(t)$	$s_{x,i}(t) = \mathcal{F}^{-1} \{ \mathcal{F}a_{x,i}(f) \mathcal{F}TF_h(f) \}$ $s_{y,i}(t) = \mathcal{F}^{-1} \{ \mathcal{F}a_{y,i}(f) \mathcal{F}TF_h(f) \}$ $s_{z,i}(t) = \mathcal{F}^{-1} \{ \mathcal{F}a_{z,i}(f) \mathcal{F}TF_z(f) \}$

	<p>Research and Development Programme on Seismic Ground Motion</p> <p>CONFIDENTIAL <i>Restricted to SIGMA scientific partners and members of the consortium, please do not pass around</i></p>	<p>Ref : SIGMA-2013-D3-97 Version : 01</p> <hr/> <p>Date : 21/10/2013 Page : 36</p>
--	--	---

## 5. Grenoble valley, France

### 5.1. Introduction

The Grenoble urban area is mostly built on the Quaternary fluvial and post-glacial deposits that fill a typical deep Alpine valley. The concern is underlined by the fact that such "alpine valley" configuration is also met in different other areas within the European Alps, and in other mountainous areas with embanked valleys filled with young, post-glacial lacustrine sediments.

Grenoble valley is geometrically complex (Figs. 5.1 – 5.3). In fact, it is a junction of three large valleys with complex geometry of the sediment-basement interface. The junction mimics letter Y. The other distinctive feature is a relatively large velocity contrast at the sediment-basement interface. Finally, the valley is surrounded by relatively high mountain ranges. All the three features pose a serious challenge for the numerical modelling of seismic motion. Even in the simplified approach neglecting the surrounding topography, the structure is relatively more challenging than, e.g., the Los Angeles basin.

The difficulty of the numerical modelling of seismic motion in complex sedimentary structure may be illustrated by the fact that the agreement between synthetics and data remains far from satisfactory, except for very low frequencies, approximately smaller than 0.1 Hz.

The concise characterization of the Grenoble valley and its investigations from the point of view of numerical modelling of seismic motion can be found in the article by Chaljub et al. (2010).

### 5.2. Computational model

In the numerical simulations we do not include the free-surface topography. The geometry of the sediment-basement interface is shown in Figs. 5.2 and 5.3. The mechanical parameters of the computational model are shown in Tab. 5.1. Although relatively complex in terms of rheology and geometry, the model is still only an approximation of the true valley. Probably, the most simplified is the shallow part of the model – given the considered frequency range.

The quality factor values were chosen infinite in the underlying very stiff bedrock. Consequently and reasonably for the assumption of the vertical incidence of the plane wave, the crustal damping is assumed negligible in the modelling. In the sediments the quality factor is taken slightly larger than that actually measured in the Montbonnot borehole,  $Q_p = 35$ . This is because



the measurements were performed at frequencies of several tens of Hz, and higher  $Q$  values are necessary for reproducing the observed low-frequency duration within the valley (Cornou 2002, Chaljub 2009).

<b>Tab. 5.1 Mechanical parameters of the Grenoble valley model</b> Coordinate $z$ is assumed in metres.					
Unit	Density (kg / m <sup>3</sup> )	S-wave speed $\beta$ (m/s)	P-wave speed $\alpha$ (m/s)	Quality factor $Q_S$	Quality factor $Q_P$
Sediments	$2124 + 0.125 z$	$300 + 19\sqrt{z}$	$1450 + 1.25 z$	50	$37.5 \alpha^2 / \beta^2$
Bedrock	2 720	3 200	5 600	$\infty$	$\infty$

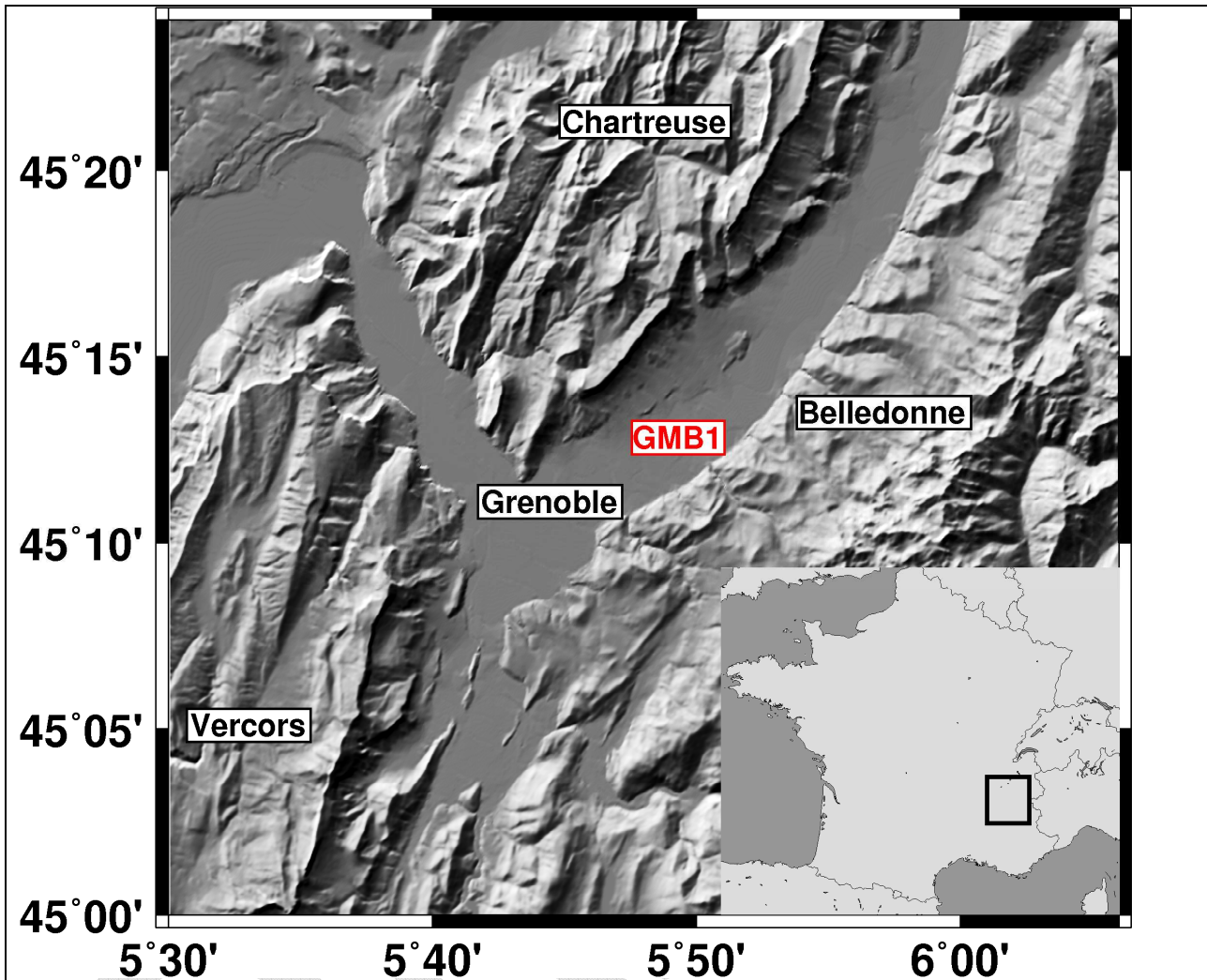


**Fig. 5.1** The 'Y'-shaped Grenoble valley surrounded by the Belledonne chain (crystalline, max. elevation approx. 3000m), and Vercors and Chartreuse (limestone massifs, max. elevation approx. 2000m). GMB1 indicates the location of the Montbonnot borehole (according to Chaljub et al. 2010).

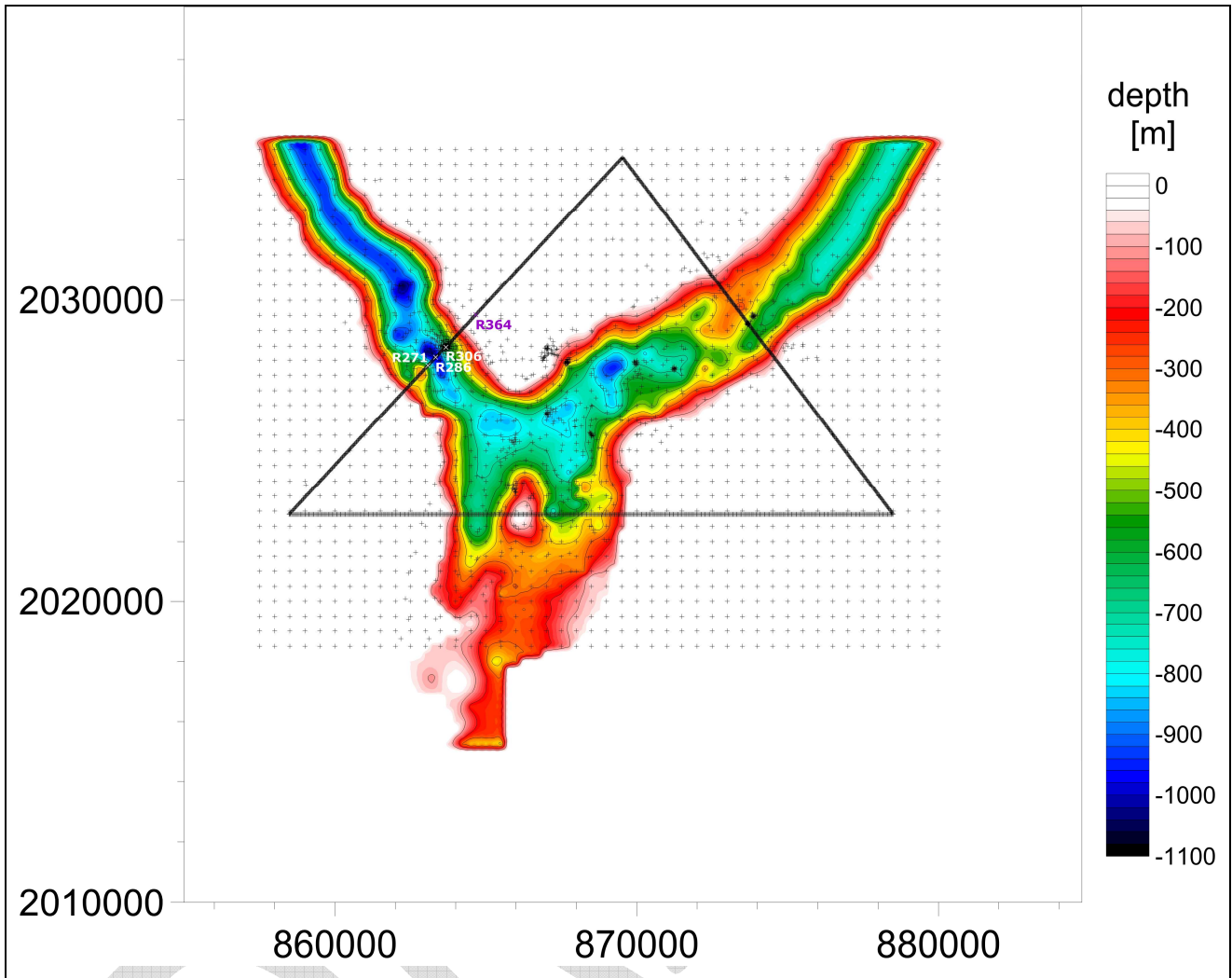



**Fig. 5.2** Thickness of sediments in the Grenoble valley. The + symbols indicate receiver positions specified for the final analysis. The black lines indicate three profiles selected for the final analysis.

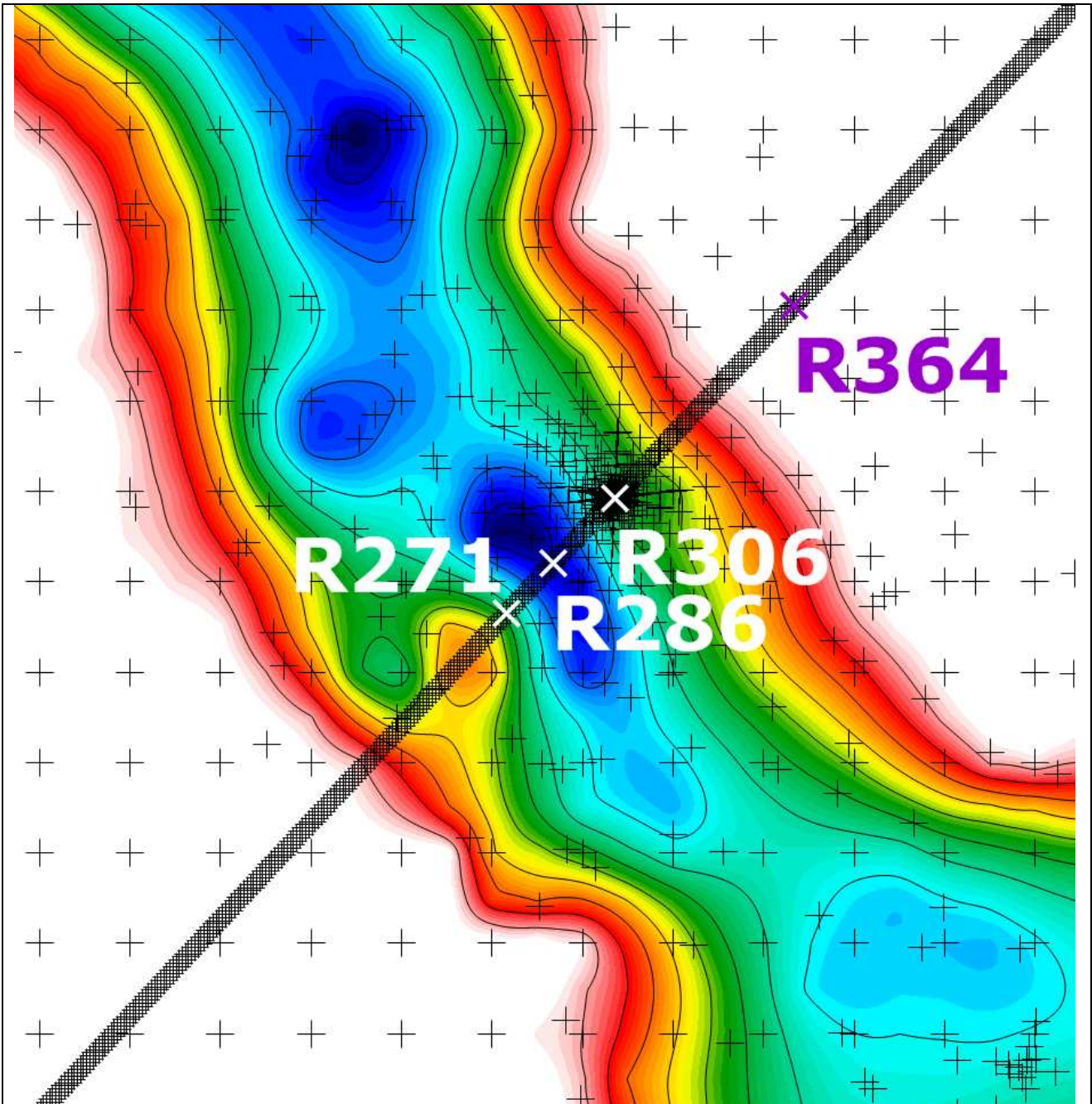


**Fig. 5.3** Detail of Fig. 5.2 showing the selected 2D profile with the four selected receivers.



	<p style="text-align: center;">Research and Development Programme on Seismic Ground Motion</p> <p style="text-align: center;">CONFIDENTIAL <i>Restricted to SIGMA scientific partners and members of the consortium, please do not pass around</i></p>	<p>Ref : SIGMA-2013-D3-97 Version : 01</p> <hr/> <p>Date : 21/10/2013 Page : 41</p>
--	--	---

### 5.3. Computational parameters

#### Space-time grid

The computational domain, a rectangular parallelepiped, is covered by a velocity-stress staggered grid. The grid spacing is 12.5 m. The grid is made of 1921 x 2001 x 104 grid cells. 50 grid spacings make the grid thickness of the PML boundary regions. The time step is 0.001 s. The used spatial grid means that the simulation should be sufficiently accurate up to 4 Hz. The simulated time window is 50 s. Computational time on IBM Power 755, 512 CPU cores: ~1000 minutes.

#### Material heterogeneity and attenuation

The true model geometry of the material interfaces as well as the smooth material heterogeneity inside the sedimentary body are accounted for in the evaluation of the effective material elastic and anelastic grid parameters as explained in Section 3.4. Here we just note that our scheme is capable to sense the true position of a material interface within the cell.


The so-called coarse grid graining (spatial distribution) of the anelastic properties is applied in the spatial discretization in order to increase computational efficiency. The  $Q$  values are specified at four frequencies - 0.04 Hz, 0.186 Hz, 0.862 Hz and 4.0 Hz. This should sufficiently accurately cover the frequency range of 0.04 – 4 Hz. The P- and S- wave speeds are specified at frequency of 1 Hz.

### 5.4. Illustrative numerical example

Here we show only selected characteristics of the simulated seismic motions – pseudoimpulse responses, amplification factors and average amplification factors. We also show selected accelerograms.

#### 5.4.1. Pseudoimpulse responses

Figures 5.1 – 5.4 (in Appendix) show the pseudoimpulse responses obtained by the 3D modelling. Each of the four figures relates to one of the four selected receivers. The top panel shows the pseudoimpulse response to the vertically incident wave polarized in the  $x$ -direction (West → East direction; EW component), that is,  $r_{xx}(t)$ ,  $r_{xy}(t)$  and  $r_{xz}(t)$ . The middle panel shows the pseudoimpulse response to the vertically incident wave polarized in the  $y$ -direction (South → North

	<p>Research and Development Programme on Seismic Ground Motion</p> <p>CONFIDENTIAL <i>Restricted to SIGMA scientific partners and members of the consortium, please do not pass around</i></p>	<p>Ref : SIGMA-2013-D3-97 Version : 01</p> <hr/> <p>Date : 21/10/2013 Page : 42</p>
--	--	---

direction; NS component), that is,  $r_{yx}(t)$ ,  $r_{yy}(t)$  and  $r_{yz}(t)$ . The bottom panel shows the pseudoimpulse response to the vertically incident wave polarized in the  $z$ -direction (vertical upward direction; UD component), that is,  $r_{zx}(t)$ ,  $r_{zy}(t)$  and  $r_{zz}(t)$ .

Figures 5.5 – 5.8 (in Appendix) show the pseudoimpulse responses obtained by the 2D modelling. Each of the four figures relates to one of the four selected receivers. The top panel shows the pseudoimpulse response to the vertically incident wave polarized in the  $x'$ -direction, that is,  $r_{x'x'}(t)$  and  $r_{x'z}(t)$ . The middle panel shows the pseudoimpulse response to the vertically incident wave polarized in the  $y'$ -direction, that is,  $r_{y'y'}(t)$ . The bottom panel shows the pseudoimpulse response to the vertically incident wave polarized in the  $z$ -direction (vertical upward direction; UD component), that is,  $r_{zx'}(t)$  and  $r_{zz}(t)$ .

Figures 5.9 – 5.12 (in Appendix) show the pseudoimpulse responses obtained by the 1D modelling. Each of the four figures relates to one of the four selected receivers. The upper panel shows the pseudoimpulse response to the vertically incident wave polarized in a horizontal direction, that is,  $r_h(t)$ . The lower panel shows the pseudoimpulse response to the vertically incident wave polarized in the  $z$ -direction (vertical upward direction; UD component), that is,  $r_z(t)$ .

#### 5.4.2. Selected accelerograms


Table 5.2 shows parameters of the 27 selected accelerograms. The accelerograms have been selected from the RESORCE database (Akkar et al. 2013) with the following criteria:

magnitude:	$4.5 < M < 7$
epicentral distance:	$\Delta < 20$ km
site class:	A
peak ground acceleration:	$PGA > 1$ m/s <sup>2</sup>

We considered those with all three components.

#### 5.4.3. Amplification factors

Figures 5.13 – 5.16 (in Appendix) show the amplification factors obtained using the 3D modelling for all 27 selected accelerograms. Each of the four figures relates to one of the four selected receivers. The upper left and right panels show the amplification factors for the  $x$  and  $y$

	<p>Research and Development Programme on Seismic Ground Motion</p> <p>CONFIDENTIAL <i>Restricted to SIGMA scientific partners and members of the consortium, please do not pass around</i></p>	<p>Ref : SIGMA-2013-D3-97 Version : 01</p> <hr/> <p>Date : 21/10/2013 Page : 43</p>
--	--	---

components, respectively. The lower left and right panels show the amplification factors for the  $z$  and  $h$  components, respectively. In each panel, the thick line shows the average amplification factor.


Figures 5.17 – 5.20 (in Appendix) show the amplification factors obtained using the 2D modelling for all 27 selected accelerograms. The structure of the figures is the same as that of Figs. 5.13 – 5.16. Similarly, Figures 5.21 – 5.24 (in Appendix) show the amplification factors obtained using the 1D modelling.

#### **5.4.4. Average amplification factors obtained from the 1D, 2D and 3D numerical simulations**

Figures 5.25 – 5.28 (in Appendix) show average the amplification factors obtained using the 3D, 2D and 1D modelling. Each of the four figures relates to one of the four selected receivers. Each panel relates to one of the four considered components ( $x$ ,  $y$ ,  $z$  and  $h$ ). Two thin red lines in each panel show the  $\pm$  standard deviation of the average amplification factor obtained using the 3D modelling.


DRAFT




	Research and Development Programme on Seismic Ground Motion	Ref : SIGMA-2013-D3-97 Version : 01
	CONFIDENTIAL <i>Restricted to SIGMA scientific partners and members of the consortium,          please do not pass around</i>	Date : 21/10/2013 Page : 44

**Tab. 5.2 Parameters of the selected accelerograms**

date time	event name	latitude [°]	longi- tude [°]	focal depth [km]	fault mech.	Mw	epic. dist. [km]	comp. orien.	Fmin [Hz]	Fmax [Hz]	PGA [m/s/s]
15.4.1978 23:33	Basso Tirreno, Italy	38.270	14.860	15	Strike- slip	6.1	18	NS	0.15	115	1.4963
								WE	0.15	100	1.2928
								UP	0.25	55	0.8048
11.5.1984 10:41	Lazio Abruzzo (Aftershock), Italy	41.732	13.921	8	Normal	5.5	15	NS	0.2	70	1.4662
								WE	0.18	55	0.8483
								UP	0.2	85	0.3771
11.5.1984 10:41	Lazio Abruzzo (Aftershock), Italy	41.732	13.921	8	Normal	5.5	6	NS	0.1	65	1.2035
								WE	0.1	999	1.2964
								UP	0.08	999	0.7148
6.10.1997 23:24	App. Umbro- Marchigiano, Italy	43.028	12.847	3.9	Normal	5.4	14	NS	0.2	999	1.4918
								WE	0.2	90	1.8444
								UP	0.12	90	0.7965
12.10.1997 11:08	App. Umbro- Marchigiano, Italy	42.906	12.920	0.1	Normal	5.2	10	NS	0.2	999	1.6841
								EW	0.2	999	1.5749
								UP	0.08	999	0.8181
14.10.1997 15:23	Umbria-Marche 3Rd Shock, Italy	42.898	12.899	7.3	Normal	5.6	12	NS	0.1	999	1.7626
								WE	0.1	75	0.9440
								UP	0.1	75	0.4363
5.4.1998 15:52	App. Umbro- Marchigiano, Italy	43.190	12.767	4.4	Normal	4.8	5	NS	0.3	90	0.9900
								WE	0.3	999	1.0084
								UP	0.2	999	0.6510
11.5.1984 13:14	Massiccio Meta, Italy	41.754	13.919	12.2	Normal	4.8	6	NS	0.4	105	1.0377
								WE	0.4	90	0.5837
								UP	0.2	100	0.3966
31.12.1988 4:07	Spitak (Aftershock), Armenia	40.950	43.990	5	Rever- se	4.2	10	NS	0.25	25	1.7342
								EW	0.25	25	1.0535
								UP	0.25	25	0.5543
30.3.1989 16:36	Spitak (Aftershock), Armenia	40.980	44.030	3	Rever- se	4.3	14	NS	0.25	25	2.0874
								EW	0.25	25	1.8723
								UP	0.25	25	1.2078
14.10.1997 15:23	Umbria-Marche 3Rd Shock, Italy	42.898	12.899	7.3	Normal	5.6	9	NS	0.25	25	3.3006
								EW	0.25	25	3.3339
								UP	0.25	25	1.5434
9.1.1988 1:02	Se Of Tirana, Albania	41.290	19.900	5	Rever- se	5.9	7	NS	0.15	20	1.1376
								EW	0.1	999	4.0476
								UP	0.15	999	0.6926
16.9.1977 23:48	Friuli, Italy	46.280	12.980	21	Rever- se	5.3	9	NS	0.3	125	1.0836
								WE	0.3	115	0.7924
								UP	0.3	150	0.4602

	<b>Research and Development Programme on Seismic Ground Motion</b>						<b>Ref : SIGMA-2013-D3-97 Version : 01</b>			
	<b>CONFIDENTIAL</b> <i>Restricted to SIGMA scientific partners and members of the consortium, please do not pass around</i>						<b>Date : 21/10/2013 Page : 45</b>			

11.5.1984 10:41	Lazio Abruzzo (Aftershock), Italy	41.732	13.921	8	Normal	5.5	13	NS	0.16	60	0.9106
								WE	0.19	100	1.7527
								UP	0.15	90	0.3495
3.4.1998 7:26	App. Umbro- Marchigiano, Italy	43.185	12.757	1.9	Normal	5.1	5	NS	0.19	85	1.1911
								WE	0.23	999	1.4762
								UP	0.45	85	1.1296
5.4.1998 15:52	App. Umbro- Marchigiano, Italy	43.190	12.767	4.4	Normal	4.8	8	NS	0.2	30	1.8187
								WE	0.2	30	1.9639
								UP	0.2	30	0.8030
28.2.1980 21:04	Val Nerina, Italy	42.800	12.967	12	--	5	6	NS	0.2	20	0.7379
								WE	0.2	20	1.2879
								UP	0.2	20	0.6606
9.9.1998 11:28	App. Lucano, Italy	40.060	15.949	29.2	Normal	5.6	10	NS	0.7	35	1.6584
								WE	0.7	35	1.5846
								UP	0.7	35	0.6383
1.4.2000 18:08	Monte Amiata, Italy	42.831	11.692	1.6	Normal	4.5	2	NS	0.5	50	1.5024
								WE	0.5	999	1.4742
								UP	0.6	999	0.9390
1.4.2000 18:08	Monte Amiata, Italy	42.831	11.692	1.6	Normal	4.5	2	NS	0.4	60	1.4652
								WE	0.4	65	0.6824
								UP	0.4	60	1.1572
26.11.2001 0:56	Casentino, Italy	43.600	12.109	5.5	Normal	4.7	3	NS	0.5	70	1.3966
								WE	0.5	55	0.6648
								UP	0.5	55	0.6565
6.4.2009 2:37	L'Aquila, Italy	42.366	13.340	10.1	Normal	5.1	2	NS	0.1	40	3.3576
								WE	0.1	40	0.9982
								UP	0.1	40	0.9886
7.4.2009 17:47	L'Aquila, Italy	42.275	13.464	15.1	Normal	5.6	15	NS	0.1	999	1.2117
								WE	0.1	35	0.9104
								UP	0.1	50	0.5593
7.4.2009 17:47	L'Aquila, Italy	42.275	13.464	15.1	Normal	5.6	10	NS	0.1	999	1.6337
								WE	0.1	999	2.2957
								UP	0.1	999	0.9851
7.4.2009 21:34	L'Aquila, Italy	42.380	13.376	7.4	Normal	4.6	2	NS	0.1	70	2.4658
								WE	0.1	999	1.3006
								UP	0.1	999	0.8176
9.4.2009 0:52	Gran Sasso, Italy	42.484	13.343	15.4	Normal	5.4	9	NS	0.07	999	1.4304
								WE	0.07	999	1.0305
								UP	0.07	999	0.4249
9.4.2009 19:38	L'Aquila, Italy	42.501	13.356	17.2	Normal	5.3	10	NS	0.07	999	1.0795
								WE	0.07	999	0.8962
								UP	0.07	999	0.6711

	<p style="text-align: center;">Research and Development Programme on Seismic Ground Motion</p> <p style="text-align: center;">CONFIDENTIAL <i>Restricted to SIGMA scientific partners and members of the consortium, please do not pass around</i></p>	<p>Ref : SIGMA-2013-D3-97 Version : 01</p> <hr/> <p>Date : 21/10/2013 Page : 46</p>
--	--	---

## 6. Conclusions

We presented methodology of the

- 3D, 2D and 1D numerical modelling of seismic motion in surface local sedimentary structures,
- evaluation of site characteristics of seismic motion.


For the purpose of the intended investigations we have developed new codes for 2D and 1D simulations – they are directly derived from the code for the 3D simulations. Consequently, the 3D, 2D and 1D simulations are methodologically and algorithmically consistent, and, moreover make the modelling computationally efficient.

We also presented an illustrative example of numerical simulations and evaluation of site characteristics for four selected receiver positions along the selected profile in the Grenoble valley.


We think that we are ready for the extensive numerical simulations and systematic investigations aiming in finding answers to questions formulated in the introduction.

## 7. References


- Akkar, S., M. A. Sandikkaya, M. Senyurt, A. Azari Sisi, B. O Ay, P. Traversa, J. Douglas, F. Cotton, L. Luzi, B. Hernandez, S. Godey 2013. Reference database for seismic ground-motion in Europe - (RESORCE). *Bull. Earthquake Eng.* DOI 10.1007/s10518-013-9506-8.
- Chaljub, E., P. Moczo, S. Tsuno, P.-Y. Bard, J. Kristek, M. Käser, M. Stupazzini, M. Kristekova 2010. Quantitative comparison of four numerical predictions of 3D ground motion in the Grenoble Valley, France. *Bull. Seism. Soc. Am.* 100, 1427-1455.
- Cornou, C. (2002). Traitement d'antenne et imagerie sismique dans l'agglomération grenobloise (Alpes Françaises): Implications pour les effets de site, Ph.D. Thesis, (260 pages, [www-igut.obs.ujf-grenoble.fr/~cornouc/PUBLIS\\_CECILE/These\\_Version\\_Finale\\_Cecile.pdf](http://www-igut.obs.ujf-grenoble.fr/~cornouc/PUBLIS_CECILE/These_Version_Finale_Cecile.pdf)), *Joseph Fourier University, Grenoble* (in French).
- Coutant, O., J. Virieux, A. Zollo 1995. Numerical source implementation in a 2D finite-difference scheme for wave propagation. *Bull. Seism. Soc. Am.* 85, 1507-1512.
- Emmerich, H., M. Korn 1987. Incorporation of attenuation into time-domain computations of seismic wave fields. *Geophysics* 52, 1252-1264.

	<p style="text-align: center;">Research and Development Programme on Seismic Ground Motion</p> <p style="text-align: center;">CONFIDENTIAL <i>Restricted to SIGMA scientific partners and members of the consortium, please do not pass around</i></p>	<p>Ref : SIGMA-2013-D3-97 Version : 01</p> <hr/> <p>Date : 21/10/2013 Page : 47</p>
--	--	---

- Graves, R. W. 1996. Simulating seismic wave propagation in 3D elastic media using staggered-grid finite differences. *Bull. Seism. Soc. Am.* 86, 1091-1106.
- Graves, R. W., S. M. Day 2003. Stability and accuracy analysis of coarse-grain viscoelastic simulations. *Bull. Seism. Soc. Am.* 93, 283-300.
- Kristek, J., P. Moczo 2003. Seismic-wave propagation in viscoelastic media with material discontinuities: A 3D fourth-order staggered-grid finite-difference modeling. *Bull. Seism. Soc. Am.* 93, 2273-2280.
- Kristek, J., P. Moczo, R. J. Archuleta 2002. Efficient methods to simulate planar free surface in the 3D 4th-order staggered-grid finite-difference schemes. *Studia Geoph. Geod.* 46, 355-381.
- Kristek, J., P. Moczo, M. Galis 2009. A brief summary of some PML formulations and discretizations for the velocity-stress equation of seismic motion. *Studia Geoph. Geod.* 53, 459-474.
- Kristek, J., P. Moczo, M. Galis 2010. Stable discontinuous staggered grid in the finitedifference modelling of seismic motion. *Geophys. J. Int.* 183, 1401-1407.
- Lebrun, B., D. Hatzfeld, and P. Y. Bard (2001). Site effect study in urban area: Experimental results in Grenoble (France), *Pure Appl. Geophys.* 158, 2543–2557.
- Levander, A. R. 1988. Fourth-order finite-difference P-SV seismograms. *Geophysics* 53, 1425-1436.
- Liu, P., R. J. Archuleta 2006. Efficient modeling of Q for 3D numerical simulation of wave propagation. *Bull. Seism. Soc. Am.* 96, 1352-1358.
- Moczo, P., E. Bystrický, J. Kristek, J. M. Carcione, M. Bouchon 1997. Hybrid modeling of SV seismic motion at inhomogeneous viscoelastic topographic structures. *Bull. Seism. Soc. Am.* 87, 1305-1323.
- Moczo, P., J. Kristek 2005. On the rheological models used for time-domain methods of seismic wave propagation. *Geophys. Res. Lett.* 32, L01306.
- Moczo, P., J. Kristek, M. Galis 2004. Simulation of the planar free surface with near-surface lateral discontinuities in the finite-difference modeling of seismic motion. *Bull. Seism. Soc. Am.* 94, 760-768.
- Moczo, P., J. Kristek, M. Galis 2014 (in press). The finite-difference modelling of earthquake motions: Waves and ruptures. *Cambridge University Press*.

	<p>Research and Development Programme on Seismic Ground Motion</p> <p>CONFIDENTIAL <i>Restricted to SIGMA scientific partners and members of the consortium, please do not pass around</i></p>	<p>Ref : SIGMA-2013-D3-97 Version : 01</p> <p>Date : 21/10/2013 Page : 48</p>
--	--	---

- Moczo, P., J. Kristek, M. Galis, E. Chaljub, V. Etienne 2011. 3-D finite-difference, finite-element, discontinuous-Galerkin and spectral-element schemes analysed for their accuracy with respect to P-wave to S-wave speed ratio. *Geophys. J. Int.* 187, 1645-1667.
- Moczo, P., J. Kristek, M. Galis, P. Pažák, M. Balažovjeh 2007a. The finite-difference and finite-element modeling of seismic wave propagation and earthquake motion. *Acta Physica Slovaca* 57, 177-406.
- Moczo, P., J. Kristek, L. Halada 2000. 3D fourth-order staggered-grid finite-difference schemes: Stability and grid dispersion. *Bull. Seism. Soc. Am.* 90, 587-603.
- Moczo, P., J. Kristek, V. Vavryčuk, R. J. Archuleta, L. Halada 2002. 3D heterogeneous staggered-grid finite-difference modeling of seismic motion with volume harmonic and arithmetic averaging of elastic moduli and densities. *Bull. Seism. Soc. Am.* 92, 3042-3066.
- Moczo, P., J. O. A. Robertsson, L. Eisner 2007b. The finite-difference time-domain method for modeling of seismic wave propagation. In R.-S. Wu, V. Maupin (eds.), *Advances in wave propagation in heterogeneous Earth*, 421-516. *Advances in Geophysics* Vol. 48, R. Dmowska (ed.), Elsevier - Academic Press.
- Rodrigues, D. 1993. Large scale modelling of seismic wave propagation. PhD. Thesis. *École Centrale Paris*.
- Virieux, J. 1986. P-SV wave propagation in heterogeneous media; velocity-stress finite-difference method. *Geophysics* 51, 889-901.

	<p>Research and Development Programme on Seismic Ground Motion</p> <p>CONFIDENTIAL <i>Restricted to SIGMA scientific partners and members of the consortium, please do not pass around</i></p>	<p>Ref : SIGMA-2013-D3-97 Version : 01</p> <p>Date : 21/10/2013 Page : 49</p>
--	--	---

## 8. Appendix

Figures of the pseudoimpulse responses, amplification factors and average amplification factors at four selected receiver positions along the selected 2D profile.

DRAFT

# 3D pseudoimpulse responses

inc. w.

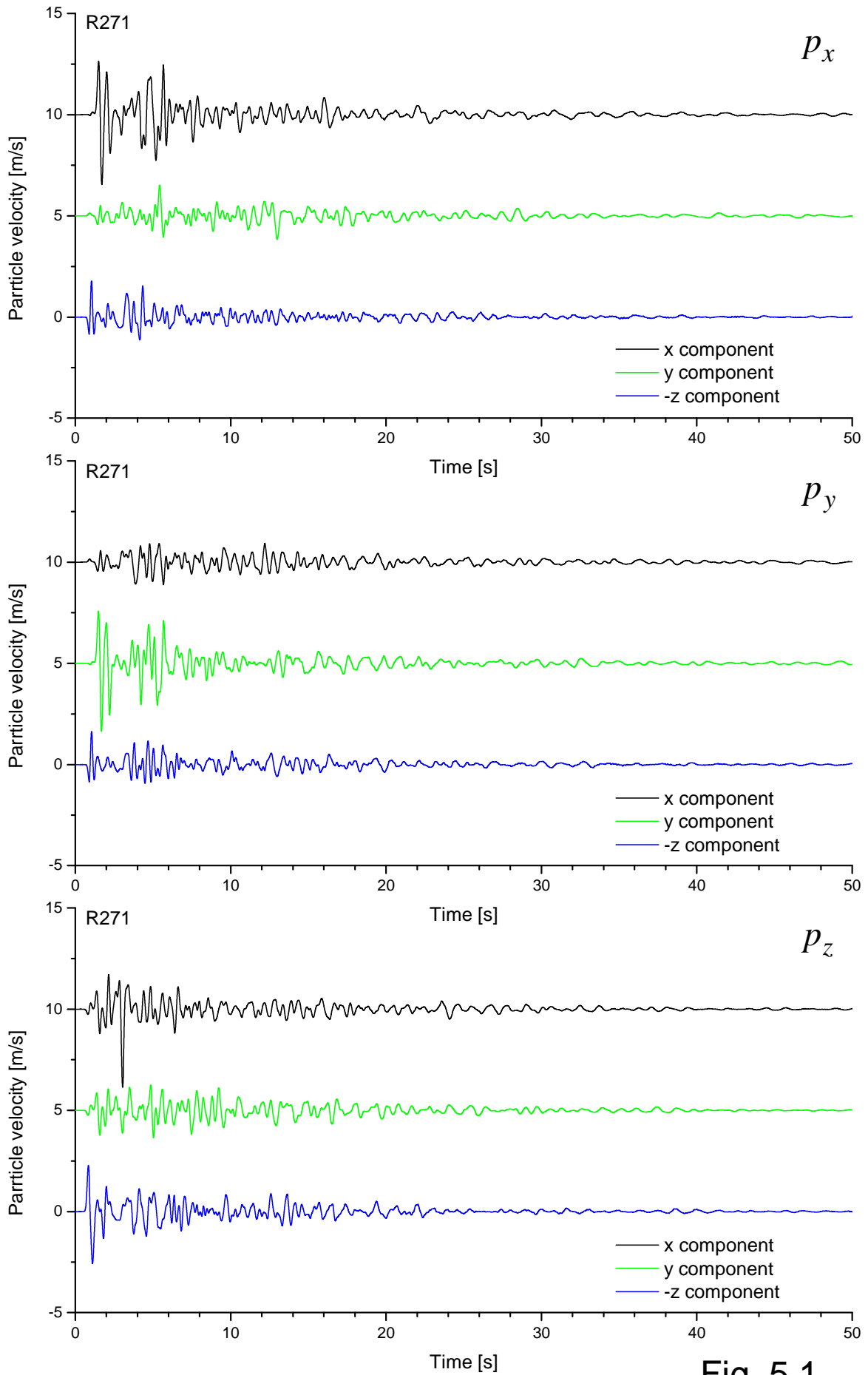


Fig. 5.1



# 3D pseudoimpulse responses

inc. w.

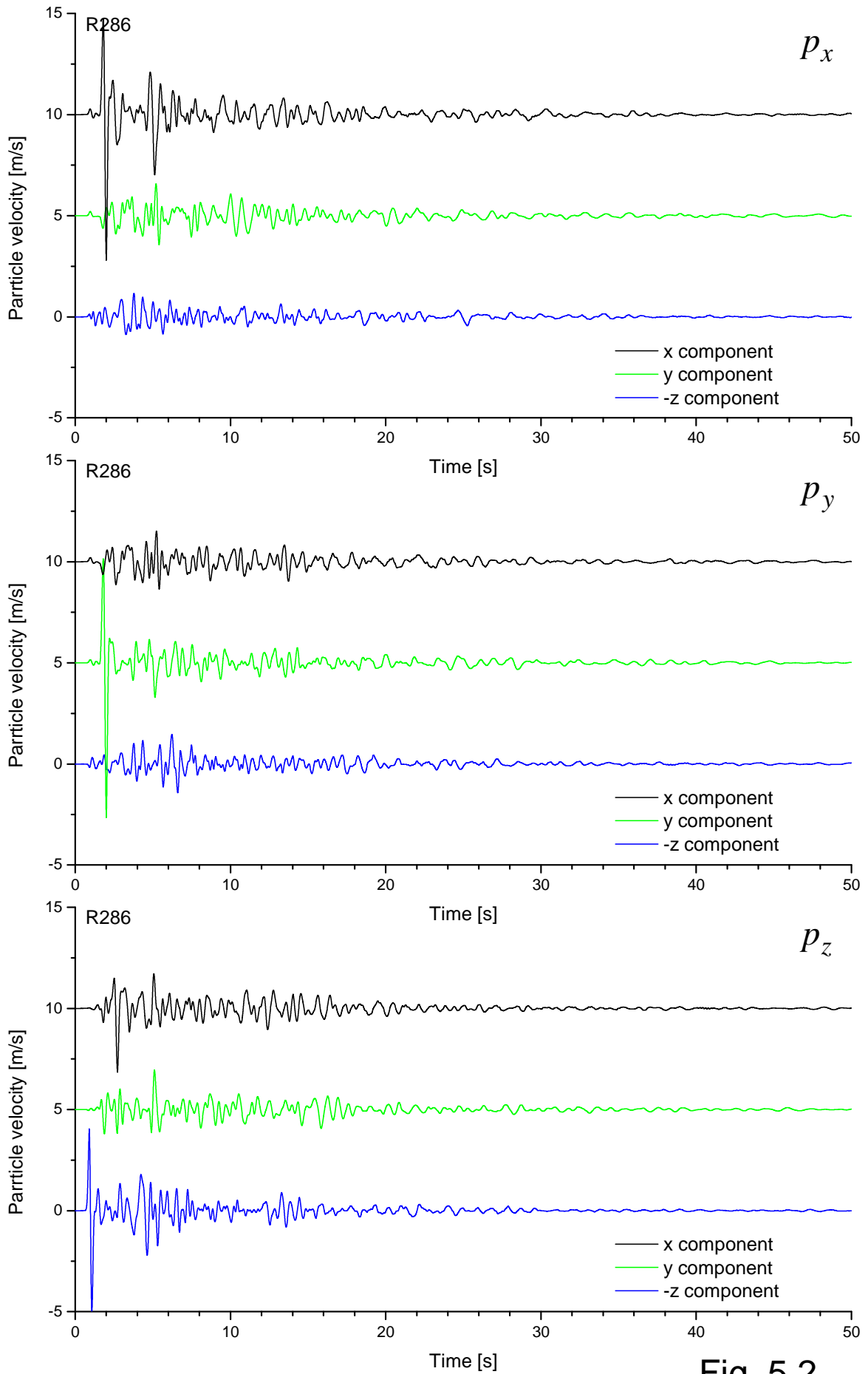


Fig. 5.2

# 3D pseudoimpulse responses

inc. w.

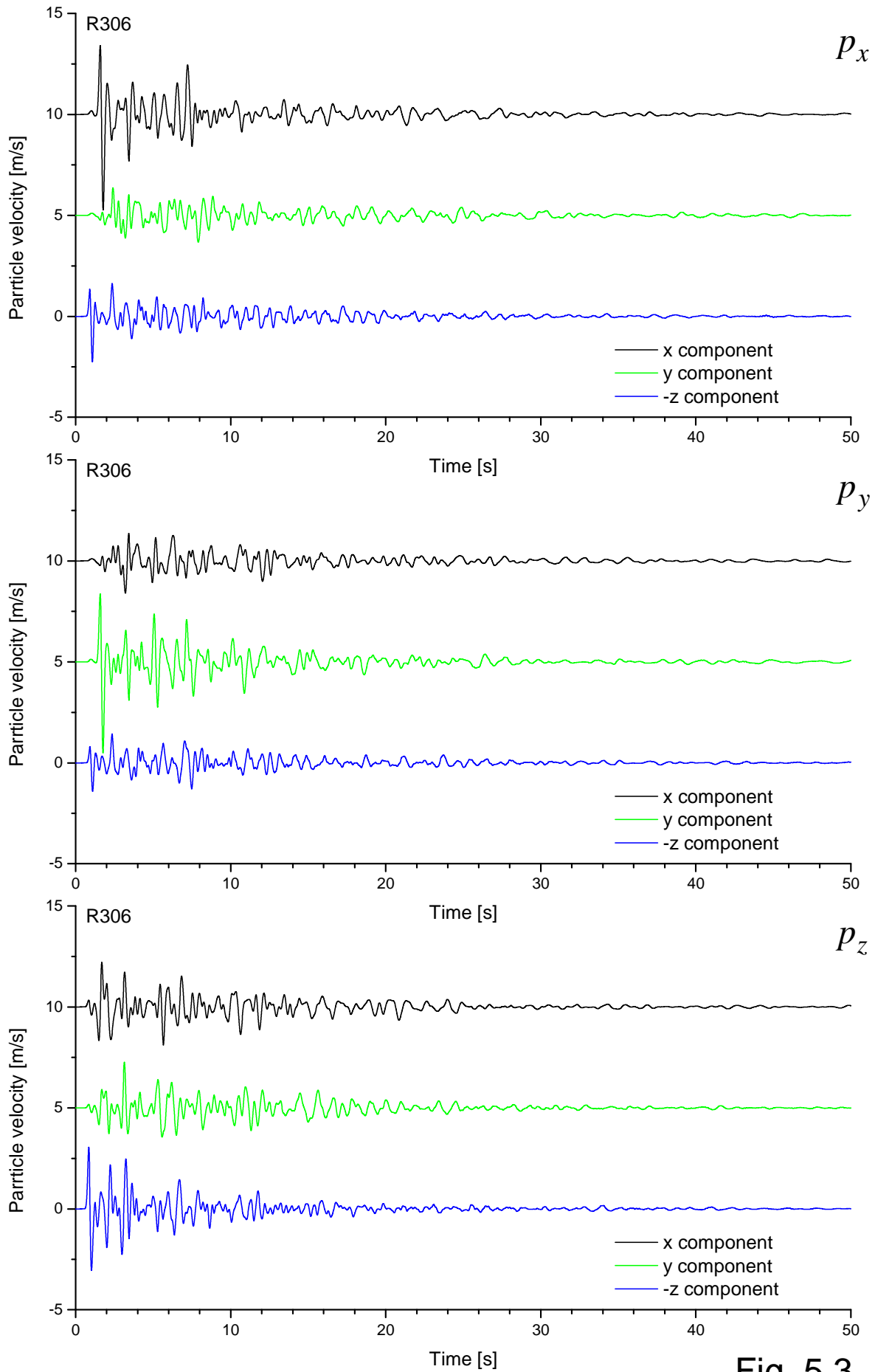


Fig. 5.3

# 3D pseudoimpulse responses

inc. w.

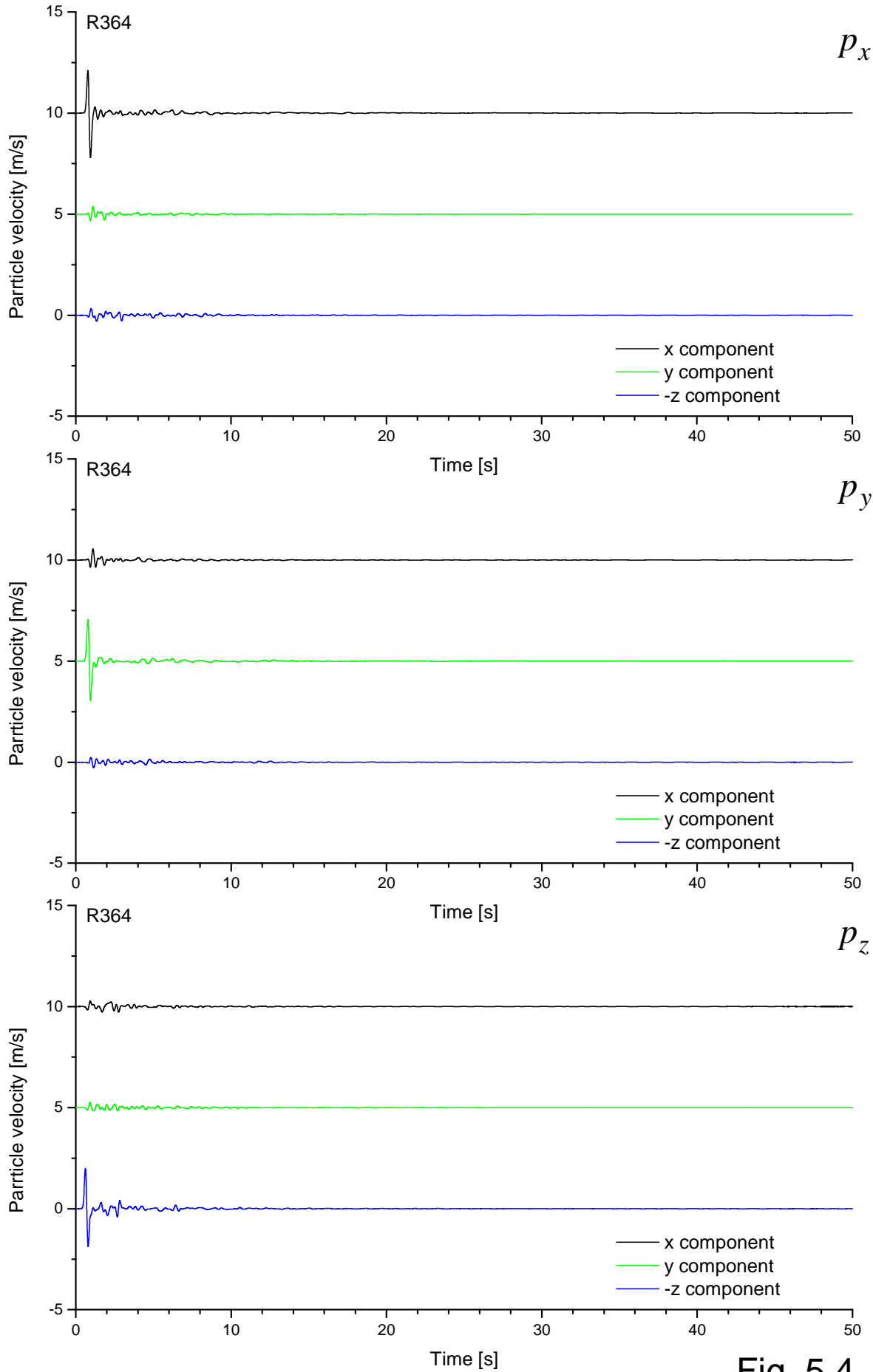


Fig. 5.4

# 2D pseudoimpulse responses

inc. w.

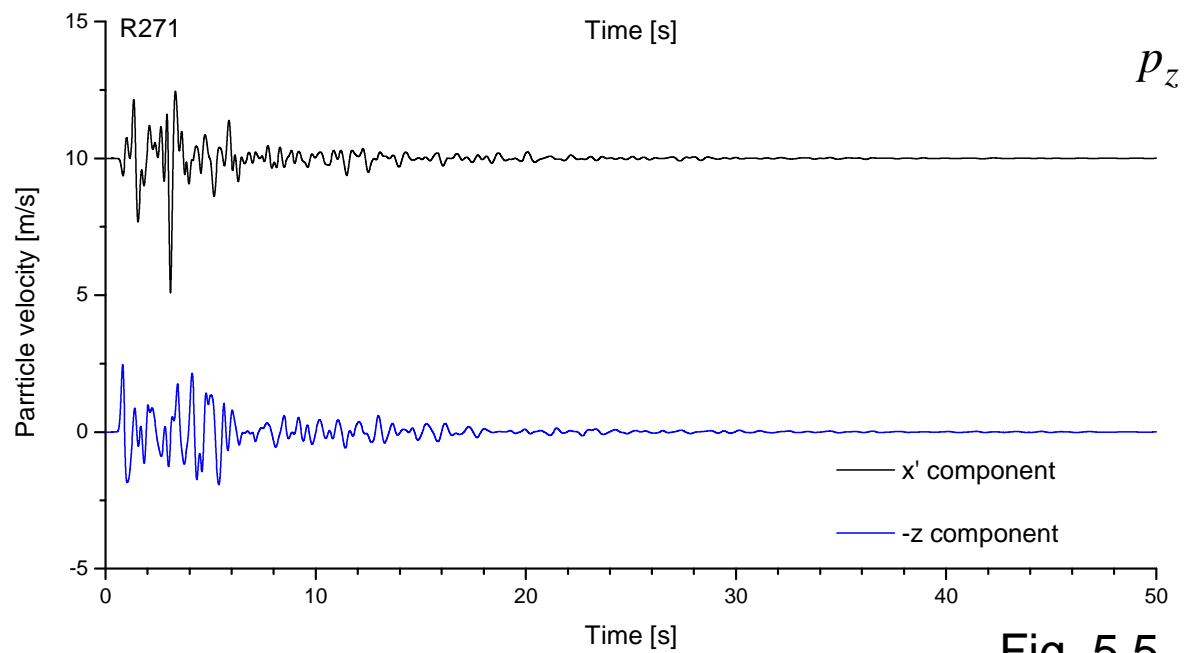
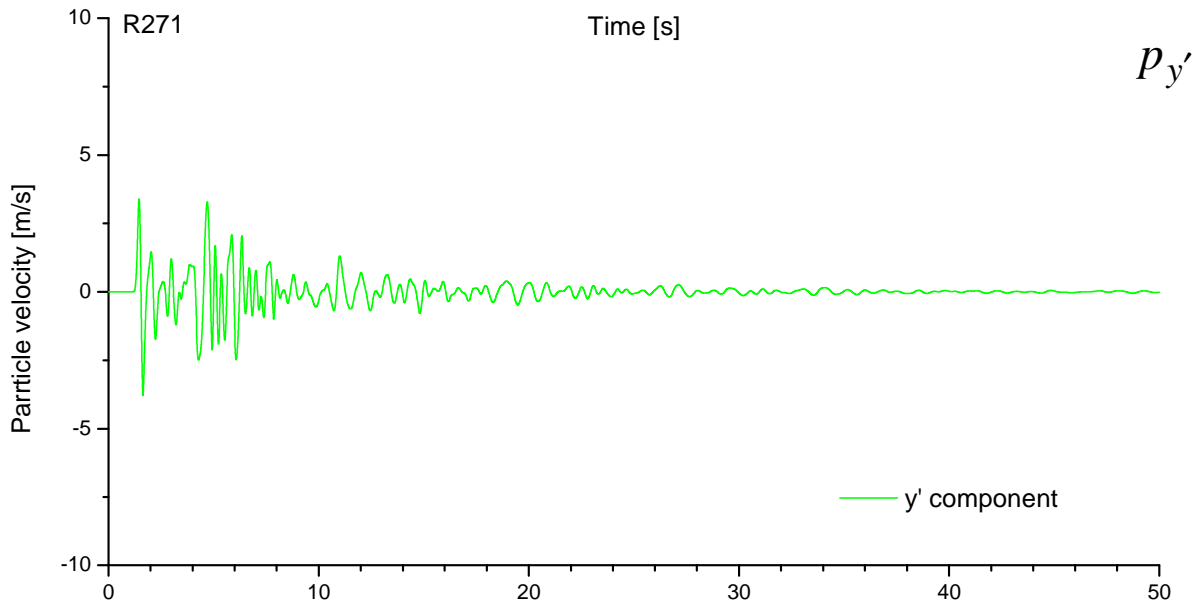
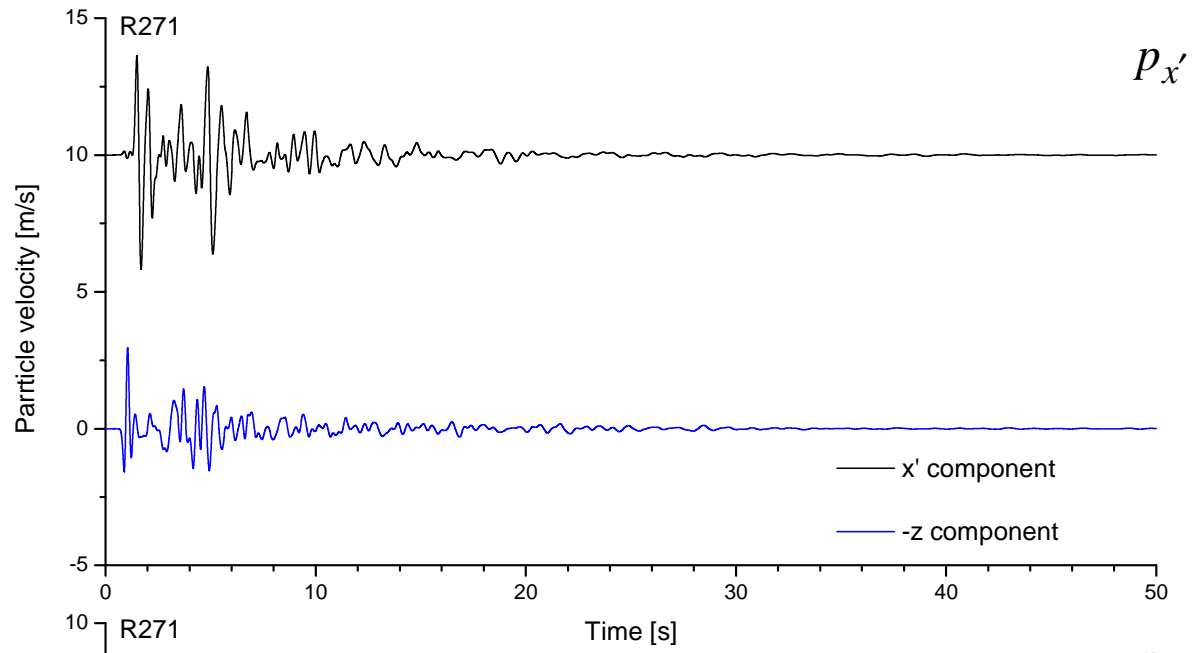
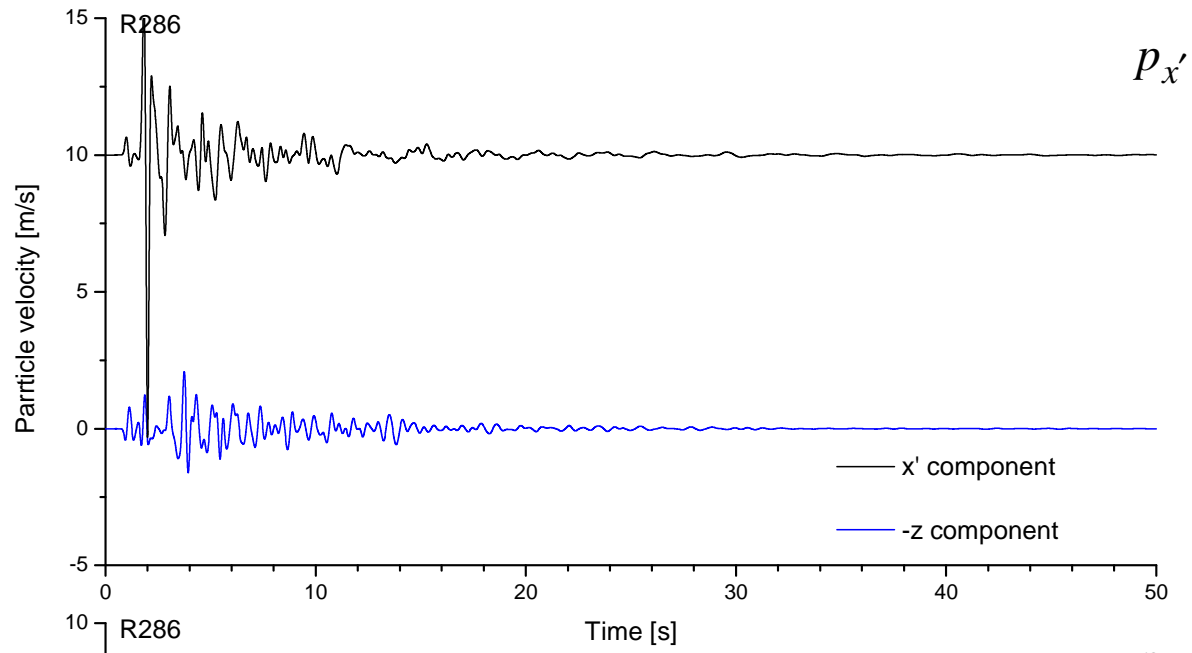


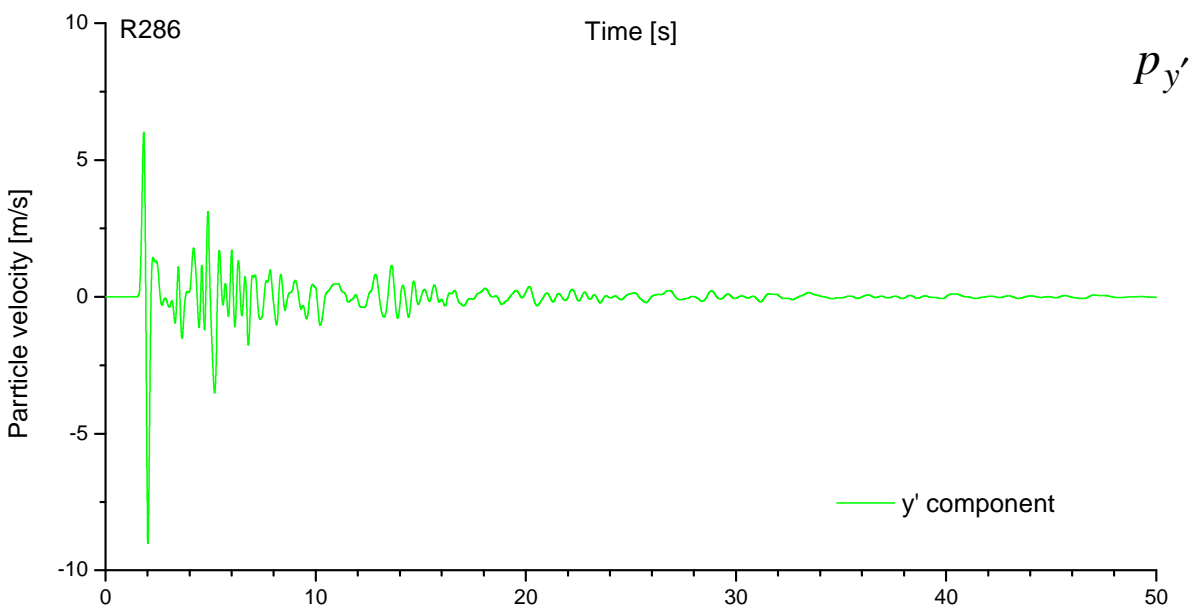
Fig. 5.5

# 2D pseudoimpulse responses

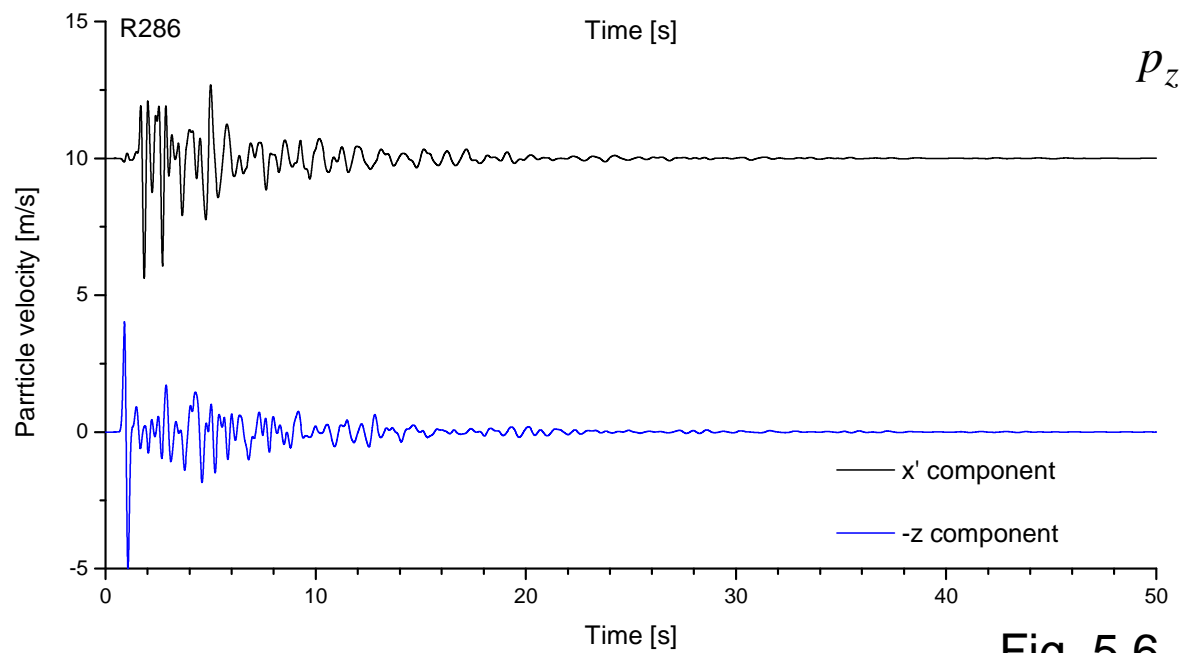
inc. w.



$P_{x'}$



$P_{y'}$



$P_{z}$

Fig. 5.6

# 2D pseudoimpulse responses

inc. w.

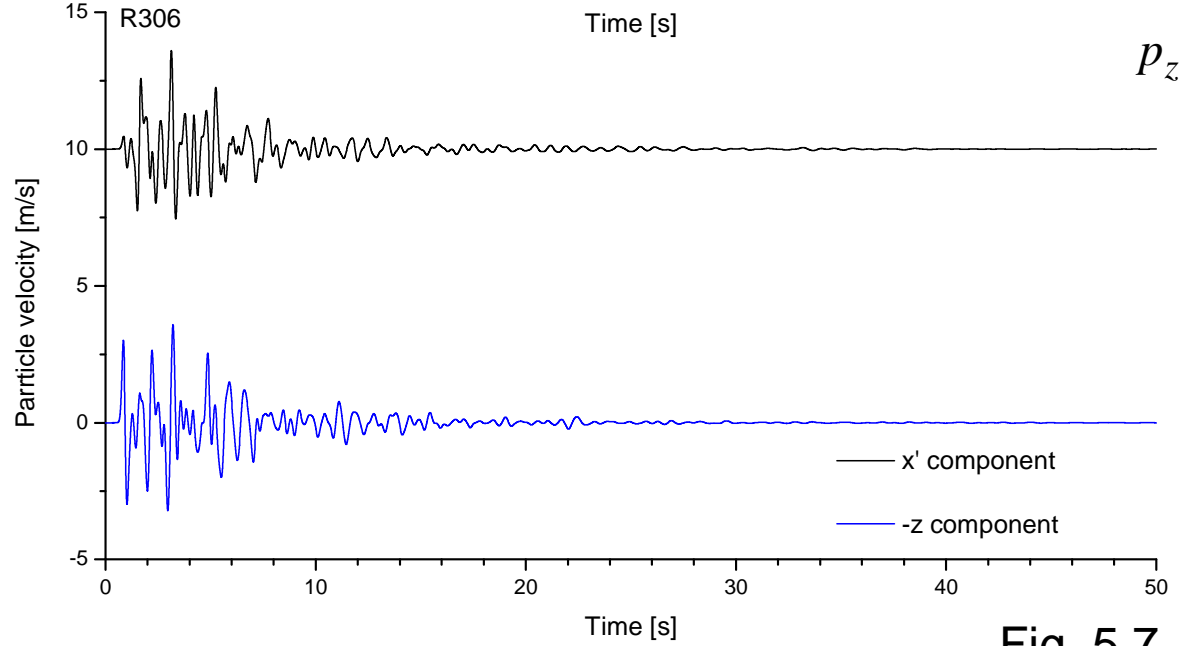
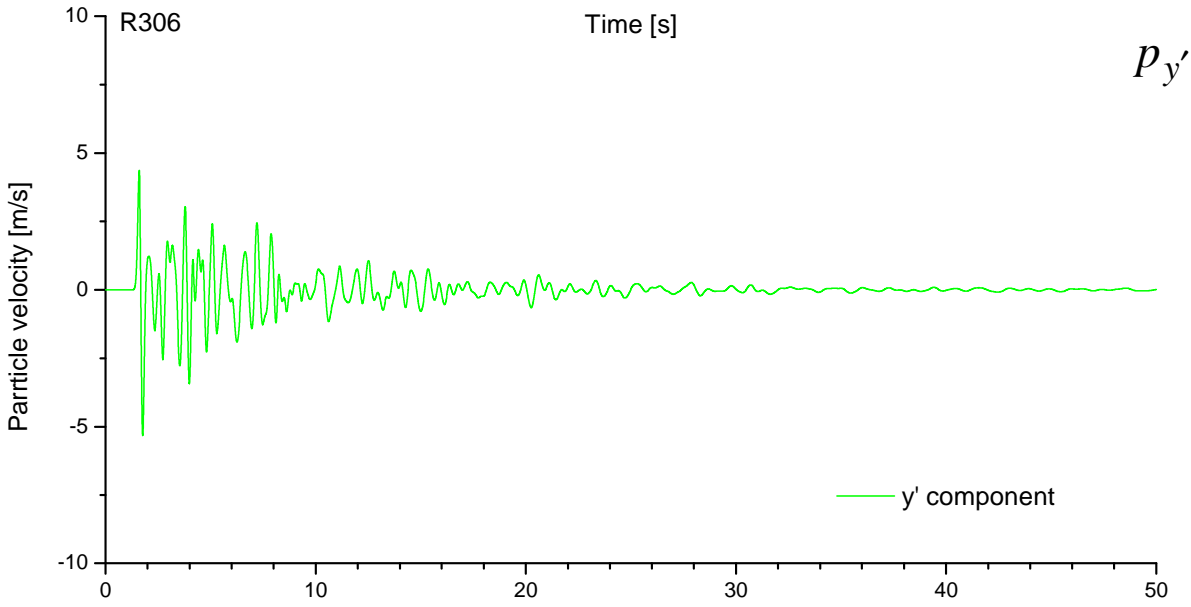
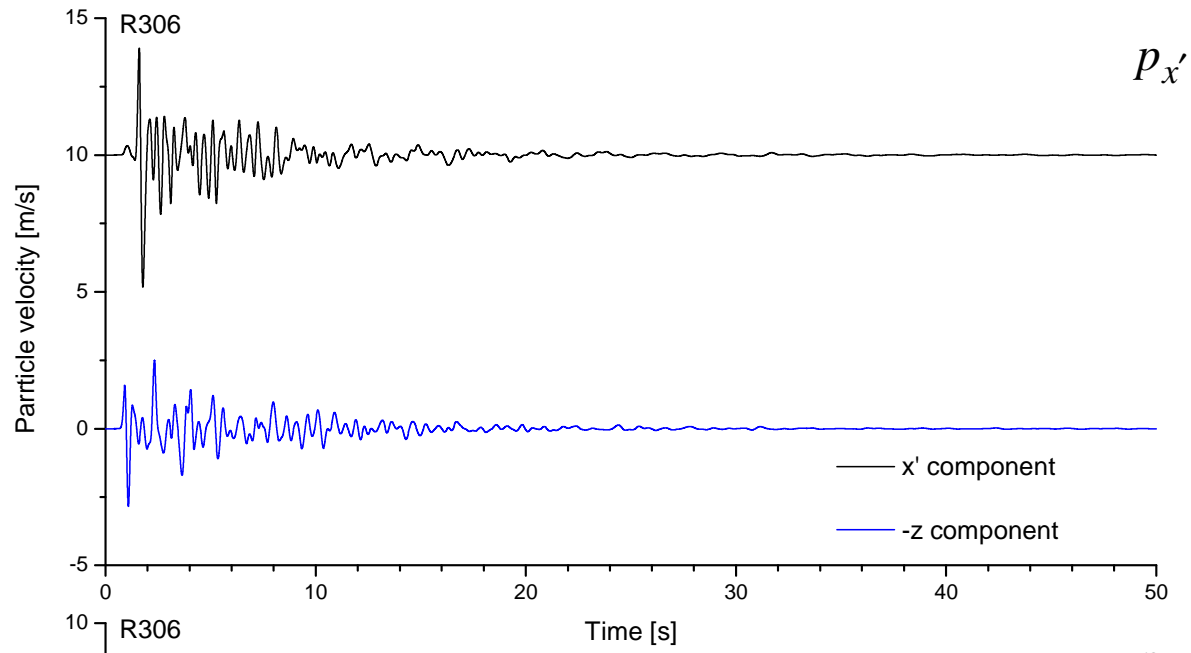


Fig. 5.7

# 2D pseudoimpulse responses

inc. w.

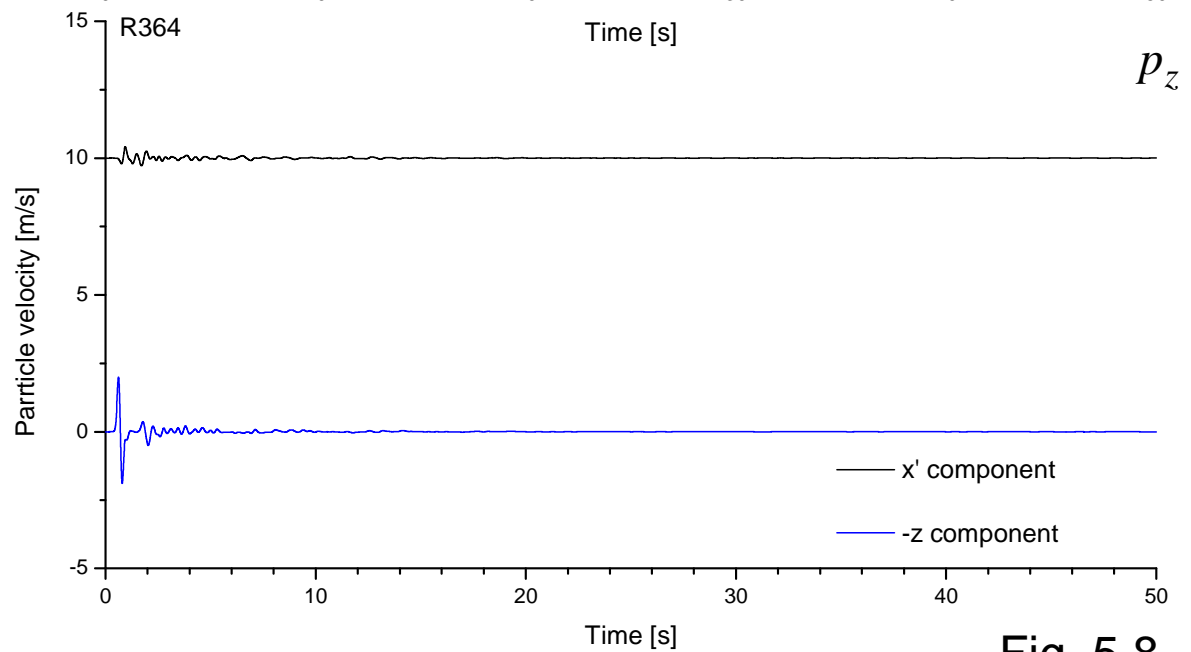
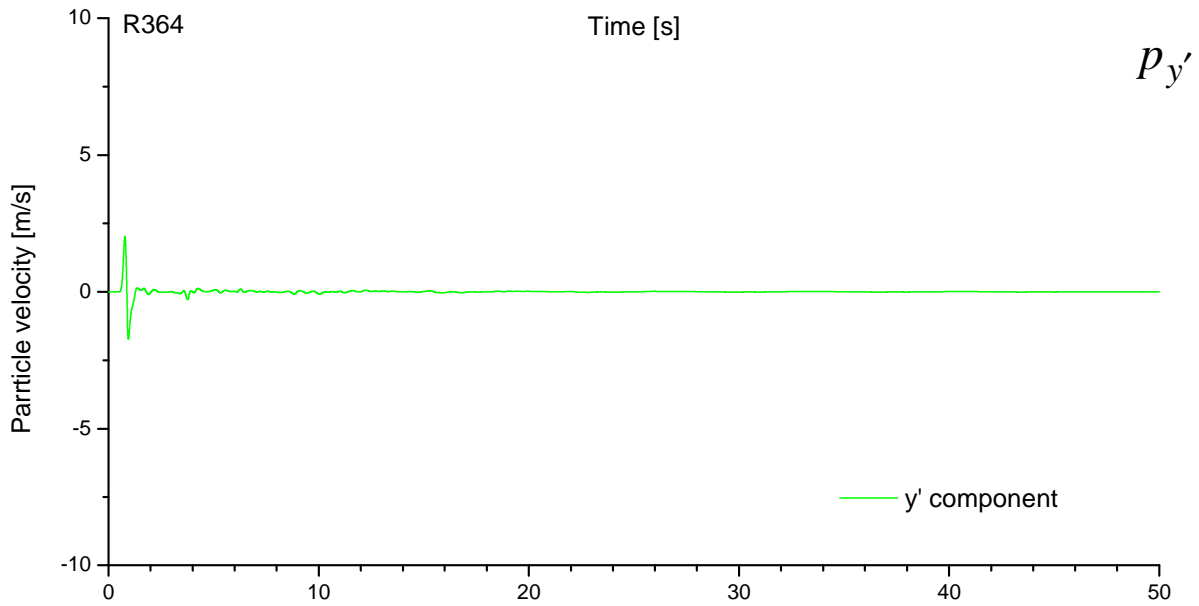
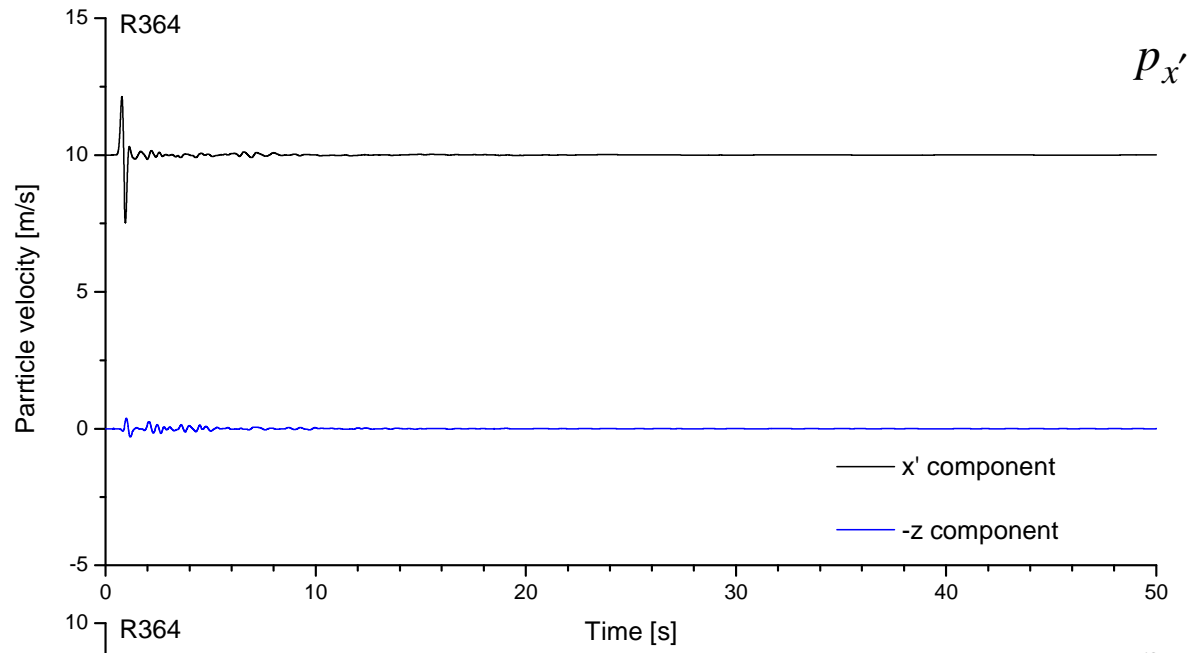


Fig. 5.8



# 1D pseudoimpulse responses

inc. w.

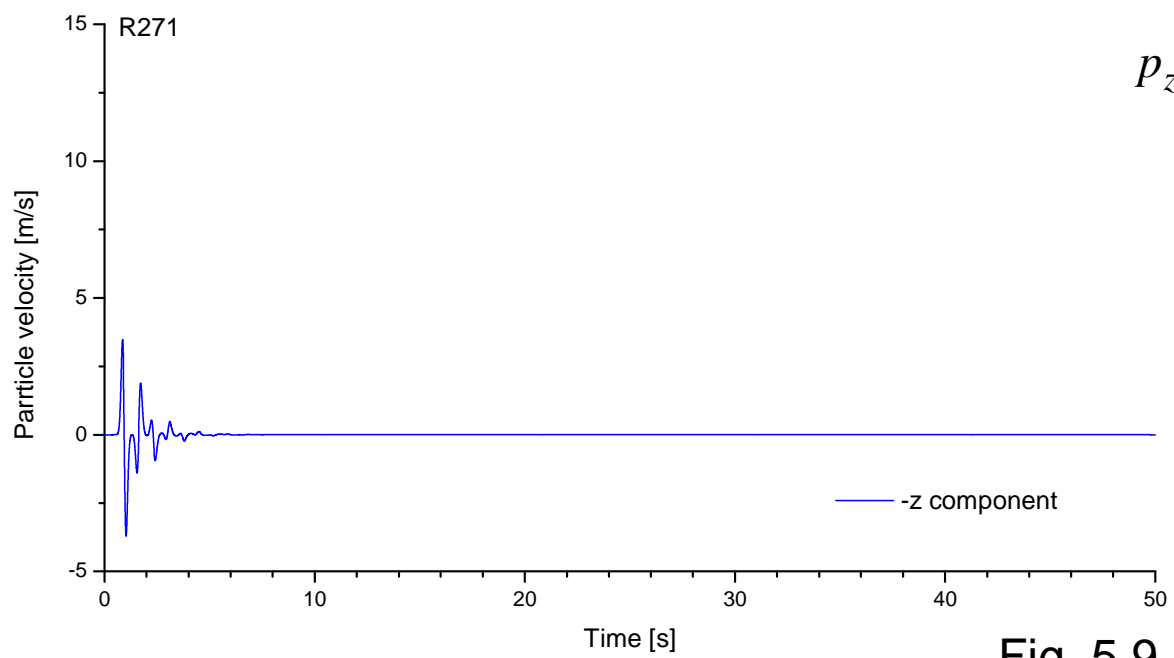
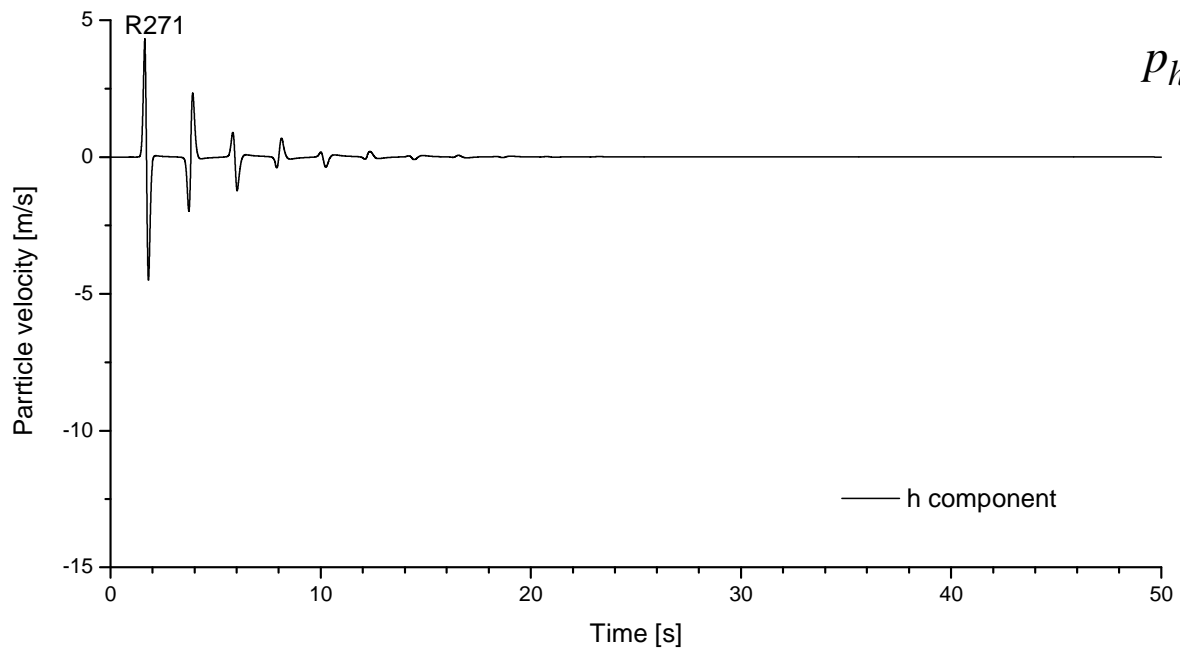


Fig. 5.9

# 1D pseudoimpulse responses

inc. w.

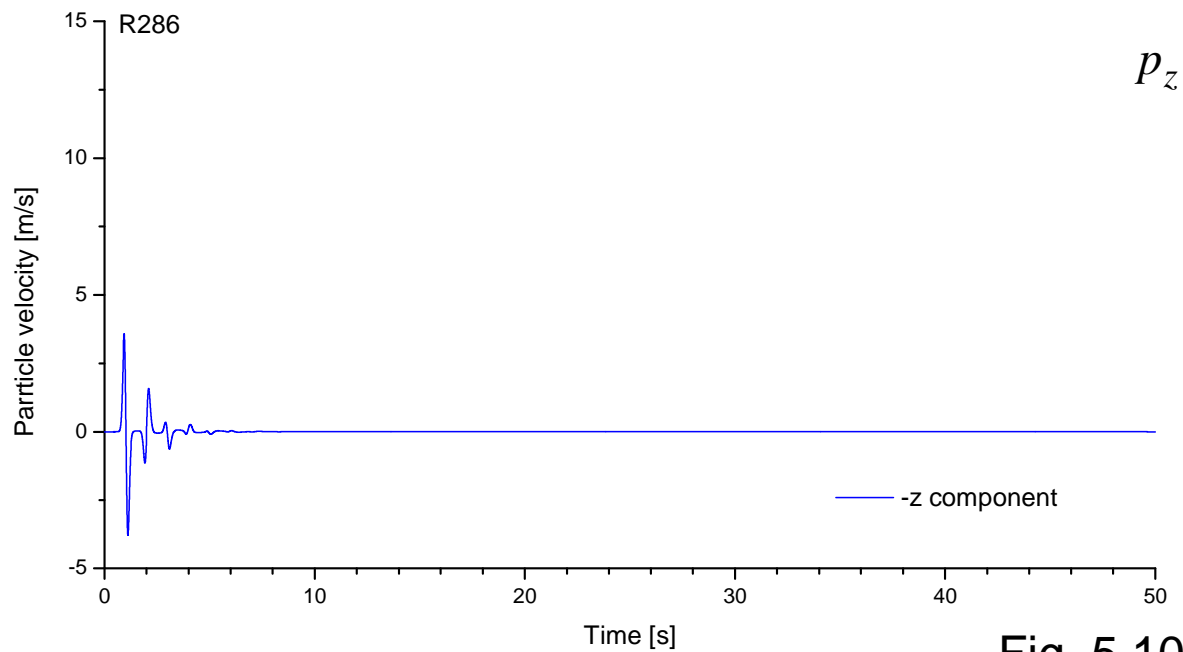
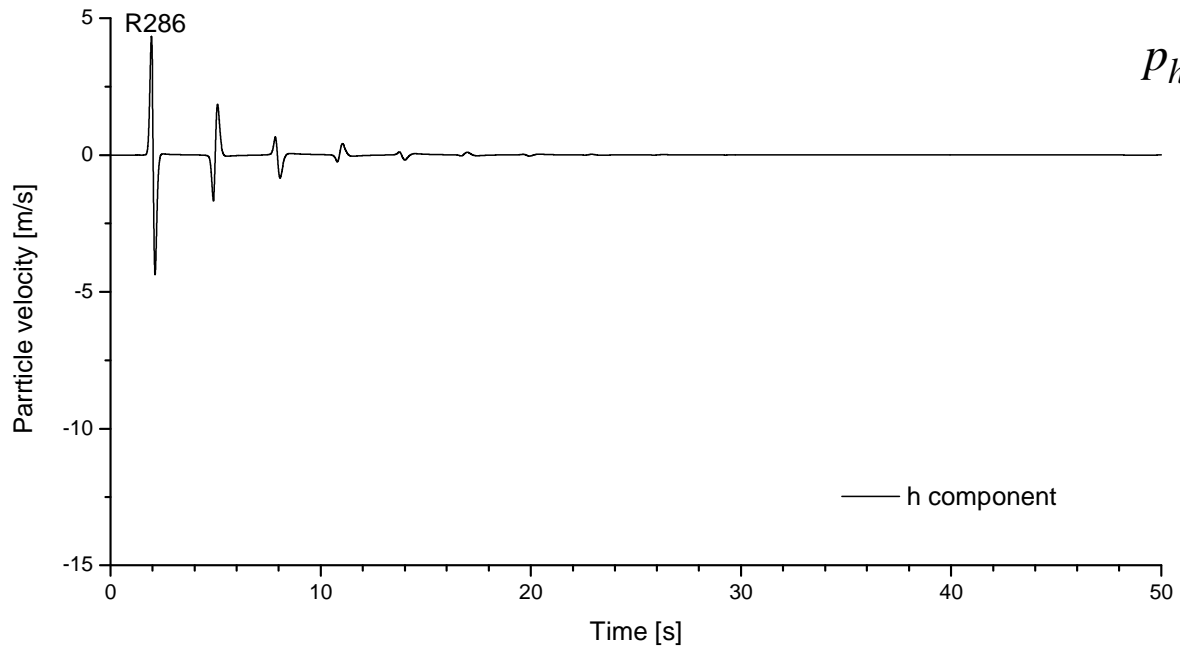


Fig. 5.10

# 1D pseudoimpulse responses

inc. w.

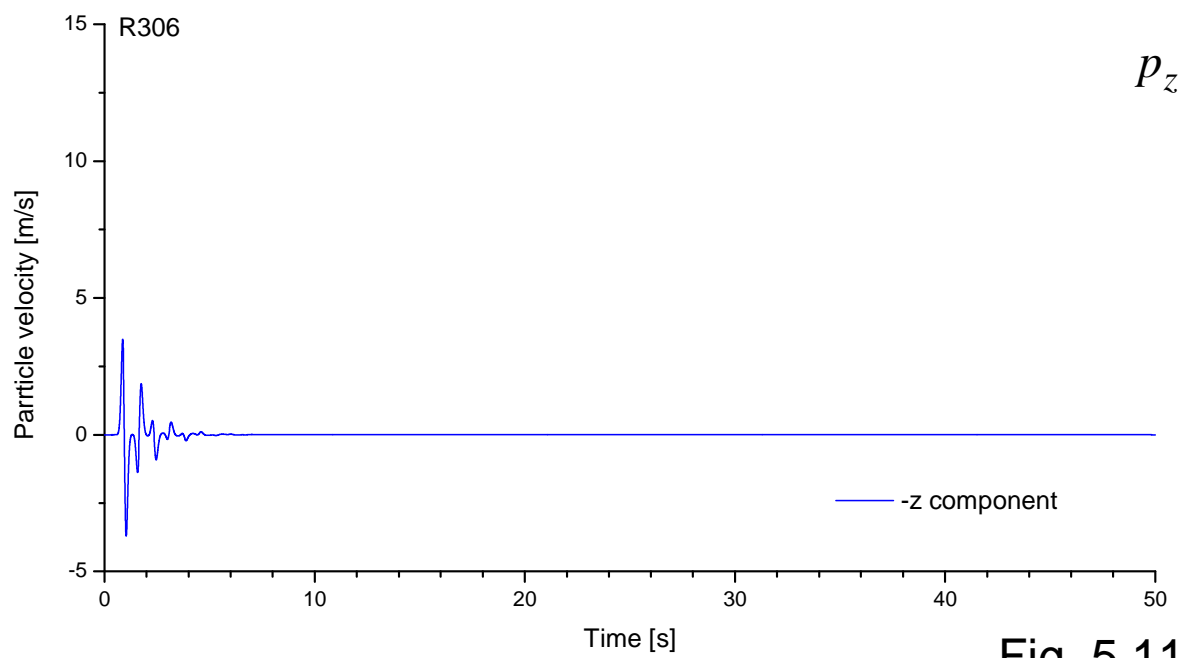
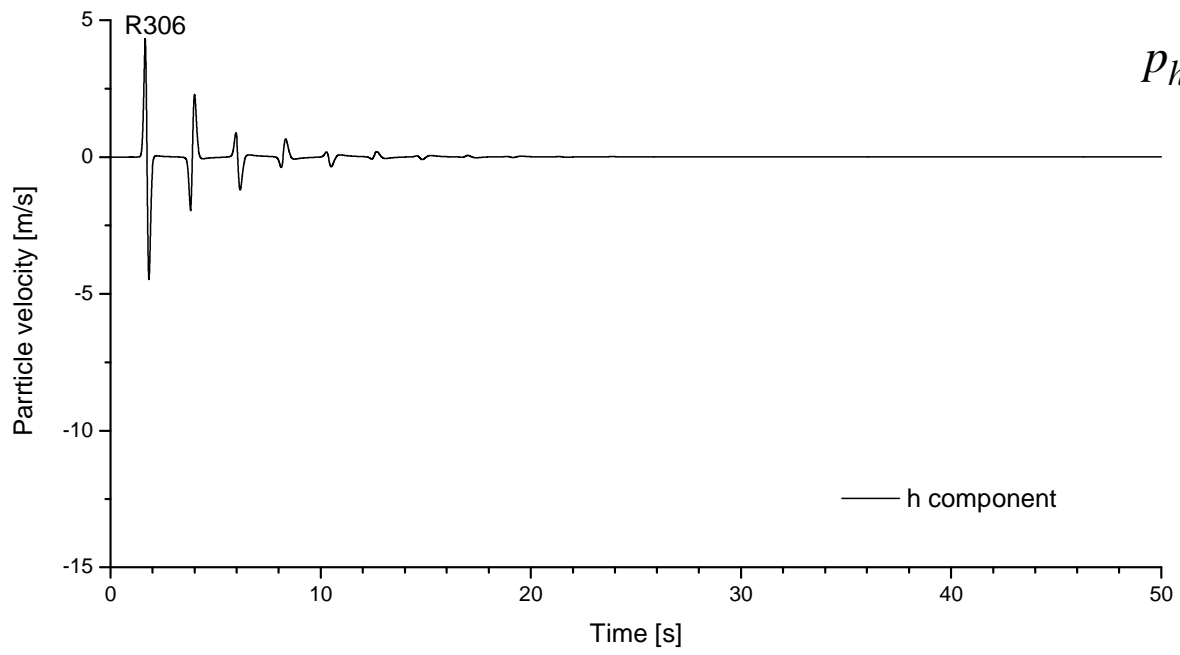


Fig. 5.11

# 1D pseudoimpulse responses

inc. w.

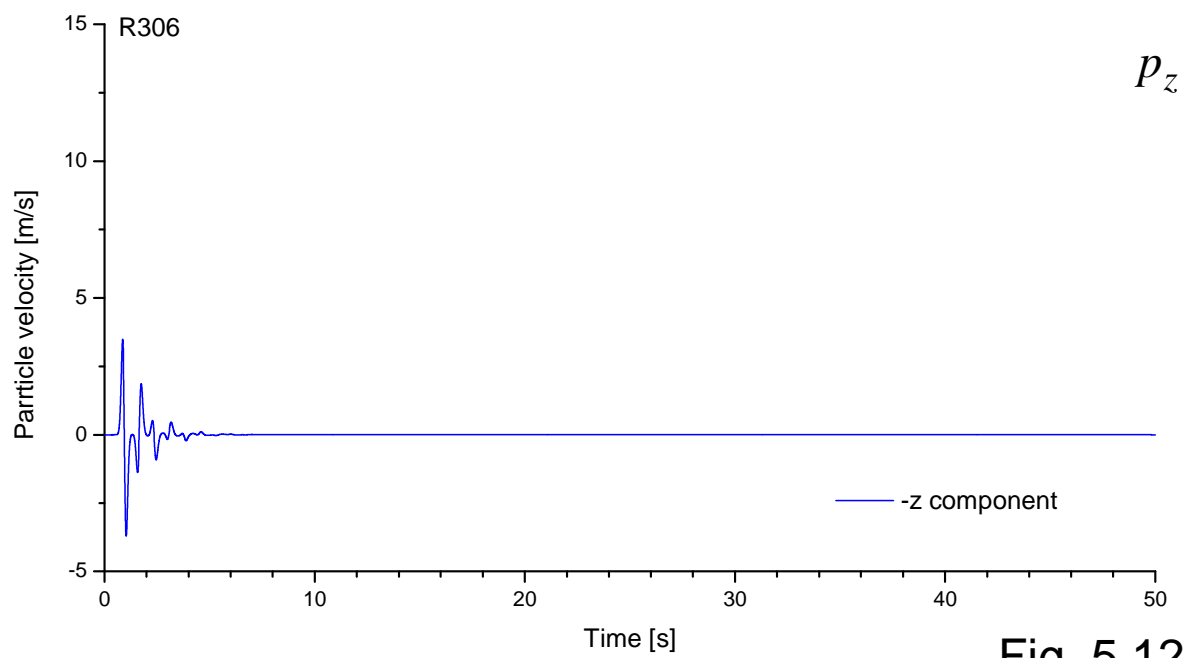
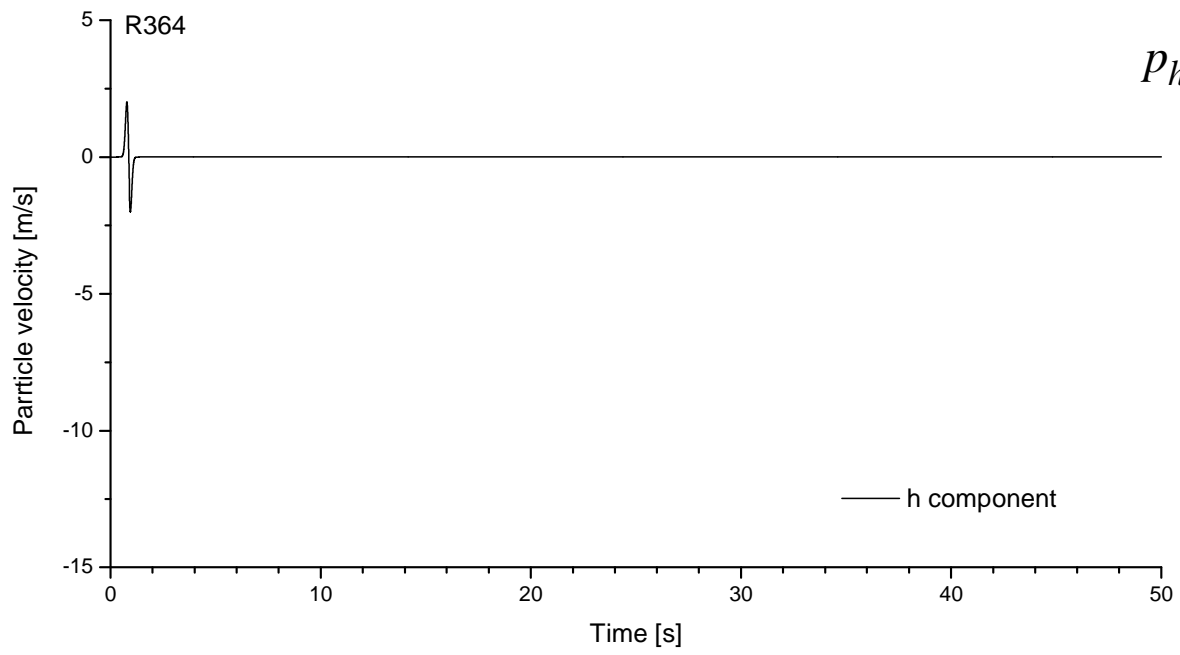
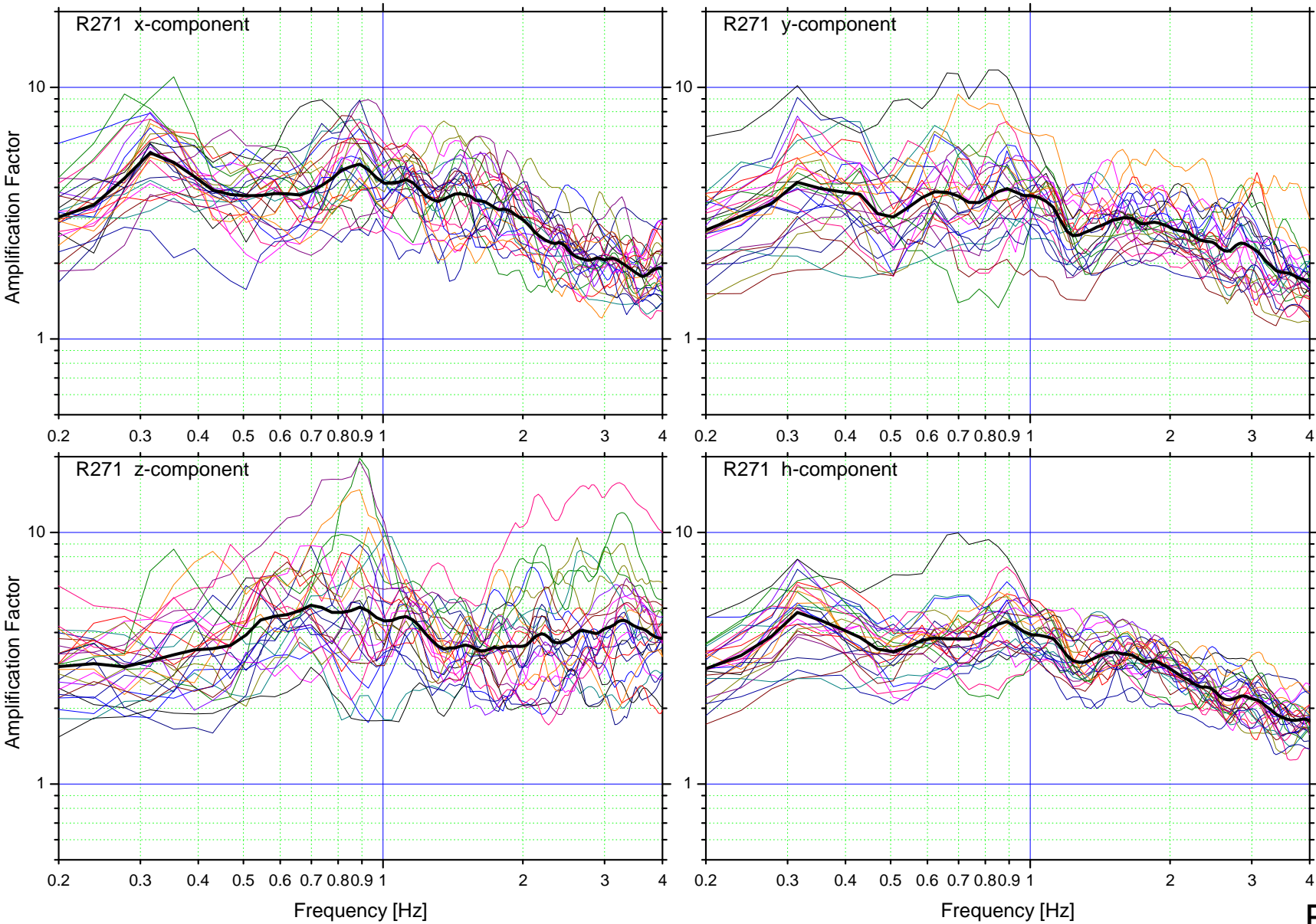
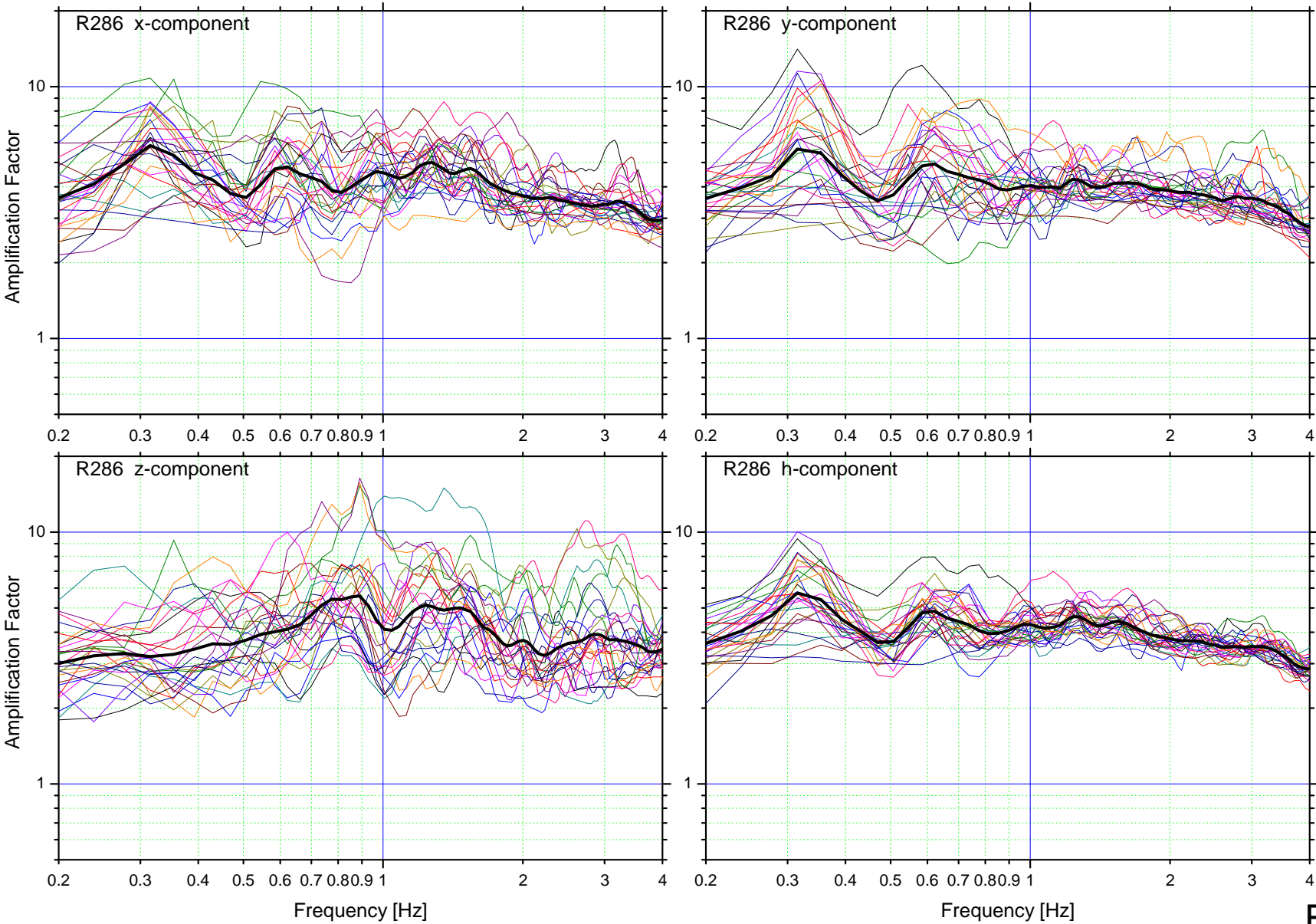


Fig. 5.12



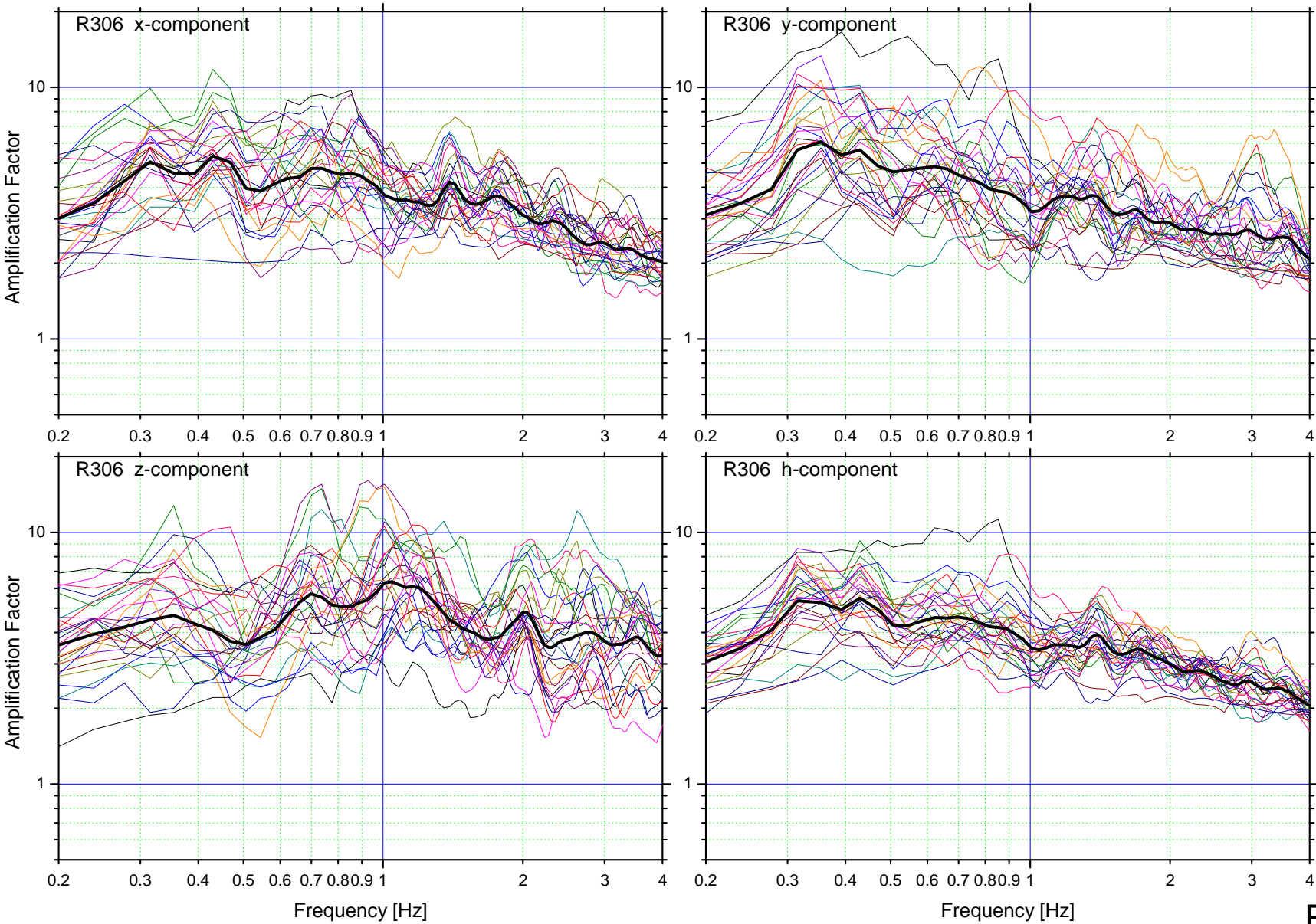
3D simulations

Fig. 5.13



3D simulations

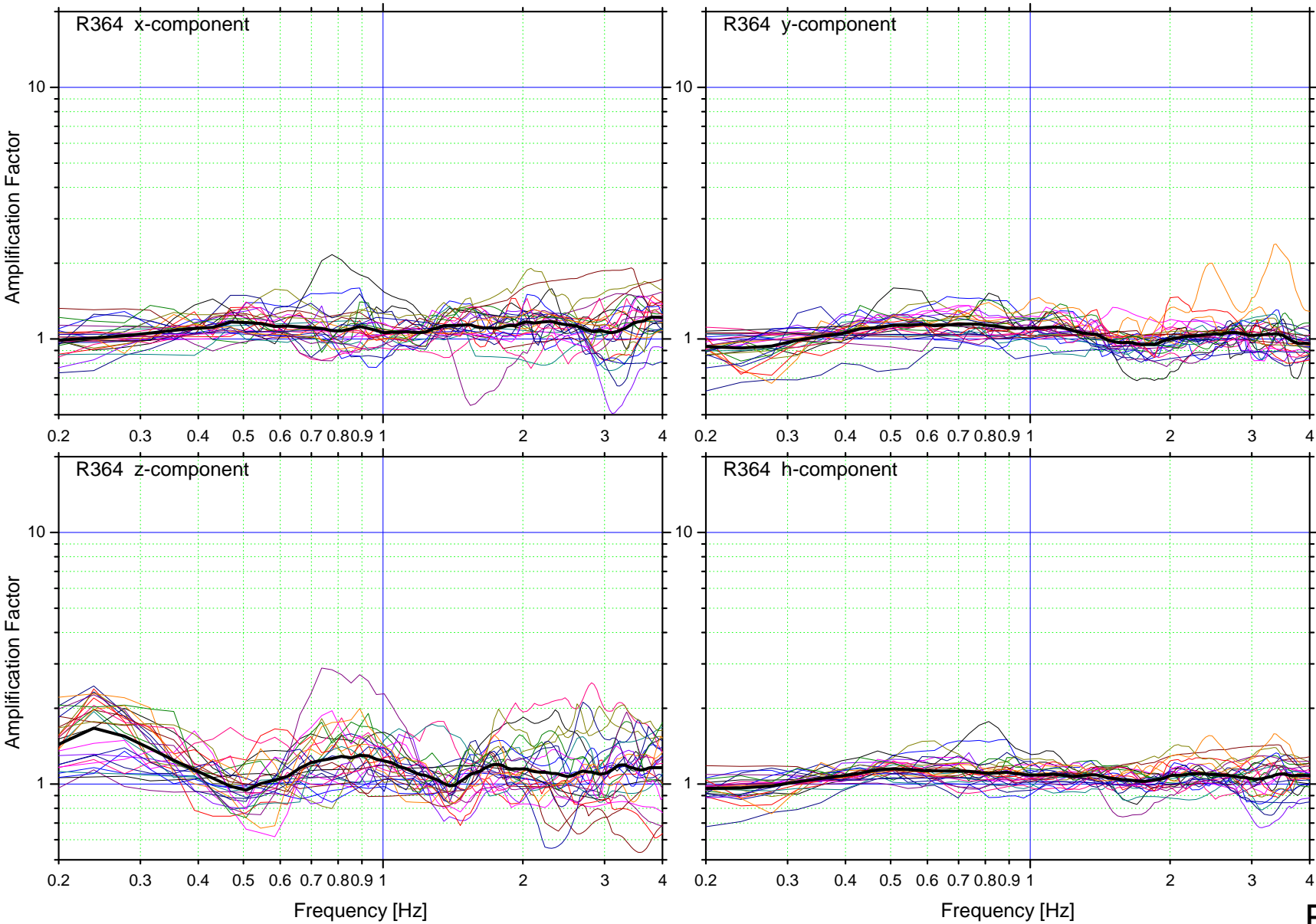
Fig. 5.14



3D simulations

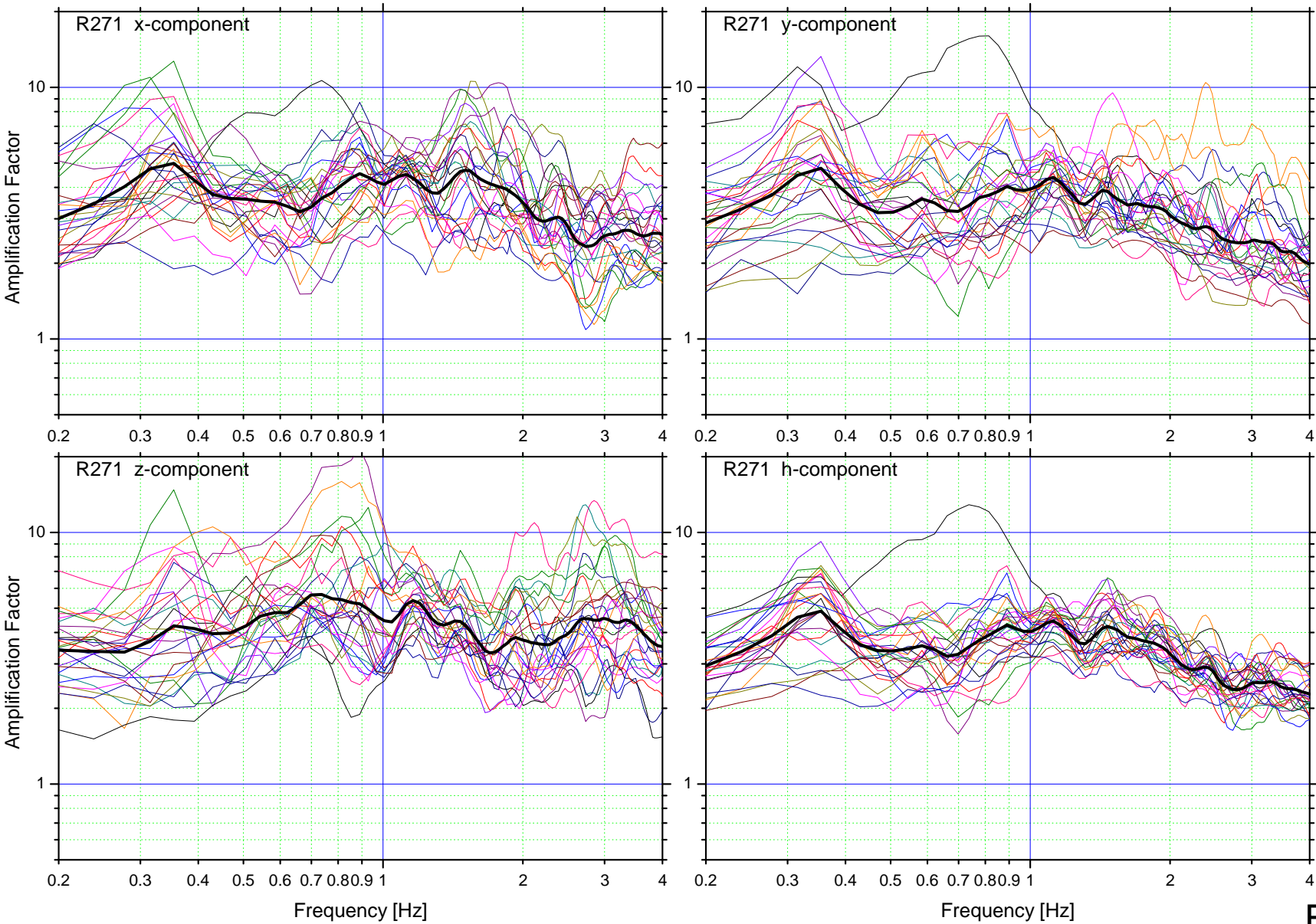
Fig. 5.15





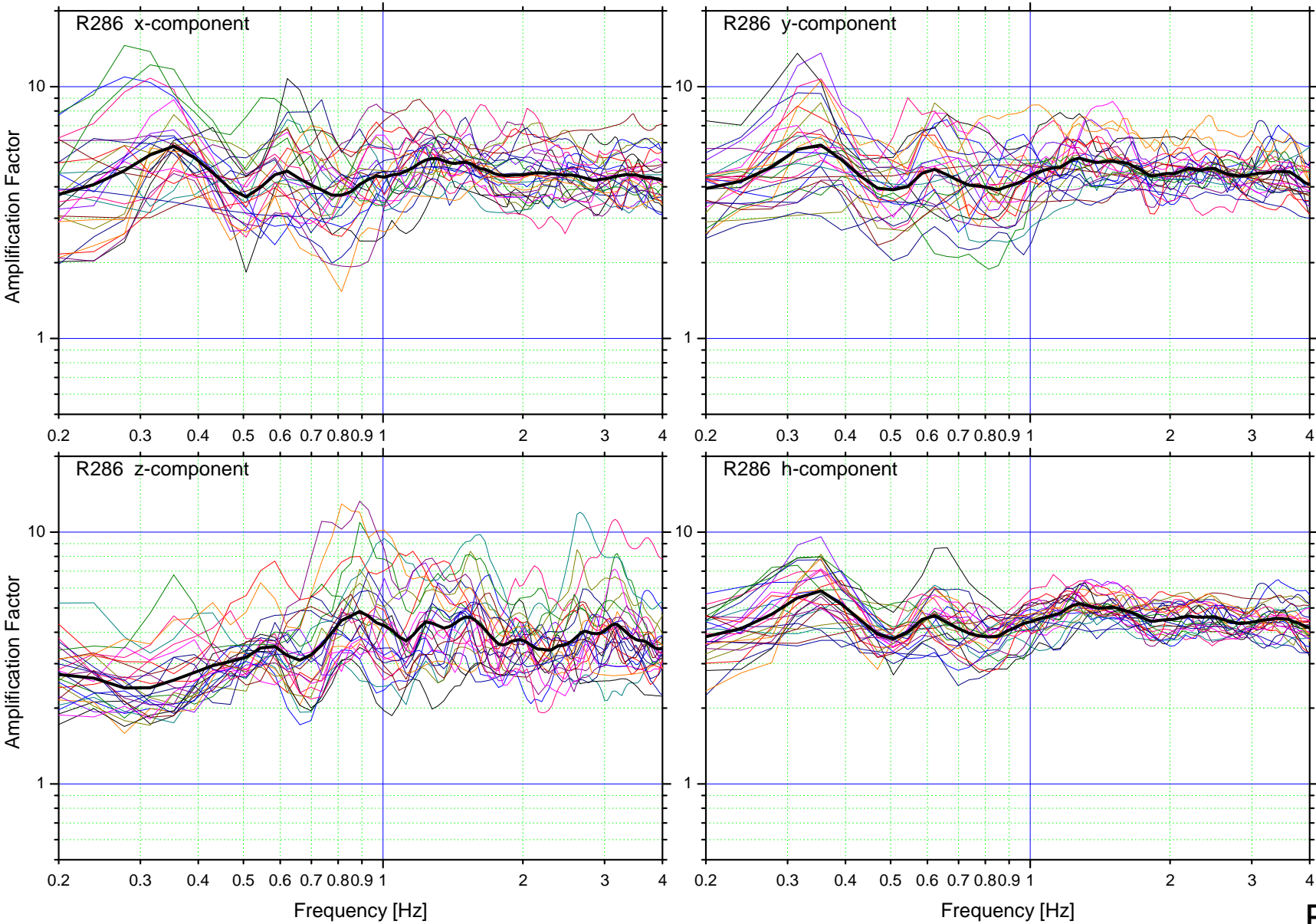
3D simulations

Fig. 5.16



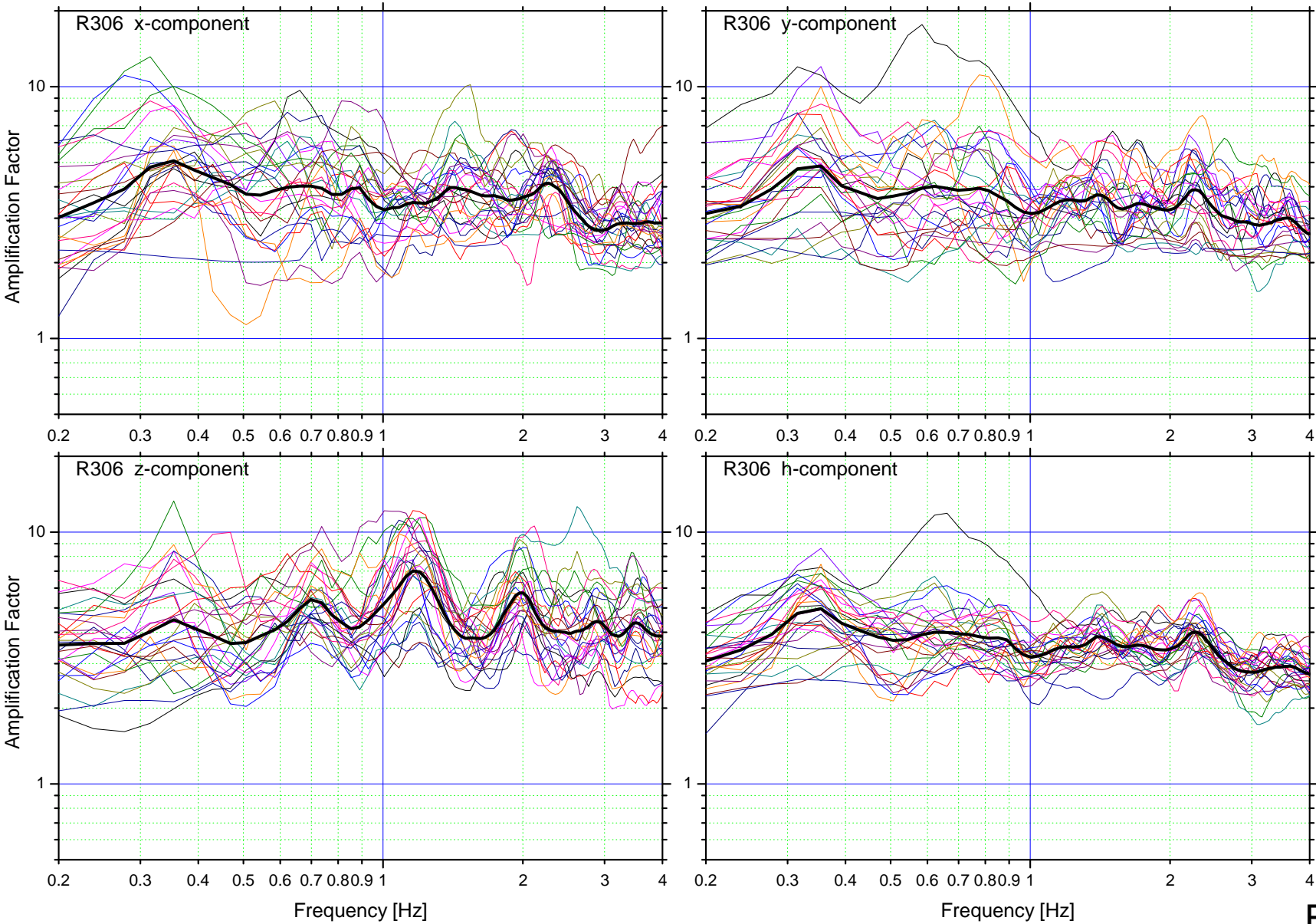
2D simulations

Fig. 5.17



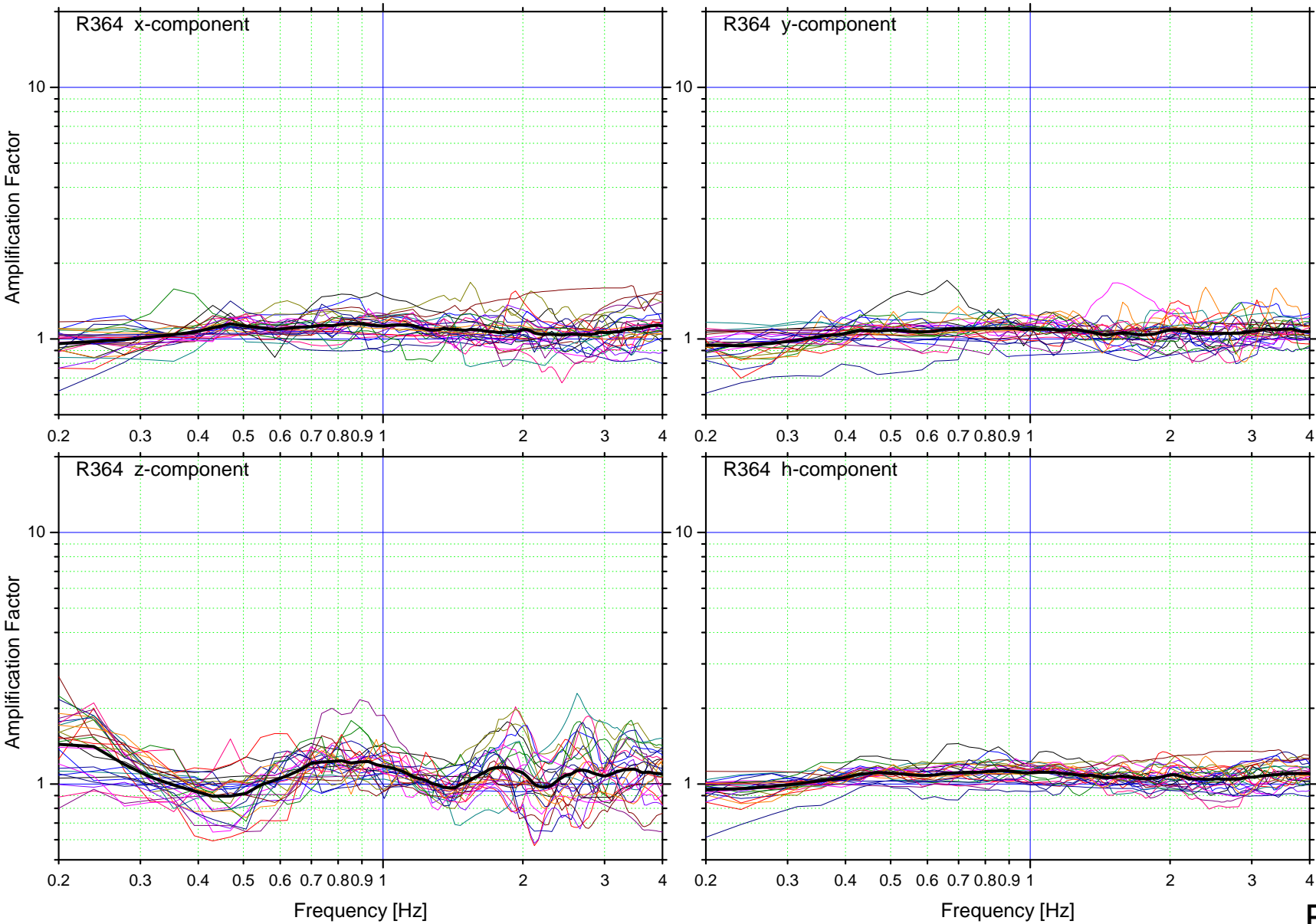
2D simulations

Fig. 5.18



2D simulations

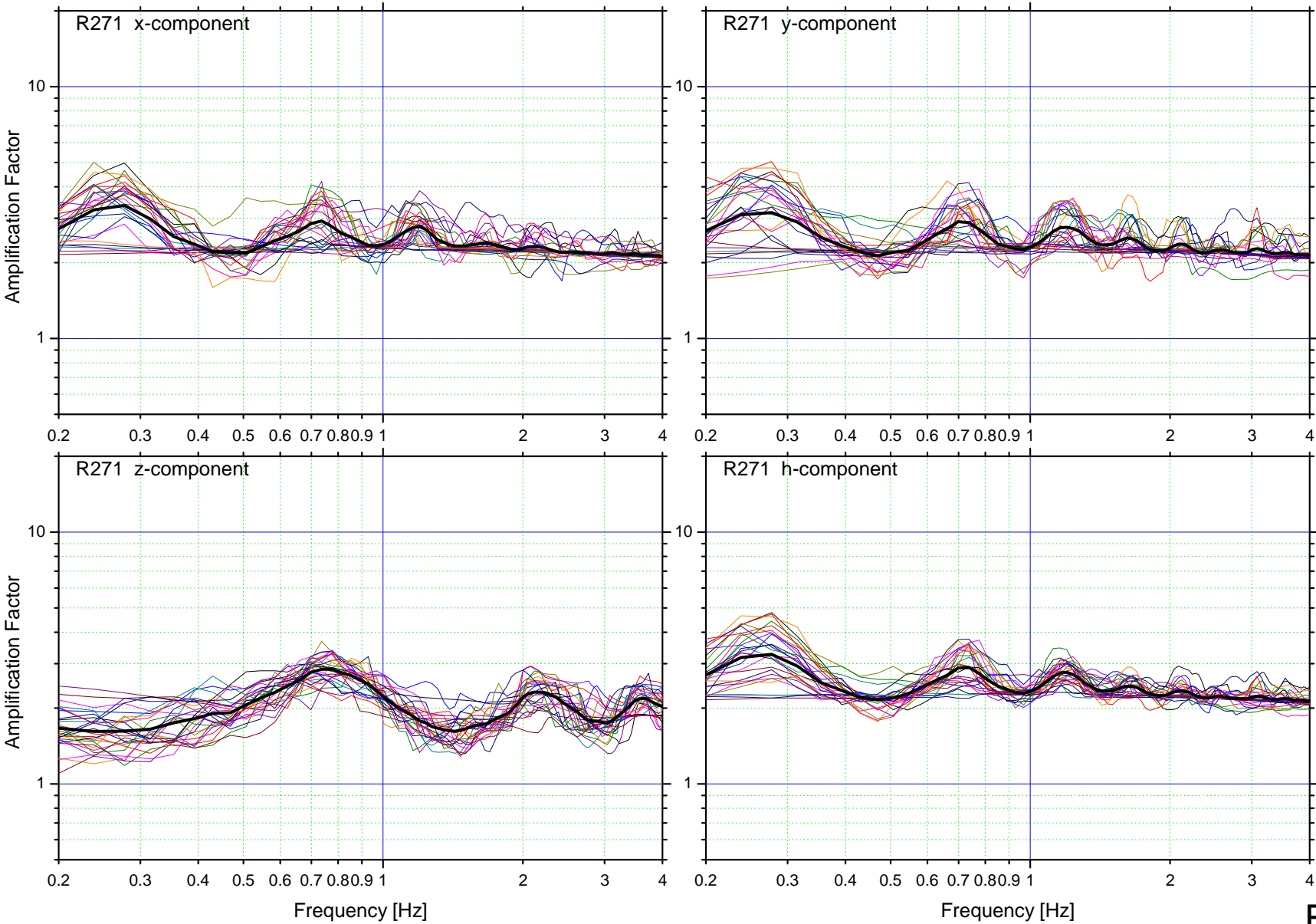
Fig. 5.19



2D simulations

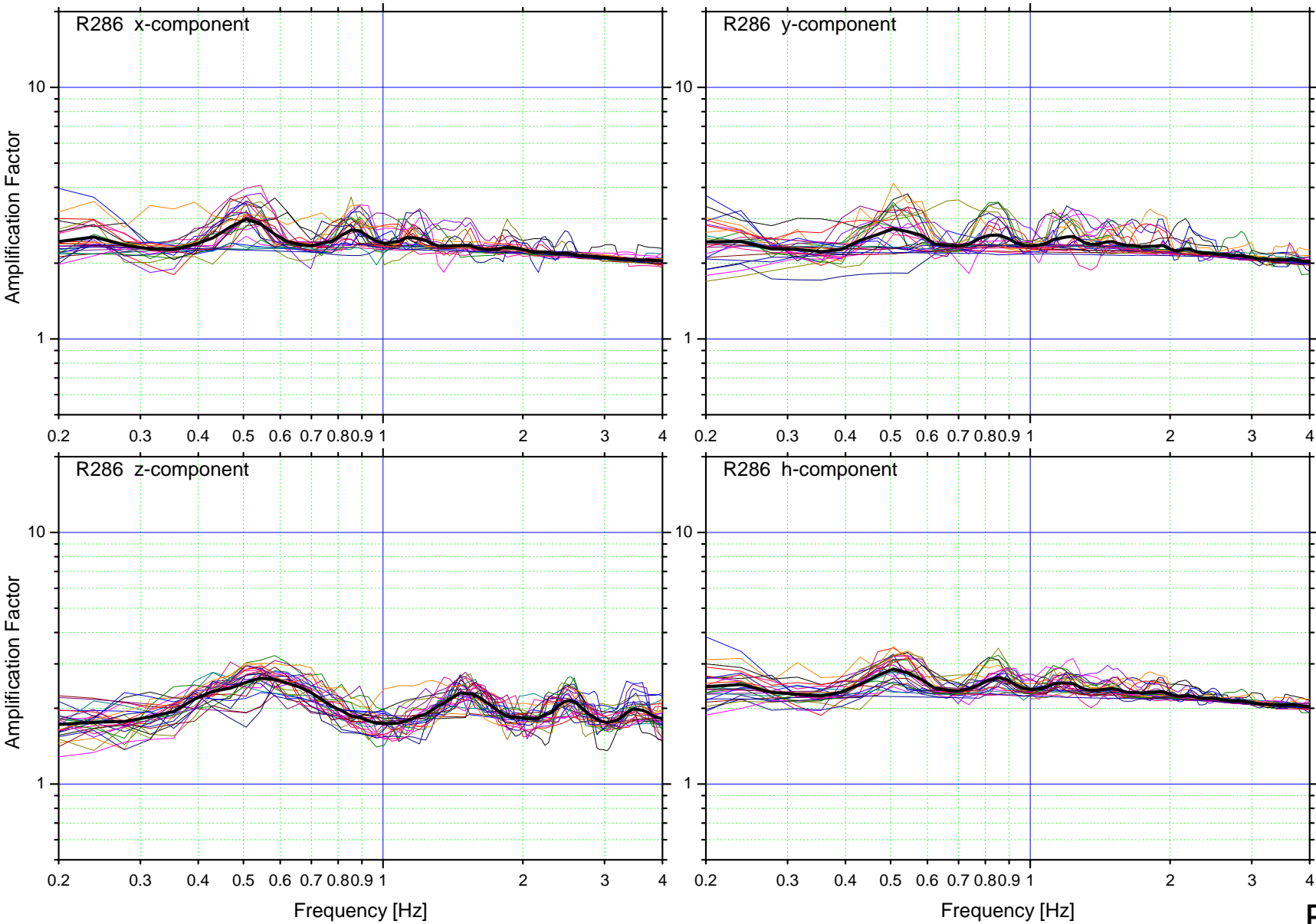
Fig. 5.20





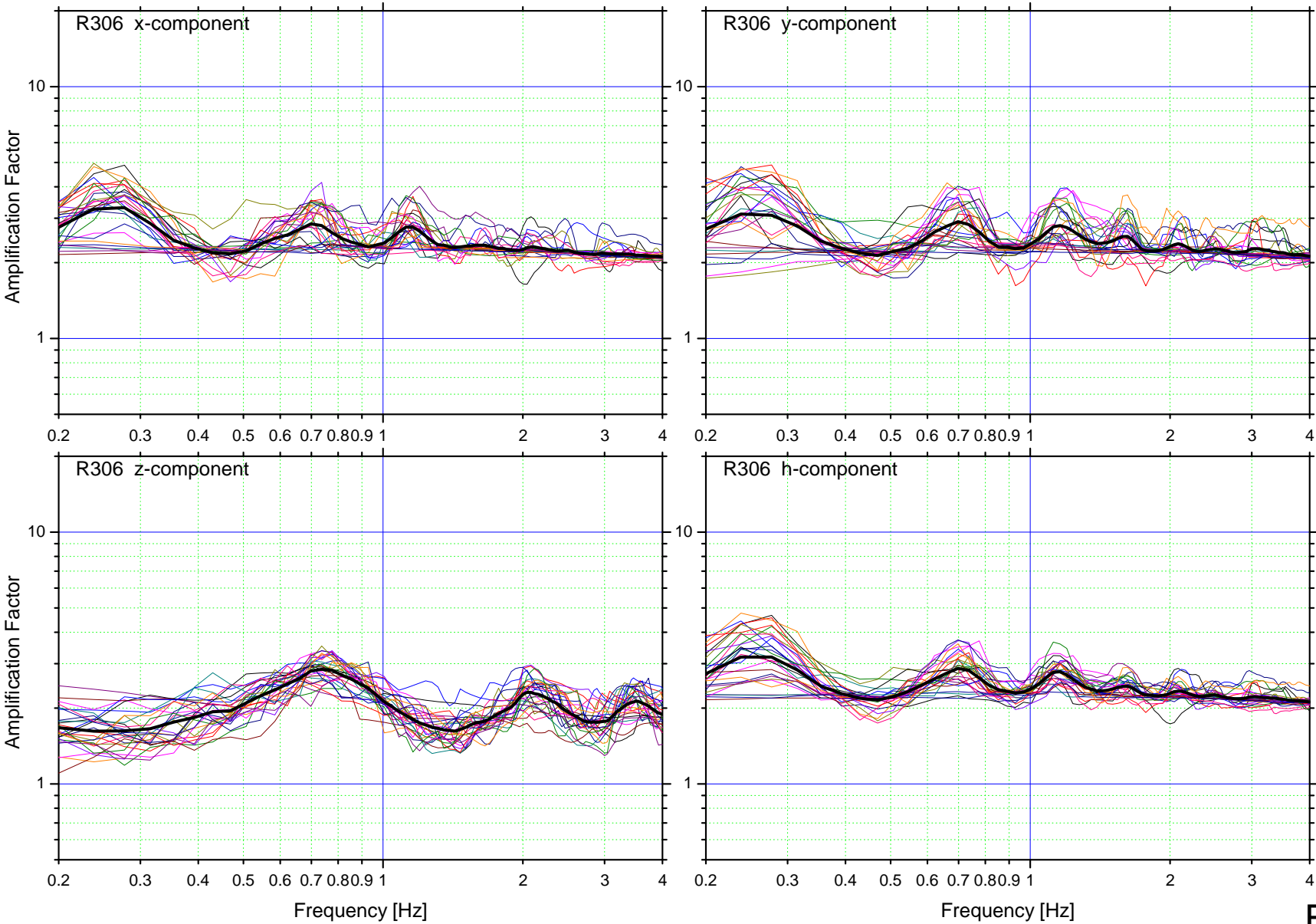
1D simulations

Fig. 5.21



1D simulations

Fig. 5.22



1D simulations

Fig. 5.23



1D simulations

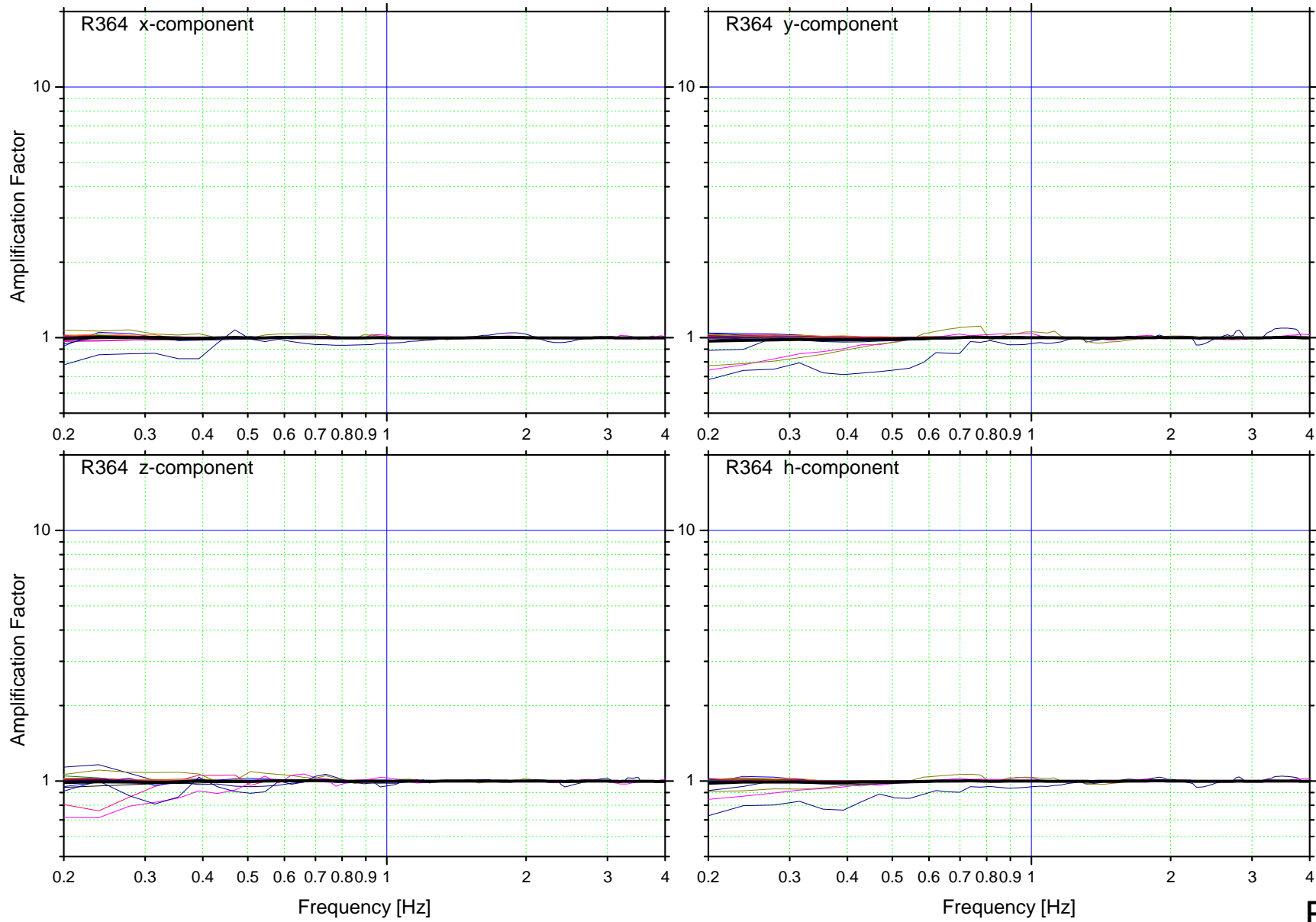
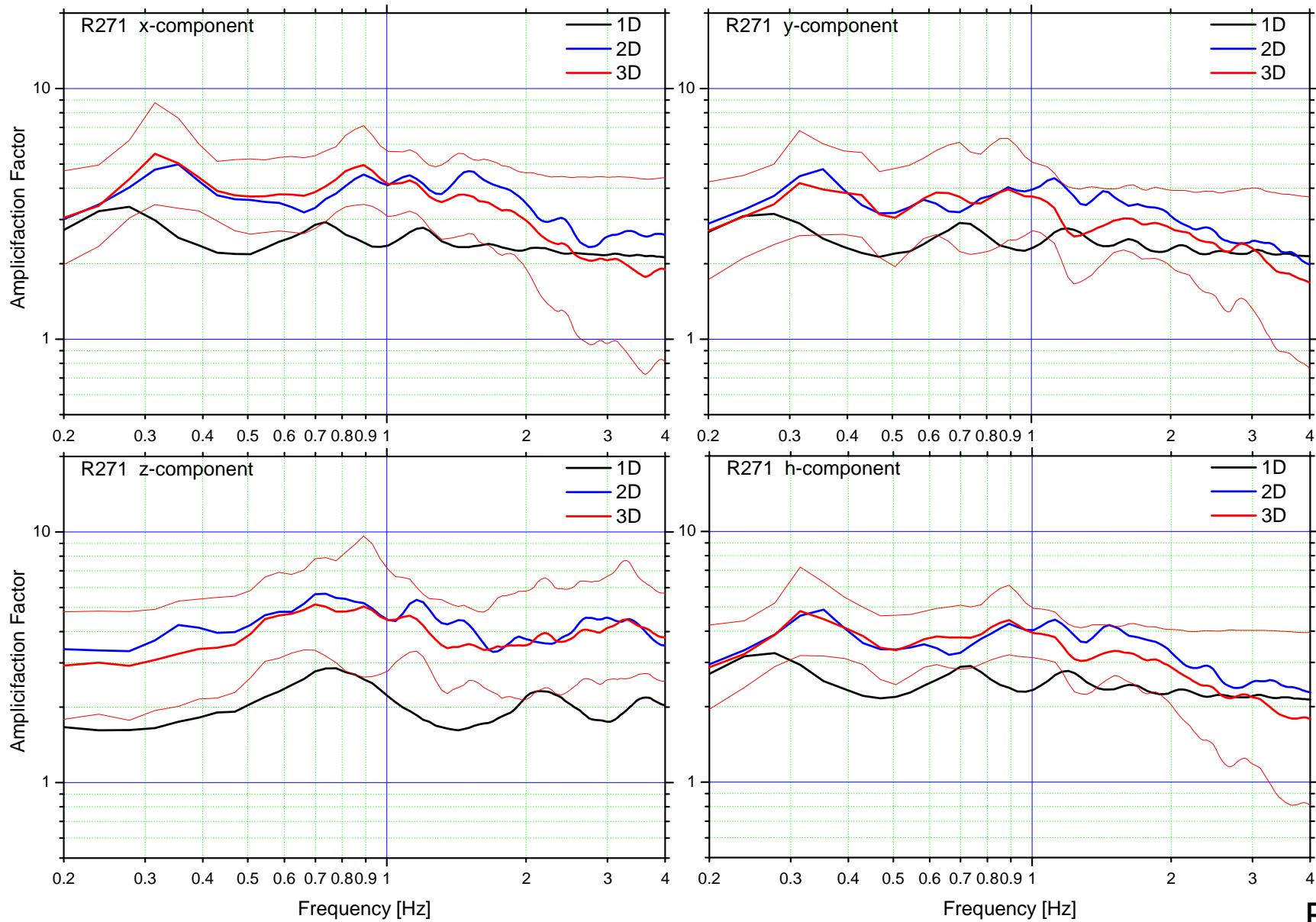
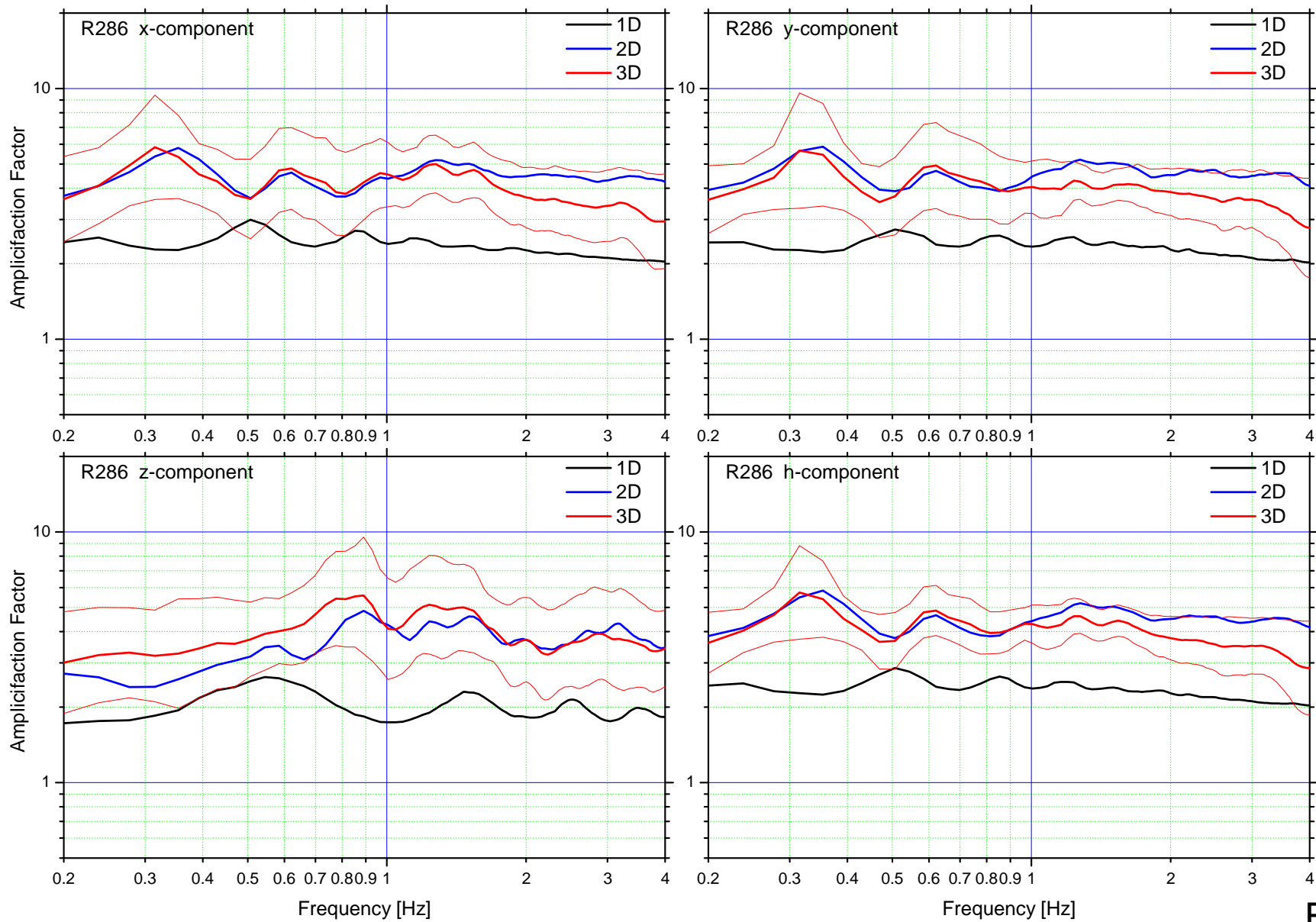


Fig. 5.24



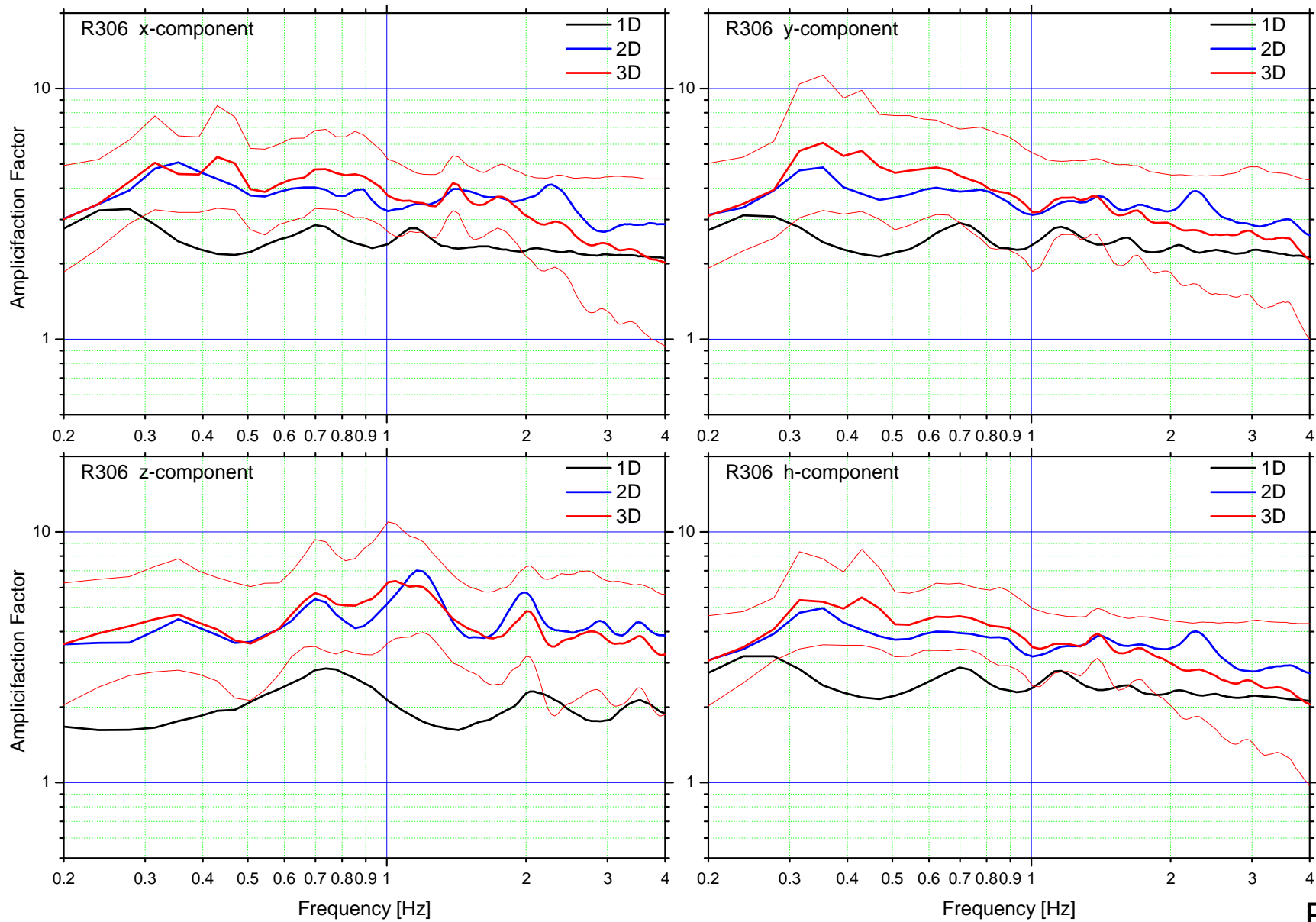
Comparison

Fig. 5.25



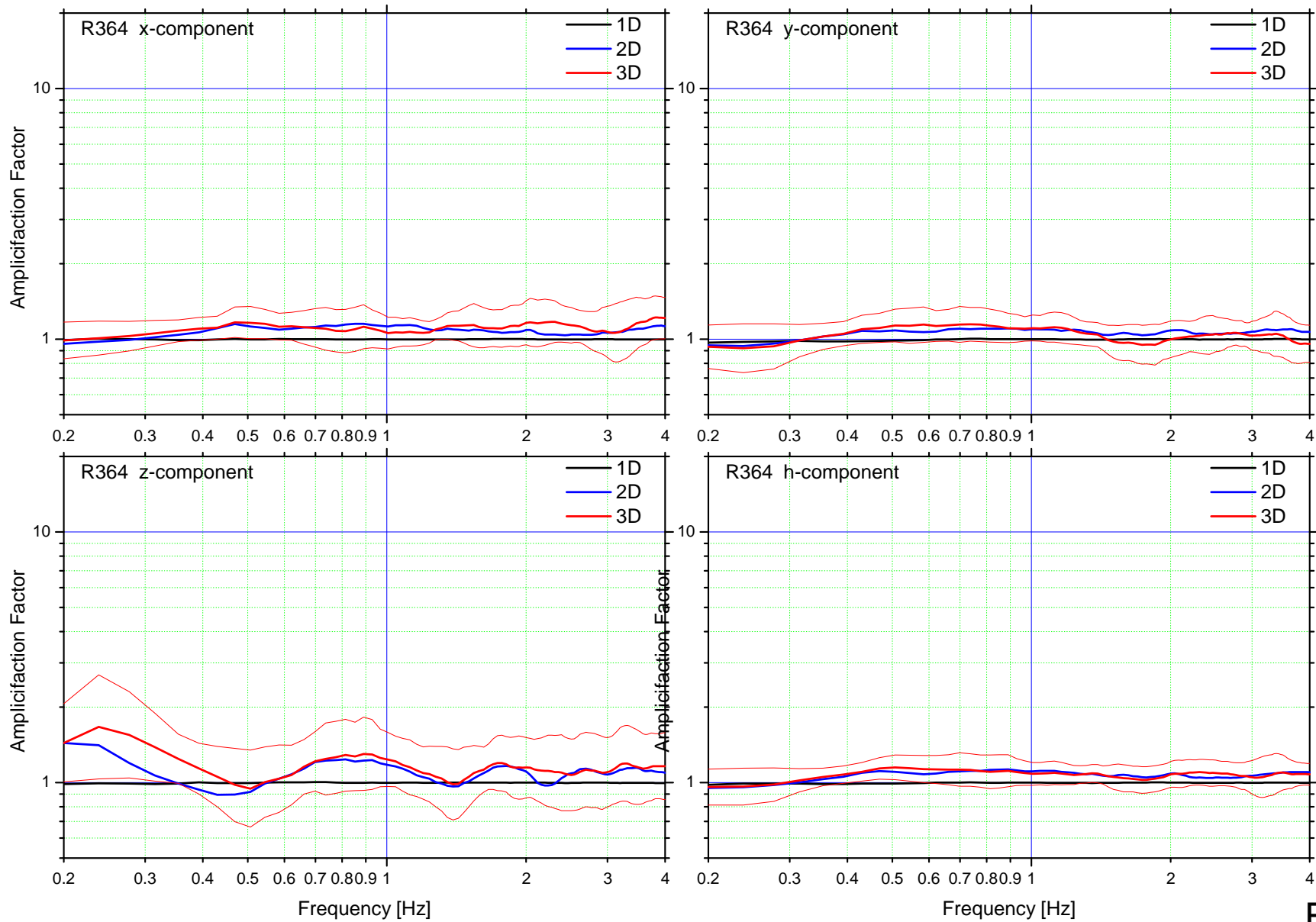
Comparison

Fig. 5.26



Comparison

Fig. 5.27



Comparison

Fig. 5.28

# **Project SIGMA**

**Review of:**  
**CHARACTERIZATION OF CLASSES OF SITES WITH A LARGE  
POTENTIAL TO CAUSE SITE EFFECTS TAKING INTO ACCOUNT  
THE GEOLOGICAL HETEROGENEITIES  
(Methodological Approach)**

(Ref : SIGMA-2013-D3-97)

*Alain Pecker*  
*October 30, 2013*

## **1. Scope of the work reviewed**

The object of the report should be as announced in the title and in the introduction to select and characterize specific sites likely to cause site effects in 1D, 2D and 3D. This work is part of WP3.

## **2. General comments**

Selection of representative sites likely to cause site effects is essential for WP3 to derive a methodology for accounting for such effects in PSHA. However the report is rather disappointing in that respect because only one page is dedicated to the description of the chosen sites, while the rest of the report focuses on numerical analyses. These developments, which occupy 27 pages, go far too much in details and are useless for ordinary people who are not forefront specialists in numerical analyses with the finite difference method. If the authors wish most of these details could be moved to an annex (at least from §3.2.4 to §4). Furthermore, it is announced in the executive summary that investigation of the sensitivity of model features to seismic motions will be carried out. At no place in the report are the sensitivity studies described: it is essential to know at this stage the parameters that will be investigated: valley dimensions, wave velocity gradient, soil layering, motion incident angle, etc...

### **2.1 Site description**

With respect to the selected site, it is not clear why the authors include the so-called canonical model in the perspective of quantifying site effects. For such a site, no site effect, as universally understood, is expected.

For the other sites the choice looks appropriate in covering typical geometries, but we would have expected a more detailed description:

- valley dimensions (width, length, depth),
- soil description : layering if any, as a minimum  $V_S$ - $V_P$  profiles, quality factor.

*Remark:* in table 2.1, the notations RS4 and RS5 would need some clarification

## 2.2 Soil constitutive model

A very general exposition of the viscoelastic constitutive soil model is provided in 3.2.3.introducing as many anelastic coefficients  $Y_l$  as wanted. From my understanding these coefficients are determined from the knowledge (measurement or estimate) of the quality factor at several frequencies. The key for the calculations of the anelastic coefficients seems to be equation (1.5); it is written that this equation, once  $Q(\omega_k)$  ( $k=1, 2, \dots$ ) are known, is solved using the least square method. Is there any reason to choose  $k$  different from  $l$ ? If both coefficients are equal the solution of equation (1.5) simply reduces to solving a set of linear algebraic equations in  $Y_l$ . If they are different some explanations would be needed to explain the choice of  $l$ .

## 2.3 Numerical analysis of the Grenoble valley

These analyses present the type of results that are expected from the numerical analyses for 1D, 2D and 3D site geometries. Analyses are carried out for 27 recorded time histories retrieved from the RESORCE database. The results are presented in terms of particle velocities at the ground surface and amplification functions.

The criteria for the choice of the time histories are rather crude, based on magnitude, focal distance and PGA. The authors must however be commended for using the RESORCE database (a good evidence of collaboration between WPs), but a more thorough discussion of the choice of time histories must be undertaken. It is in particular strongly recommended that this choice be made in collaboration with WP5 who will be the end users of the PSHA.

It would have been appreciated to have some comments on the results of the numerical analyses and not a simple set of uncommented figures; for example comparisons between the three geometric models seem to indicate that going for a 3D model in the Grenoble valley is not worthy; 2D and 3D analyses are very similar. Is it a general trend for the Grenoble valley or would some minor changes in some parameters (sensitivity studies) overrule this conclusion?

Would not it be interesting from an engineering standpoint to use other parameters than the Fourier amplification function to characterize site effects: response spectrum ratios as it is commonly done (Pegasos and Pegasos Refinement Project)?

## Review of the SIGMA Deliverable D3.97

### "Characterization of classes of sites with a large potential to cause site effects taking into account the geological heterogeneities (Methodological approach)"

(Authors : J. Kristek, P. Moczo, F. Hollender, 21/10/2013)

This report presents the methodology that will be followed to investigate the "overamplification" due to laterally varying underground structures for a number of site geometries. While results are presented in this report only for a small number of sites (four, located on a 2D cross-section in the Grenoble area), the goal is to apply this approach to extensive numerical simulations for 7 different geometries.

This report is clearly written and easy to follow. One may regret the apparent lack of balance between the methodological part (numerical method, post-processing approach to get the amplification factors, which include many equations : 30 pages), and the example results (10 pages , with only little discussion, probably due to time shortage); I think however it is good for the SIGMA project to have a report documenting the numerical simulation approach in a relatively concise way, as it will be extensively used afterwards. I anticipate the future reports will focus on the interpretation of results that will be derived with this methodology for a collection of complex geometries, and the way it can/should be used for practical design purposes

#### Specific comments

##### ***Local surface geological structures (p. 4-6 / Table 2.1) :***

This section presents very shortly the qualitative features of the 7 various types of sites to be considered. I did not understand very well what is the meaning or the purpose of the "canonical sites" which are half-spaces : would not it be better to consider, for each type of structure, a "local" reference corresponding to the local "outcropping bedrock", which might include some kind of weathering and thus differ from a "homogeneous half-space" ?

I would have expected, together with an overview of the geometry of the various sites, some more quantitative information of the geometrical characteristics of each site (thickness, width) and on the velocity profiles and impedance contrasts to get a comparative overview about the expected frequency ranges and amplification levels, together with the target maximum frequencies. Also, although it is not the main scope of the present computations, it will be useful at some time to have an idea about the variability of local reference rock conditions from one site to another, in view of better capturing the possible issues at the interface between axes 2 (rock hazard) and 3 (soil hazard). I anticipate however this will be detailed in future reports.

##### ***Numerical simulation of seismic motion (p. 7-24) :***

The main scope of this section is to present the implementation details of the FD numerical scheme to be used for all the computations (all carried in the linear viscoelastic domain). The 3D model is coupled with numerically consistent 2D and 1D models in order to isolate the respective importance of 3D, 2D and 1D effects.

I did not check all the equations presented in this report, as I am fully confident in the expertise of the authors and the extreme care they attach to the accuracy and reliability of their computations. They successfully participated to numerous benchmarking exercises, including the ESG2006 and E2VP on the Grenoble and Euroseistest sites, respectively.

Of particular interest for practical purposes are the following items :



- A well controlled implementation of attenuation
- a careful accounting of material discontinuities
- the efficiency of the non-reflecting boundaries
- the versatility of the excitation (point sources, finite sources with arbitrary kinematics, vertically propagating plane waves)

As I understand it, the main limitations of this code in its present implementation are the following:

- it cannot easily handle obliquely incident plane waves. This could be seen as a drawback for some sensitivity studies in cases with shallow near sources, but it could then be replaced by point (or finite) sources at carefully selected locations.
- It can handle only flat free surfaces and cannot therefore consider the effect of surface topography. I consider this is not a major issue, as pure topographic effects are marginal compared to valley effects; this may however add some complexity for the development of models for real sites which do have a non-planar free surface as it needs some consistent corrections for the free surface and underground interfaces.

***Analysis of numerical simulations (p. 24-35) + Grenoble case example (p. 36-45 :***

The 3D simulations are intended to be performed basically for vertically incident plane waves, so that it can be easily compared with 2D and 1D response.

The "raw", direct outputs of the FD simulations are time domain response functions to quasi-Dirac smoothed displacement pulses (Gabor wavelets), which are later convolved with a series of real accelerograms in order to derive engineering oriented parameters (such as amplification factors on response spectra), and compare them in the 3D, 2D and 1D cases through a statistics of the results obtained with all the considered input accelerograms. For the Grenoble case considered here as a first example, the engineering parameters are the amplification factor of response spectra. The approach is sound, I suggest however that some specific issues should be more clearly emphasized in the report to be sure the readers can be explicitly aware of them

- Multidirectionality of input motion

The 3D case is indeed a 3D-3C case, which means 3D geometry with 3 Component input: it is assumed that the two horizontal motions (polarized in the East and North direction) are carried by vertically incident plane S waves, and the vertical component by a vertically incident plane P wave. This assumption is obviously incorrect in the reality (there are P wave contributions in the horizontal components, and S wave contributions on the vertical component, and there are also oblique and surface wave contributions on both), but it is acceptable from an engineering viewpoint: it is indeed difficult to have another option when considering vertically incident plane waves, which is the standard case for most 1D studies. The only other options are to include the source in the model, but then the comparison with 1D or 2D cases becomes more difficult or at least more time consuming.

The three dimensional character of the input motion also raises some specific issues for the comparison with the 2D and 1D cases : a rotation of component along SH and SV components depending on the profile direction (as rightly indicated in the report), and one single component (East or North) for the 1D case. As a consequence, the total energy input is different in the three cases and the comparison of the single component amplification ratios includes both the effects of the 3D (or 2D) geometry of the underground, and the multidirectionality (or not) of the input motion: The  $AF_h$  amplification factor is therefore probably the most meaningful horizontal amplification factor compared to  $AF_x$  and  $AF_y$ , while  $AF_z$  is the most strongly affected by the coupling between horizontal and vertical components in the 2D and 3D cases

One possible option could be to consider separately the 3D effects of each single component horizontal input (comparing 3D-1C and 1D-1C) but then the 2D case for non EW or NS profiles corresponds to a different input. I do not have any simple solution, the option taken by the authors is probably the best one, but this 3-directionality of the input has to be kept in mind for the interpretation of the result.

- Choice of accelerograms

The derivation of statistics on engineering parameters of ground motion requires the use of a set of input accelerograms with varying frequency contents (amplitude and phase). The present report uses a set of 27 3C accelerograms corresponding to short distance, rock recordings for magnitudes 4.5 to 7. A look at the corresponding response spectra (not shown in the present report, but kindly provided by the authors after a direct request) shows that they do span a very satisfactory range of variability in terms of frequency contents, with predominant frequencies from 3 to 20 Hz.

- It is not clear whether this selection is valid only for the Grenoble site or will be the same for all the other sites (the latter option would seem reasonable for me)
- I am wondering whether this set of 27 could not be reduced to around 10, in order to minimize the cost of post-processing. This reduction would imply an analysis of the scatter of input spectra, and of the corresponding scatter in output results, such as amplification factors: what is the minimum number of input accelerograms to have a robust estimate of this output scatter, especially in the 3D case where the Grenoble example exhibits the larger scatter
- When the final set is selected, It would be good to have an appendix with the corresponding time histories and spectra

- Specific results for each site

- In addition to the 1D, 2D and 3D amplification factors, it could be useful to display also "aggravation factors" (i.e., the overamplification due to non 1D effect :  $AF_{2D}/AF_{1D}$  or  $AF_{3D}/AF_{1D}$ )
- It would be interesting also to consider the effect of underground structure dimensionality on some other quantities more sensitive to the signal duration than the response spectra : Fourier transfer functions, CAV, duration, ... (following the E2VP experience)

- Specific results for the Grenoble case

Some discussions on the displayed results would have been welcome ! Here are some items I personally noticed

- The underlying bedrock is very hard ( $V_s = 3.2$  km/s), which will imply a specific tuning of the rock hazard with respect to "standard" rock conditions
- The pseudoimpulse time domain responses exhibit a very long duration and a strong component to component coupling<sup>1</sup>
- It would be good to quantify the scatter on the amplification factor through a frequency-dependent standard deviation, not only in the 3D case, but also in the 2D and 1D cases: I anticipate it would show a significantly larger scatter for the 3D case, intermediate for the 2D case, and minimum for the 1D case
- For the specific sites chosen, the mean 2D and 3D results are almost comparable: this may be understood considering the almost 2D structure in this NW branch of the basin. it would be instructive to know if this result stands for other receivers located in downtown Grenoble where the geometry is fully 3D.

### **Conclusions (p. 46)**

I think the methodology presented here is sound and able to quantify the genuine effects of the geometry of the underground structure. What is not yet clear is the number of receivers that will be considered for each site (given the 3D structure of the sites displayed in Table 2.1, this number may be huge), and how the potentially huge set of results can be managed, considering also the

---

<sup>1</sup> there is an error on Figure 5.12 bottom which duplicates the impulse response for receiver R306 instead of R364

announced sensitivity studies with variations on the structure or on the excitation. It would be good to present what are the options presently considered for the future computations

Grenoble, 07/11/2013

Pierre-Yves BARD